2014-03-26

Application of Dynamic Upscaling for Thermal Reservoir Simulation

Picone, Matteo M.

UNIVERSITY OF CALGARY

Application of Dynamic Upscaling for Thermal Reservoir Simulation

By

Matteo Mario Picone

A THESIS

SUBMITTED TO THE FACULTY OF GRADUATE STUDIES

IN PARTIAL FULFILMENT OF THE REQUIREMENTS FOR THE

DEGREE OF MASTER OF ENGINEERING

DEPARTMENT OF CHEMICAL AND PETROLEUM ENGINEERING

CALGARY, ALBERTA

March 2014

Abstract

Reservoir simulation is inherently an imperfect tool for forecasting. However, given sufficient analysis and post-processing, the areas of uncertainty can be quantified and effort can be made to mitigate their impact and improve the confidence in the prediction. The focus of the research documented here is to analyze the extent to which grid size definition and the location and quantity of reservoir heterogeneities impact the performance of a simulation-based recovery process. In analysing two different sets of models (binary and facies-based), a new methodology was developed and applied to mitigate the observed difference in the forecasted result. When the observations are coupled, it suggests that an increase in near wellbore reservoir heterogeneity, as indicated by a reduction in gridblock connectivity, has an increased impact upon the simulation results when compared to the impact of strictly length scale definition of heterogeneity. Additionally, the impact of length scales can be normalized when the focus is upon connectivity within the reservoir model.

Acknowledgements

I would like to thank Arnfinn Kjosavik for helping to conceive this idea. Our original conversations serve as the foundation to this work. Secondly, I would like to thank Dr. Ian Gates who not only served as an academic mentor and was instrumental in fine tuning many of the details, but was also very kind and patient during the entire process.

Finally, I would like to thank my family. To my parents who always empowered my brother and I to achieve our goals. They are the foundation to my life and represent everything good I have accomplished thus far. Life is nothing if not for family.

And to my wife, Kim, you are the other half, the missing piece. And our love is unconditional.

Table of Contents

List of Tables

List of Figures and Illustrations

List of Symbols, Abbreviations and Nomenclature

Symbol	Definition
A	Area
B	Oil Formation Volume Factor
c	Compressibility
c_p	Heat Capacity
C_{max}	Optimum Connectivity for the Given Cell
∇	Derivative Operator
$\bar{f}$	Face-Averaged Fractional Flow
f_i	Fractional Flow
g	Acceleration due to Gravity
h	Height
k	Thermal Conductivity Constant of the Material
i	Gridblock Notation
k_{abs}	Absolute Permeability
k_{eff}	Effective Permeability
k_e^x	Effective Permeability
K_{eq}	Equivalent Permeability
Kh	Horizontal Permeability
k_{rl}	Relative Liquid Permeability
Kv	Vertical Permeability
L	Length
n	Number of Outcomes
n	Time-step Notation
NI	Steam Chamber Development, x-direction
NJ	Steam Chamber Development, y-direction
NK	Steam Chamber Development, z-direction
P	Pressure
P	Probability of Occurrence or Weight
p_l	Liquid Pressure
q	Sink (production) or Source (injection) Term
Q	Volumetric Rate
Sg	Gas Saturation
So	Oil Saturation
Sw	Water Saturation
So_r	Residual Oil Saturation
Sw_{irr}	Irreducible Water Saturation
T	Temperature
t	Time
K_{TH}	Thermal Conductivity
$thcong$	Thermal Conductivity, Gas
$thcono$	Thermal Conductivity, Oil

$thconr$	Thermal Conductivity, Rock
$thcons$	Thermal Conductivity, Solid
$thconw$	Thermal Conductivity, Water
T	Transmissibility
T_R	Reservoir Temperature
T_S	Saturation Temperature
V	Volume
V_c	Condensate Convective Velocity
v_l^c	Convective Liquid Velocity of the System
x	Value Assignment
x	x-direction

Greek Symbol	**Definition**
Δ	Delta (Change in Quantity)
δ	Partial Derivative
κ_{mix}	Thermal Conductivity, Volume Weighted
λ	Mobility
$\bar{\lambda}_t$	Face-Averaged Total Mobility
μ	Mean
μ	Viscosity
μ_l	Liquid Viscosity
v	Velocity
ρ_l	Liquid Density
$\rho \boldsymbol{v}$	Mass Velocity Vector
σ	Standard Deviation
Σ	Summation
ϕ	Porosity
ϕ_e	Effective Porosity
φ_f	Fluid Porosity
φ_v	Void Porosity
ω	Averaging Constant (Arithmetic, Harmonic, or Geometric)
ω_i	Weight Assignment

Epigraph

"Lost to the treasures that compel us…"

Alert Status Red

Matthew Good, White Light Rock & Roll Review

CHAPTER 1 – INTRODUCTION

1.1 Background and Introductory Concepts

The process of thermal oil recovery is an evolving tertiary production technique commonly used for oil sands reservoirs in Western Canada. Thermal recovery processes target hydrocarbon plays where the fluid is immobile at in-situ reservoir conditions and consequently requires heat to achieve flow. The heat is often in the form of the enthalpy of vaporized water. The Athabasca Oil Sands region is one of three significant oil sands deposits within the province of Alberta. The Athabasca region mainly consists of the Wabiskaw-McMurray (clastic) and Grosmont (carbonate) Formations. The other two major oil sands plays in Alberta are the Cold Lake deposit which mainly consists of the Clearwater Formation and the Peace River deposit which comprises the Bluesky-Gething Formations, as indicated in **Figure 1.1.1**. According to the Alberta Energy Regulator (AER), formerly known as the Energy Resources Conservation Board (ERCB), Alberta's Energy Reserves for 2012 and the Supply/Demand forecasts for 2013-2022 highlight that Alberta has approximately 26.68 billion m^3 of established remaining crude bitumen reserves[1]. Approximately 80% of those reserves are considered recoverable by in-situ technologies, such as Steam-Assisted Gravity Drainage (SAGD) and Cyclic Steam Stimulation (CSS). Due to the location, depth, reservoir architecture and in-situ properties of the bitumen, SAGD is the most viable commercial thermal recovery technology currently operated in the Athabasca Wabiskaw-McMurray region. Conversely, CSS is mostly practiced in Cold Lake and Peace River where the oil sands formations are deeper and are overlain by a thick, competent caprock which is required for the elevated injection pressures (often 2-5MPa greater than

SAGD). The pay intervals tend to have poorer vertical continuity than that of a McMurray deposit and tend to produce at higher gas-to-oil ratios (GORs). CSS production GORs are often 10-25m^3/m^3 for the first several cycles, compared to production GORs of approximately 5-8m^3/m^3 for SAGD well pairs operated in the McMurray Formation.

Figure 1.1.1 – Schematic Highlighting the Three Major Oil Sands Areas within Alberta[2]

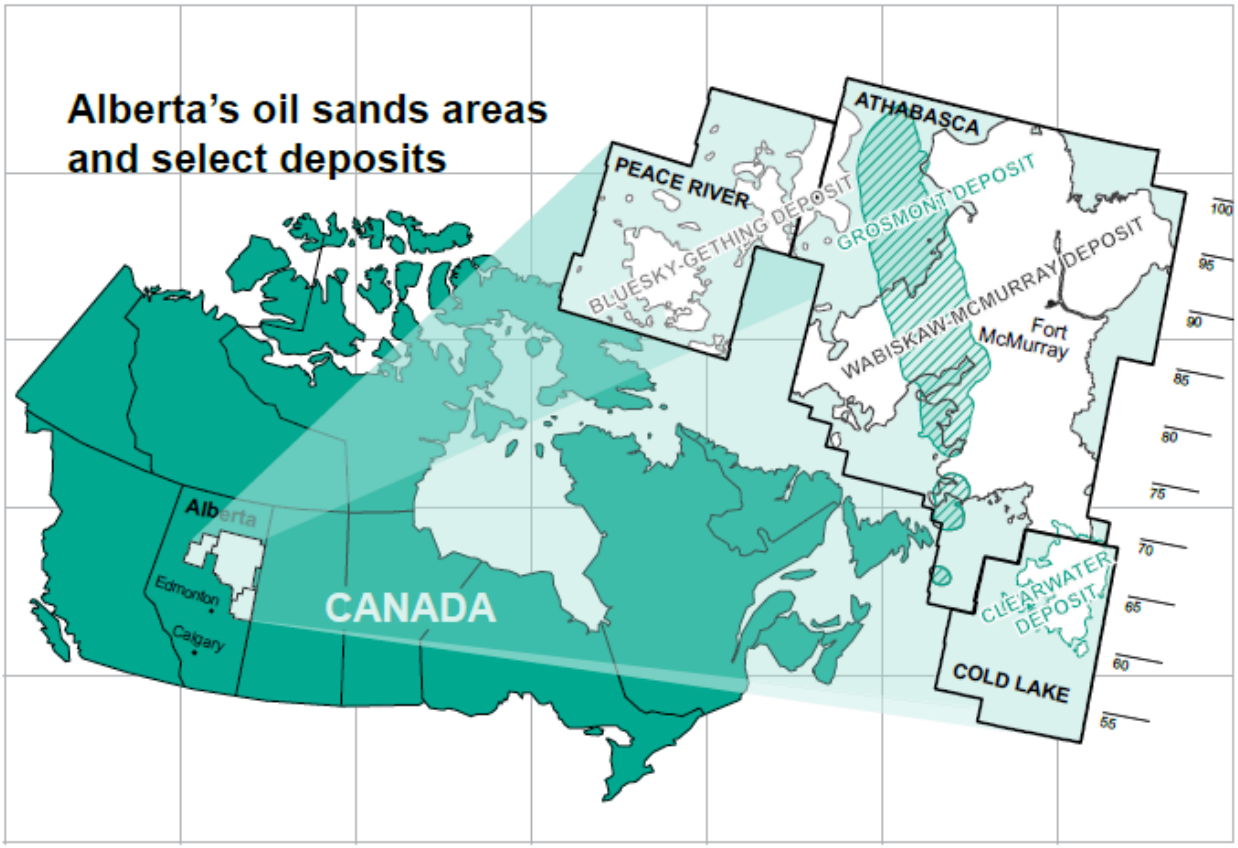

SAGD in an idealized sense involves the completion of two parallel horizontal wells typically 800-1,000m in length with a vertical separation between them equal to approximately 5m. The upper well continuously injects high-pressure steam into the formation and mobilizes highly viscous extra heavy oil (EHO, also known as bitumen), as indicated in **Figure 1.1.2**. Bitumen has

an API (American Petroleum Institute) gravity of approximately 8-10°API. The viscosity of bitumen reduces by up to five orders of magnitude after it is heated to saturated steam conditions, often in excess of 200°C, and flows downward under the action of gravity into the producer well. The mobilized bitumen is produced in combination with water and formation gases often in the form of an oil-in-water emulsion. The produced water consists of formation, lean or transition zone, bottom water and condensed steam. The formation gases consist of free reservoir gas, gases that evolve out of solution, or gases generated through the process of aquathermolysis. The formation depth and reservoir pressure are such that the emulsion stream must often be lifted to surface by using an artificial lift technique, such as Gas Lift (GL) or Electric Submersible Pumps (ESP).

Figure 1.1.2 - Cross-sectional View of the Steam-Assisted Gravity Drainage Process[3]

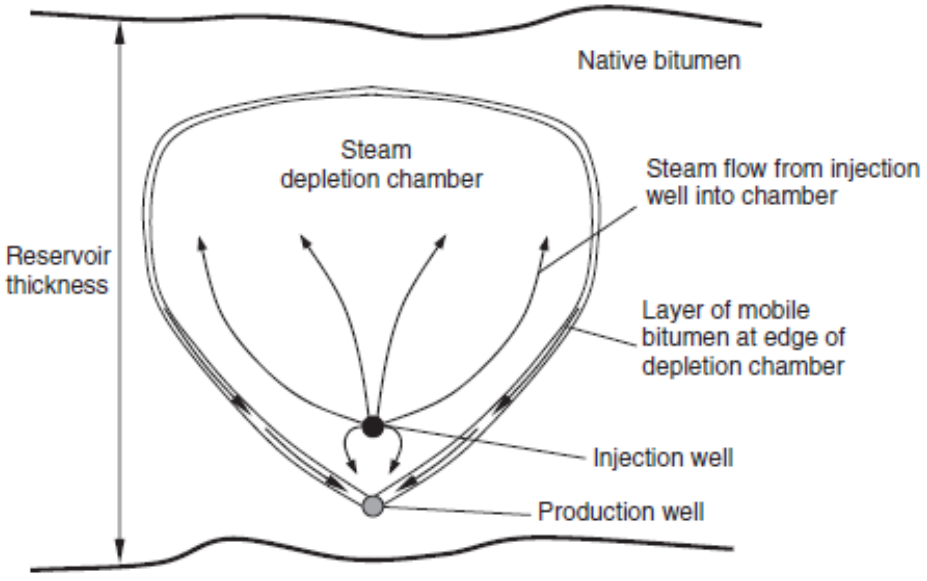

Provided the reservoir geology is favourable, a uniform steam chamber can grow along the horizontal section of the well pair and significant heat conformance can develop in the pay interval. However, even in this idealized state, SAGD is extremely energy intensive as natural gas is consumed as fuel to vaporize the water into steam for injection. Unfortunately, this process is required to develop communication between the pair and to maintain operation and production until a wind-down or blow-down phase is implemented. In addition to the energy requirement, the steam is the principle medium in which the energy is transferred into the reservoir. In some instances solvent can be injected simultaneously with steam (Solvent Co-Injection, SCI) to improve the mobility of the bitumen by reducing viscosity, however, 100% steam injection is a common operational methodology with many of the current producers in Alberta. As a result, SAGD is energy and water intensive and on average requires three units of injected steam on a cold water equivalent (CWE) basis to produce one unit of bitumen. This relationship and concept is further indicated in **Section 3.5, Figure 3.5.1**. While the input requirement is significant, the produced water volumes and the required handling is equally challenging, as produced water cuts often range from 70 to 85% of the produced emulsion stream.

The success and economic viability of SAGD is dependent on the ability to efficiently deliver high quality steam to the reservoir and transfer latent to the bitumen and reduce its in-situ viscosity to enhance mobility. This continuous cycle is improved when thermal losses are minimized. From a subsurface perspective, a principle operational challenge associated with SAGD is the reservoir geology and proportions and distribution of facies. Variation in geology and depositional environment impacts production efficiency and daily operation. If the pay interval is discontinuous with variable roof intervals and is characterized by higher proportions

of reservoir heterogeneities, then the ability to develop a uniform steam chamber efficiently and maximize well utilization is reduced. The variation in performance can be observed with respect to wellbore subcool. Subcool represents the temperature difference between the injector and producer well and the degree to which an area has developed a steam chamber. Provided a conventional liner completion, subcool targets for a given well pair are approximately 10-15^{o}C. Subcool represents the liquid inventory and heat conformance in that particular location along the well pair. SAGD well pairs with homogenous properties tend to have consistent subcool values. SAGD well pairs with poorer geology tend to have variable heat conformance and larger variation in subcool distribution. It should be noted that other reservoir features can significantly impact SAGD operations such as bottom and top thief zones, but for the purpose of this thesis that topic will not be explored further.

Therefore, in practice, it is important to characterize the reservoir fully to capture features of the geology that challenge steam injectivity, steam flow, oil mobilization, and oil drainage in SAGD. This often entails analysis and integration of petrophysics, geophysics, geology, geochemistry, production, reservoir and drilling engineering to properly characterize the reservoir.

As part of the multidisciplinary analysis, reservoir engineering via reservoir simulation, can optimize recovery performance and facilitate field development planning. For subsurface operations, key field development decisions are often made based on the results of numerical reservoir simulation. A typical work-flow, which includes a continuous feed-back loop of dynamic data into the geological model in order to tune and improve the reservoir characterization, is presented in **Figure 1.1.3**[4]. While numerical modelling is one component to

the geoscience-engineering work-flow, it is fundamental to capture anticipated field behaviour. These simulation studies are often the foundation of many business plans and reserves reports, which are directly linked to economics and project viability.

Figure 1.1.3 – Geoscience-Engineering Work-flow[4]

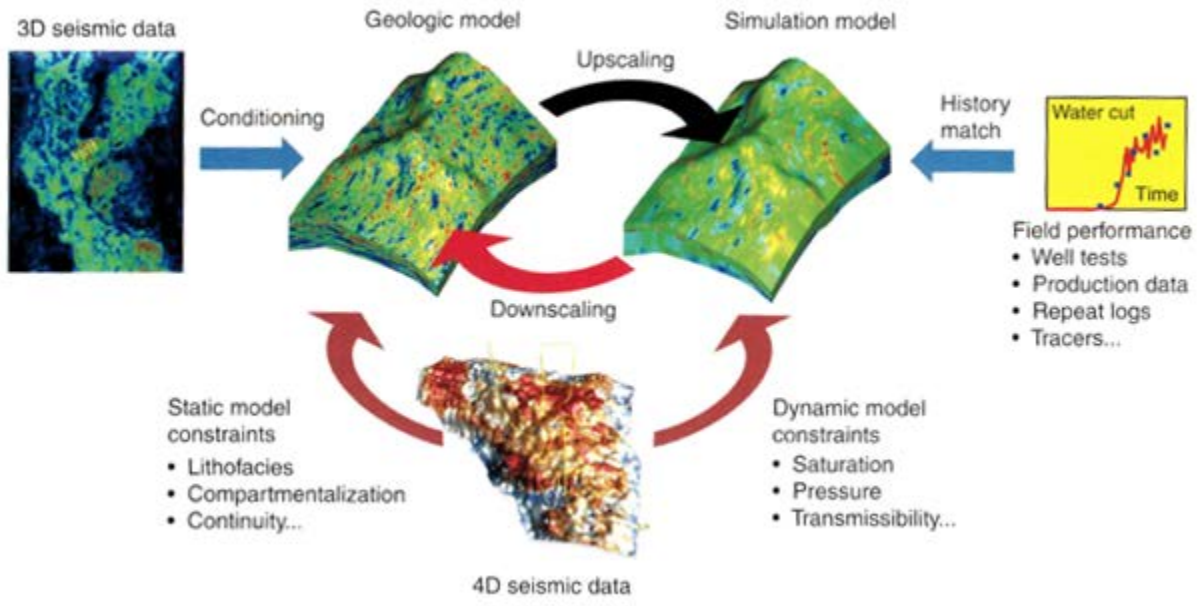

Historically, a geological model is constructed from reservoir evaluation data such as well logs, core data, three-dimensional (3D) and four-dimensional (4D) seismic interpretations, and outcrop studies. Often, geological models that are constructed in geological modelling software packages encompass several millions cells (a cell is the fundamental discretization unit in a geological model). However, direct conversion of these geological models to reservoir simulation models is not possible due to hardware and software limitations. Given modern computational capabilities, reservoir models which hope to achieve practical execution times must remain below about 5-10

million gridblocks, which is also dependent on PVT characterization and numerical tuning. One way to deal with the conversion of a detailed geological model to a reservoir simulation model, and still provide a reasonable representation of the geological environment, is through upscaling. Upscaling is the exercise where a coarse grid is generated with properties that provide a reasonable representation of a fine-gridded property distribution.

Extensive publications have been written on the development of techniques for scaling petrophysical properties between the reservoir simulation and geological models, as is the upscaling and downscaling notation used in **Figure 1.1.3**. Those publications will be discussed in detail in **Section 2.1** and **2.2**.

Within the work-flow, one of the challenges faced by SAGD reservoir simulation is that fine grid resolution is required to track temperature fronts in the reservoir. This is especially true when thermal fronts lead to high temperature gradients spanning a few meters or less. Simulation of finely gridded reservoir models is very computational intensive and impractical to run for Optimization, Sensitivity Analysis (SA) or History Matching (HM) studies where hundreds to thousands of runs are required. Consequently, modelling of the SAGD process is done with fine gridding perpendicular to the wellbore where the temperature gradients are largest, typically dimensions of 1m in the cross-well direction by 1m in the vertical direction or 2m in the cross-well direction by 1m in the vertical direction. However, grid resolution parallel the wellbore tends to be coarser, typically between 25m to 100m per gridblock.

1.2 Problem Statement

The research documented here focuses on the differences in the numerical solutions obtained from a reservoir simulator as a function of length scales and distribution and quantity of reservoir facies. Therefore, for the research documented in this thesis, the term dynamic upscaling is being used to refer to this process. Coarse gridblock size along the wellbore is reasonable simplification provided the temperature gradient is not significant in that direction. However, with the introduction of facies-based reservoir models with reservoir heterogeneities, large temperature gradients parallel the wellbore can be introduced. To capture the movement of the temperature advance in steam chamber, it is necessary to introduce dynamic upscaling parameters to more accurately model the movement of the thermal front in the coarse heterogeneous simulation model.

The purpose of the research documented in this thesis is to highlight the impact of dynamic upscaling on reservoir models and discuss the techniques that can be used to offset the impact of grid coarsening while still taking advantage of the reduction in simulation time and improved accuracy of the coarse models.

1.3 Organization of Thesis

The thesis consists of six chapters which highlight the progression of ideas and learnings when discussing and applying dynamic upscaling parameters to a thermal simulation work-flow.

Chapter 1 is intended to discuss the background information and fundamental concepts for SAGD performance, both operationally and how it is approximated in numerical modelling.

Chapter 2 affords a detailed literature review on all the work that has come before and supports the purpose and motivation of this thesis in exploring a previously undiscussed area. Chapter 3 discusses all the modelling inputs and various data required to populate a geological model for import into reservoir simulation software. The configuration of the data-set is the most important step as the quality of the input impacts the degree to which the data is applicable and useable on a larger scale. Chapter 3 also begins to introduce the concept of dynamic upscaling and the fundamental definitions that shape the technical approach. Chapter 4 is the heart of the report, in that it organizes and presents all the results from the work-flow and quantifies the magnitude of the outcome. Chapter 4 further expands upon the concepts in Chapter 3 and details the specifics of the history matching process, which was the approach used to evaluate the impact of reservoir heterogeneities and length scales in simulation. Chapter 5 further synthesizes the date presented in Chapter 4 by applying the SAGD Productivity Index tool to the work-flow. Chapter 5 is a natural progression from Chapter 4 in that it answers several needs and identifies restrictions in analyzing the data that has be summarized to that point. It includes the final application of the analytical solution and the modelling assumptions and limitations that are inherent in the thesis. Chapter 6 is focused on the inferences and conclusions developed from the information documented in the thesis, but also provides recommendations to expand the work-flow and strengthen the work moving forward. Finally, the Appendices section is intended to support and provide specific detail about certain sections of the thesis. It is supplemental to the information provided in the aforementioned chapters.

CHAPTER 2 – LITERATURE REVIEW

In this chapter, a literature review on the techniques that have been developed in the past to handle uncertainty associated with grid coarsening is discussed. Stochastic geological modelling involves the generation of several realizations of equal probability for a distribution of various petrophysical values, such as fluid saturations and directional permeability. These geostatistical models can successfully represent the geological variation within a depth interval on a fine scale. However, due to hardware and software limitations, this intense level of detail is unmanageable for export to flow simulations. As a result, to reduce the number of data points and corresponding grid density, averaging techniques are applied to upscale the fine scale petrophysical values to larger grid scales appropriate for dynamic studies. Ultimately, the ambition is that results obtained from the representative coarser grid perform comparably to that of the fine grid.

2.1 Upscaling for Reservoir Simulation

The first several approaches for upscaling focus on conventional oil reservoir simulation, such as the black oil formulation. Of which emphasis will be placed on numerical techniques as opposed to analytical techniques, such as arithmetic or harmonic means. For example, single-phase upscaling, as described by Beggs et al. (1989)[5], is an algorithm that calculates an effective permeability, while maintaining the same total flow of the single-phase fluid through the coarse, homogenous block as that which was obtained from the fine, heterogeneous block. It is considered the simplest form of upscaling. Specifically, the application of the Pressure-Solver

Method for upscaling solves the single-phase flow calculation with certain boundary conditions, yielding an effective permeability from the fine gridded model. The most prevalent assumption regarding the Pressure-Solver Method is to define no-flow conditions at the boundary of the cube that is being analyzed. The Pressure-Solver Method permits directional effective permeability and full-tensor effective permeability calculations. The directional (diagonal tensor) effective permeability in the x-direction is given by:

$$k_e^x = -\mu \Delta x \frac{Q}{A} \tag{2.1}$$

White et al. (1987)[6], Durlofsky et al. (1992)[7], and King, M.J. (1993)[8] have tested periodic boundary conditions to calculate the full-tensor effective permeability. The principle limitation is the inability to enter the tensor method into most commercial simulators, despite its improved accuracy. Pickup (1992)[9] has also used periodic boundary conditions to calculate effective permeability.

Other single-phase upscaling techniques include the renormalization technique, which offers a more direct and faster method to calculate effective permeability, despite a reduction in accuracy. The technique focuses on taking a larger problem-set and dissecting it into a hierarchy of smaller and more manageable problems. The work was based upon King's (1989)[10] use of a resistor-network analogy to determine effective permeability on sequences of 2 by 2 cells. It should be noted that renormalization is not limited to 2 by 2 cells.

In two-phase upscaling, the absolute permeability is inadequate to fully describe the heterogeneous medium. Therefore, King et al. (1993)[11] developed a methodology to utilize renormalization for two-phase upscaling. Christie et al. (1996)[12] would later expand upon the original renormalization approach, which is built upon the single-phase normalization method. The production from each gridblock, that has modeled a miniature flow simulation through each heterogeneous sub-grid at each level and cell, is monitored and the effective relative permeability is calculated as a function of face-averaged fractional flow and total mobility:

$$\bar{f} = \sum f_i v A \Big/ \sum v A \tag{2.2}$$

$$\bar{\lambda_t} = \sum \lambda_{ti} k_i A_i \Big/ \sum k_i A_i \tag{2.3}$$

In addition, the use of pseudo function techniques is a diverse area in upscaling. Many different versions of pseudo functions have been applied over the years. Pseudo function techniques, as summarized by Soedarmo (1994)[13] can be classified into three categories dependent on the magnitude of: (1) viscous forces, (2) gravitational forces and (3) capillary forces.

The categories can be defined as follows:

(a) Horizontal displacement as a function of viscous forces dominant,

(b) Gravity segregation and viscous cross-flow dominant,

(c) Dynamic pseudo function which simultaneously account for all viscous, gravitational and capillary interactions.

However, these methods can be restrictive, especially the first two. Instead, the use of numerical modelling to obtain useable solutions is preferred. Dynamic (space and time) pseudo functions have been proposed by Jacks et al. (1973)[14] and Kyte and Berry (1975)[15] for improved upscaling by replacement of a fine gridded model based upon original saturation dependent functions with a coarser mesh of effective or representative properties. Darcy's Law was required to calculate the pseudo functions for Kyte and Berry (1975). Lasseter et al. (1986)[16] further expanded upon the Kyte and Berry (1975) method by presenting a multi-scale upscaling methodology suitable for heterogeneous reservoirs. Lasseter et al. work was scaled up from laboratory data. Kossack et al. (1989)[17] proposed a scale up procedure from various flow regimes and geological descriptions. The numerical work performed was designed to verify the effects of different flow regimes on pseudo function curves in the homogenous, layered and random geological types.

Additionally, Stone (1991)[18] introduced the use of average total mobility to avoid the need to calculate phase potential on a coarser gird, as required by Kyte and Berry (1975). Stone (1991) also introduced fractional flow formulation instead of calculating the flow using Darcy's Law. These effective properties can be thought of as pseudo relative permeability and capillary pressure functions, represented as a pseudo fraction flow curve.

Alabert and Corre (1991)[19] explored three-phase flow in an environment of 3D models of varying heterogeneity. The flow parameters are directionally dependent. Guérillot and Verdiére (1995)[20] and Verdiére and Thomas (1996)[21] utilized two grids to determine the appropriate upscaled solution. The pressure equation was determined from a coarse grid solution and the

saturation distribution was determined by the fine grid solution. The methodology was later referred to as the Dual Mesh Method.

A major limitation in the application of dynamic pseudo functions is the inherent length or time dependency of fluid dynamics across the simulated grid boundaries. Therefore, length-dependent pseudo functions have been proposed to improve upon the dynamic pseudo functions. Taggart et al. (1995)[22] have shown that superior recovery and flow predictions can be obtained with length-dependent functions by incorporating the curvature of the characteristic fine grid simulation curves, as opposed to those based upon velocity models.

Unfortunately, despite the large number of pseudo function approaches, there is not one agreed upon method to perform upscaling in this way. This discrepancy has motivated the need for other approaches and further research.

An emerging area is the application of an adaptive process within the reservoir models, as proposed by Guedes et al (1999)[23], and is focused on managing a higher volume of data within the dynamic model than originally proposed with the earlier methods by the solution of the sub-domain (SD) and coarse grid. This multi-scale computational model for multiphase flow implicitly treats upscaling without the use of pseudo functions. Fundamentally, **Figure 2.1.1** describes the main processes executed, at each time step, by the multi-scale computational method.

Figure 2.1.1 – Multi-scale Computational Model[23]

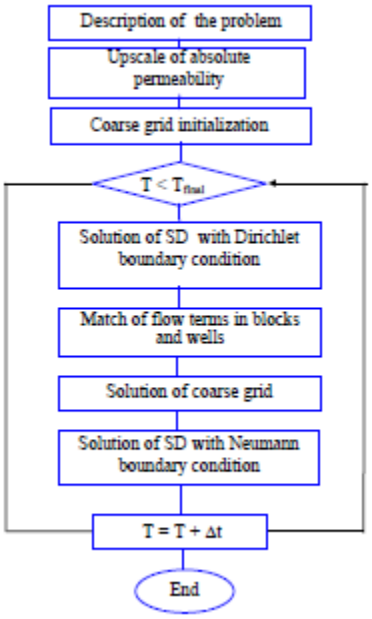

It should also be noted that while a Cartesian grid has been applied in the work-flow developed here, as the geological features are aligned with the grid definition, there has been advancements within industry to implement a Corner Point Geometry (CPG) as the depositional features of most models are often not aligned with the choice of gird, impacting the representation of the effective properties. This methodology was first proposed by Ponting (1989)[24], whereby a more flexible CPG can be implemented to handle more complex reservoir boundaries and reservoir heterogeneities. The CPG grid can be constructed by using three techniques: (1) streamline technique as proposed by Agut et al. (1998)[25], (2) elastic adjustment as proposed by Garcia et al. (1990)[26] or (3) geological modelling built from stochastic simulations. This grid definition is coupled with averaging techniques to upscale fine resolution permeability to larger scales

appropriate for simulation. The application of power law averaging is implemented on CPG meshes:

$$K_{eq} = \left(\frac{1}{n}\sum_{i=1}^{n} k_i^{\omega}\right)^{1/\omega}, \omega \in [-1, 1] \quad (2.4)$$

Ultimately, the literature review thus far has been focused on the early methods for upscaling, often as it relates to representing the fine gridded result as a coarse gridded proxy for conventional oil and gas models. But the literature does not focus on the impact of varying length scales within simulation after upscaling. What error is associated with a coarse grid definition compared to a fine grid definition of identical petrophysical properties when simulated? This is different than the upscaling presented above. For the purpose of the thesis, the approach can be thought of as analyzing the difference after a fine gridded model is upscaled and exported at a specific grid definition. How does the performance change if the model was further subdivided?

To ensure this approach has not be studied before, further research was performed to analyze the extent to which upscaling has been applied for thermal simulation, while focusing on work that could improve the predictive ability of the coarse dynamic model.

2.2 Upscaling for Thermal Reservoir Models

The use of upscaling for thermal models is of most interest and relevance to the work-flow proposed in the thesis. Of the published literature, the approach that has garnered the most

momentum is dynamic sub-gridding. This topic has been reviewed as it relates to SAGD. Dynamic gridding has been further analyzed by Lacroix et al. (2003)[27] as a tool to update the mesh definition throughout the run-life of the model but is performed external to the reservoir simulator as opposed to within the simulator. The overriding motivation for this approach is that it is easier to develop a mesh generator than to implement the sub-gridding directly in the reservoir model. Alternatively, Lacroix et al. (2003) commented on the ability to have the sub-gridding directly developed in the model. Given that updating the actual reservoir model dynamically has the most application to this thesis, it will be discussed further. Christensen et al. (2004)[28] presented a paper focused on the use on dynamic gridding within a 3D SAGD model, whereby fine gridding is reserved for the bitumen-chamber interface, and coarser gridding is reserved for areas with lesser change (such as, areas of the steam chamber with constant temperature). However, the application of the dynamic gridding feature has several limitations and can be difficult to implement. For example, when applying this technique, the user is advised to simulate a fine gridded model to study the behaviour of several parameters, such as temperature, molar fractions and saturation. Only after this preliminary study and review of the magnitude of the gradients of these variables, can the user accurately define the thresholds which force amalgamation and de-amalgamation. There is the risk that cells may be amalgamated across the steam-bitumen interface, resulting in reduced accuracy of the forecast. Therefore thresholds should be as small as possible to ensure proper dynamic gridding, consequently increasing simulation time.

While the implementation of this technique has a lot of potential, especially if the user has a strong understanding of SAGD dynamics, the author wanted to more closely study the impact of

geological variation on performance and the movement of the temperature and steam fronts in homogenous and heterogeneous simulation models. Additionally, the technique proposed offers the user a tool to screen and filter large sets of static models, representing multiple realizations. Characterization and understanding of the impact of the reservoir variations as a function of length scale was as important of a deliverable as proposing an alternative technique to dynamic gridding.

The research presented in this thesis attempts to answer several questions, which have been perceived as absent in the published literature for SAGD simulations. Such as, to what extent can we relate the variation in reservoir quality to performance? How does varying the grid definition impact our forecasts, when the petrophysical properties remain unchanged? To what extent does block volume impact the heat and fluid transfer? By performing the exercise outlined in this thesis, the reader will enhance their understanding of the physics of SAGD.

CHAPTER 3 – MODELLING CONCEPTS

3.1 Numerical Modelling Process

In the research done for this thesis, the simulation study was designed to encompass both binary models and facies-based geological models to quantify the impact of reservoir heterogeneities for different length scales. The static model (the geological model) is fundamental in the modelling process as the quality of the result will be a function of the input parameters. It is necessary to capture any uncertainty and assumptions in the construction phase to identity potential errors or inconsistencies upon completion of the simulations. These assumptions are further elaborated on in **Section 5.3**. The following section highlights the fundamental tools and inputs used to define models used in the research.

3.2 Modelling Tools

Computer Modelling Group's (CMG) suite of reservoir simulation tools was the primary software used in this study. The reservoir models were built by using Builder™ (Versions 2011.10 and 2012.10)[29] and simulated by using the thermal reservoir simulator, Steam, Thermal and Advanced Processes Reservoir Simulator, STARS™ (Versions 2011.10 and 2012.10)[30]. The STARS™ models were coupled with the Computer Assisted History Matching, Optimization, Sensitivity and Uncertainty Assessment Tool, CMOST™ (Versions 2011.10 and 2012.10)[31]. CMOST™ automates simulation runs from the base case model and then submits and analyzes the data from a range of sensitivity parameters and values to achieve an optimal solution set.

Ultimately, it permits the reservoir engineer to identify uncertainty and improve simulation forecasts. Finally, all results were analyzed by using the CMG Results post-processing tools (Versions 2011.10 and 2012.10)[32].

STARS™ is the thermal software commonly used for SAGD processes within the oil sands industry. For the purpose of this study, FlexWell™ was not employed and sink-source model approximation was favoured because the foundation of this report focuses on reservoir performance and interaction of gridblocks and not wellbore hydraulics. Also, no geomehanical assumptions were implemented into the study.

3.3 Model Grid Definitions

The methodology to create simulation models was to generate representative 3D binary models and representative 3D facies-based models. Universal to all models was three reservoir inputs: (1) PVT characterization, (2) relative permeability curves and (3) thermal properties. These datasets were not manipulated during the course of the study. They were sourced from a combination of literature[33-35] and default parameters outlined in the CMG data-manuals. In this way, the input parameters should simply been seen as constant inputs across the set of models. It should also be noted that nominal numerical tuning was performed on the models in the study, however, a small sub-set of coarse and fine models were reviewed to ensure the run performance metrics were favourable, such as total time step cuts, solver failures and material balance error. Given this sample of performance, it was decided that the configuration was appropriate for global use. The numerical configuration was based upon CMG recommended parameters and

ranges, which represent the default for STARS™ related simulations. The parallelization configuration (including number of processors) was identical for all model types.

The models were constructed with one of six grid definitions. For example, the primary grid definition as defined on an (*i*, *j*, *k*) basis was (4m, 100m, 1m) and gridblock counts in each direction equal to (25, 3, 30) gridblocks = 2,250 gridblocks. These models represent one-third the average length of a SAGD well pair to accelerate run time and reduce the dependence on hardware and software. This approximation represents the upper limit in reservoir simulation coarseness when simulating the SAGD process and is referred to as a coarse model approximation. A fine model approximation involves refining the grid to a (1m, 1m, 1m) discretization. Additional details of the grid configurations are described in **Section 3.7**. The dimensional notation used in this thesis is depicted in **Figure 3.3.1**.

Figure 3.3.1 – Standard Dimensional Notation

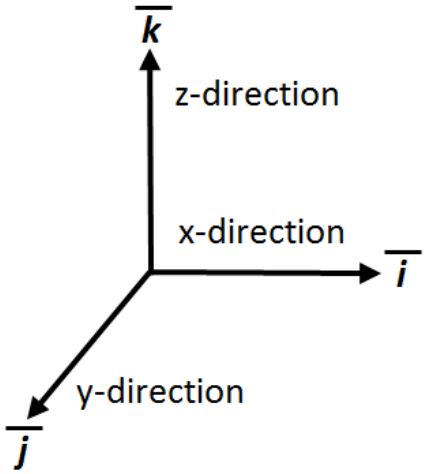

3.4 Editing an Existing Grid

Each coarse gridded model will have a unique distribution of reservoir facies, however, their corresponding find gridded models (1m, 1m, 1m) are simply a manipulation of the coarse gridded distribution. In that way, the location and quantity of reservoir properties from the coarse grid to the fine grid are maintained. For example, **Figure 3.4.1** idealizes the fundamental process of grid refinement within the contexts of this paper. The colour palate represents a particular set of petrophysical values and its distribution within the grid. Also, the placement of the wells within the schematic (injector and producer well) are idealized, as all the injection and production nodes are centered in their respective gridblock.

Figure 3.4.1 – Schematic of Grid Refinement Process, View in the Cross-Well Direction (*i*, *k*-direction)

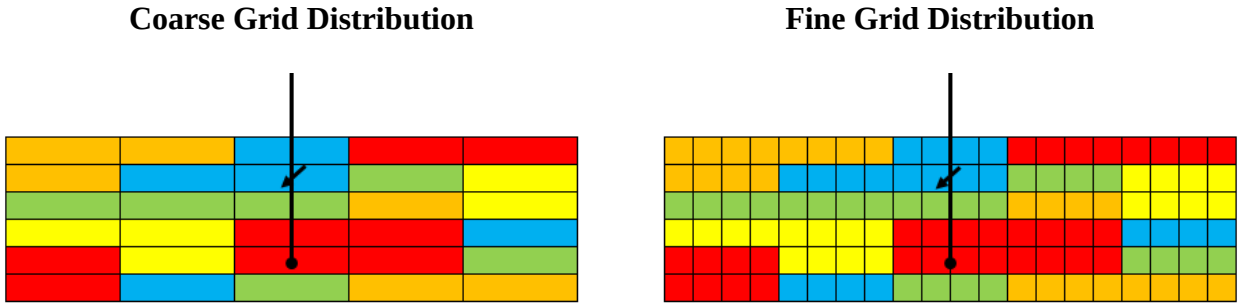

The models were originally refined by using two techniques within Builder™. Split grid plane and Cartesian refine. The split grid plane feature permits the user to specify a uniform or non-uniform number of blocks divisions in each respective direction. The Cartesian refine feature also permits the user to specify a uniform or non-uniform number of blocks divisions in each respective direction. However, Cartesian refine will not refine non-reservoir blocks, which will

be represented as Facie Type B in **Section 3.7**. Based upon the sensitivity analysis that was performed on several type models, there is no major distinction between the production results with split grid plane and Cartesian refine. For the purpose of comparison, coarse models were refined to selective dimensions to generate a quick comparison when compared to simulating the fine grid definition. The results are presented in **Figure 3.4.2**. However, as part of the tuning process to ensure reduced simulation time, the split grid plane method tended to have the fastest simulation times, as highlighted in **Table 3.4.1**. In addition to the acceleration in run-time, the inability of Cartesian refine to segment non-reservoir blocks could have an impact upon the rate of thermal conductivity in that given cell, when comparing the performance between coarse and fine gridded reservoir blocks of different block volumes. This option may potentially impact future results.

Therefore, the split grid plane feature was employed as the local refined grid technique due to its ease of use and complete refinement of the entire grid. It eliminated the inconsistency between variable shale content and the number of gridblocks refined on a model basis.

Table 3.4.1 – Comparison of Simulation Time for Different Refinement Techniques

Binary Model Association	**Shale Volume (%)**	**Dimensions *i, j, k* (m)**	**Split Grid Plane Simulation Time (hh:mm:ss)**	**Cartesian Refine Simulation Time (hh:mm:ss)**
Type-C	5	4, 25, 1	00:07:06	00:07:09
Type-D	5	2, 100, 1	00:01:39	00:01:52
Type-F	5	2, 25, 1	00:17:00	00:25:33

Figure 3.4.2 – Comparison of Production Profiles for Different Refinement Techniques

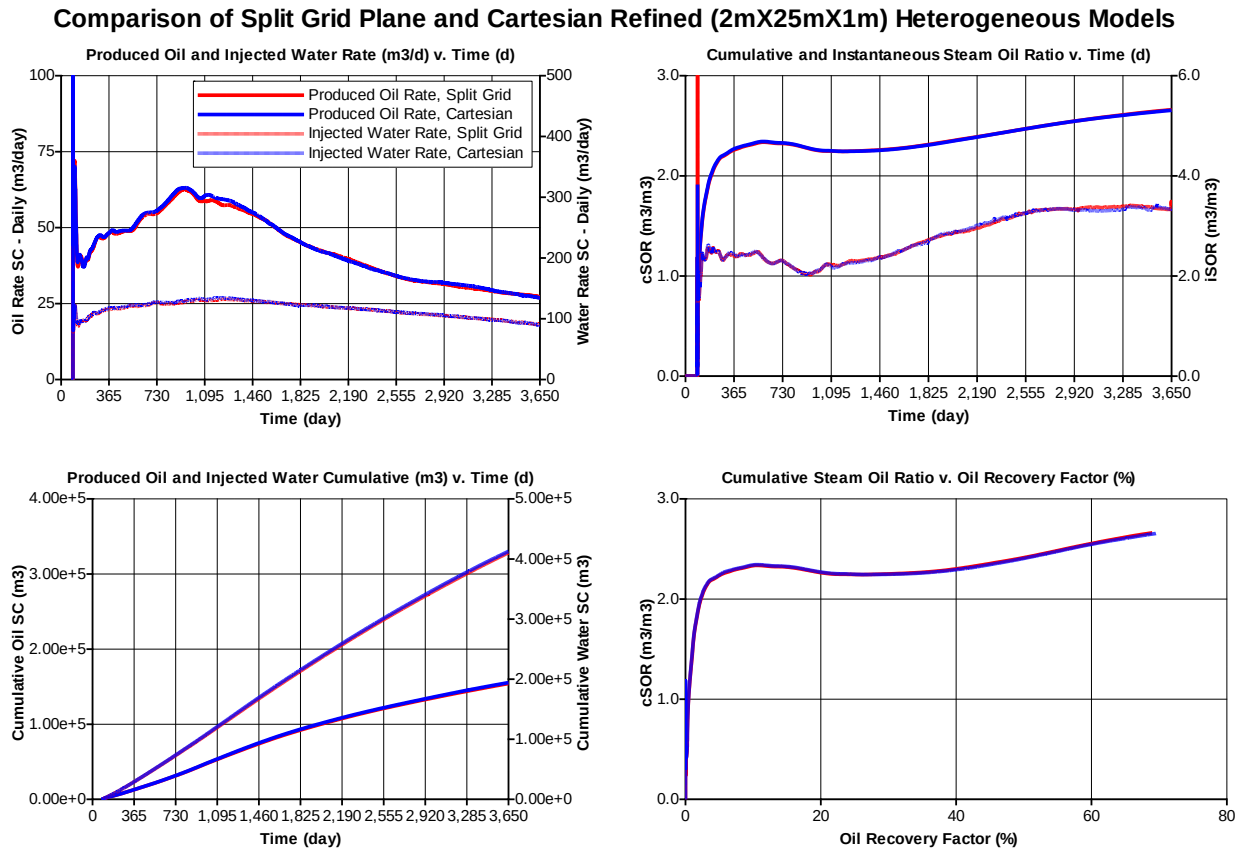

3.5 Reservoir Parameters

The models were configured as listed in **Table 3.5.1**. With respect to the initial GOR, it was calculated by using initial phase mole fractions of bitumen and methane within the oil phase. The mole fraction of bitumen component (C_2H_6+) in the oil phase is 90% and the mole fraction of methane (CH_4) component in the oil phase is 10%. This combination of bitumen and methane in the oil phase generates an initial GOR of approximately 4.8m^3/m^3. To initiate the models, neither bitumen nor methane was defined in the gaseous phases.

Table 3.5.1 – Single Well Pair Reservoir Simulation Properties and Input Parameters

Parameter	Unit	Value
Base Case, Cell Definition *(i, j, k)*	cells	25, 3, 1
Base Case, Grid Dimensions *(i, j, k)*	m	4, 100, 1
SAGDable Interval *(k-direction)*	m	30
Reference Depth *(k-direction)*	mTVD	400
Initial Reservoir Temperature	^{o}C	12
Initial Reservoir Pressure	kPa	2,000
Initial Gas-to-Oil Ratio	m^3/ m^3	4.8
Upper Interval *(k-direction)*	m (vertical cell layers)	10 (1-10)
Middle Interval *(k-direction)*	m (vertical cell layers)	10 (11-20)
Lower Interval *(k-direction)*	m (vertical cell layers)	10 (21-30)
Depth of Injector	m (vertical cell layer)	22.5 (23)
Depth of Producer (2.5m off base)	m (vertical cell layer)	27.5 (28)

3.5.1 SAGD Circulation, Constraint Set-Up

During the SAGD circulation phase, both the injection and production well inject steam for a specified period of time to establish communication between the two wells to condition the well pairs for conversion to SAGD. Within STARS™ the process is idealized with nodal heaters that simulate the behaviour of injecting steam uniformly along the wellbore without the actual injection of steam. Both wells were shut-in during the circulation phase and the details of the well configuration are outlined in **Table 3.5.1.1** and **3.5.1.2**.

Table 3.5.1.1 – Circulation Well, Constraint Configuration

Parameter	Unit	Value or Parameter
Well Geometry	-	*j*-direction
Max Steam Constraint	m^3/d	3.0
Maximum Bottom-Hole Pressure	kPa	3,500
Maximum Total Liquid Rate (water and oil phase)	m^3/d	1,000
Well Radius	m	0.086
Geometric Factor for the Well Element	unitless	0.249
Inflow Fraction (wfrac)	unitless	1.0
Well Skin Factor	unitless	0.0

Table 3.5.1.2 – Circulation Heater Configuration

Parameter	Unit	Value or Parameter
Well Heater Duration	days	90
Heating Rate	J/day-m	2.40E+9
Heater Target Temperature	^oC	240

3.5.2 SAGD Production Phase, Constraint Set-Up

During the SAGD production phase, the injection well continuously injects high pressure steam whereas the production well is controlled by pressure and fluid intake constraints. The details of the injection and production well constraints are outlined in **Tables 3.5.2.1** and **3.5.2.2**.

Table 3.5.2.1 – SAGD Production Phase, Constraint Set-Up - Injection Well

Parameter	Unit	Value or Parameter
Well Geometry	-	*j*-direction
Temperature	^oC	242.5
Maximum Bottom-Hole Pressure	kPa	3,500
Quality	unitless	0.95
Maximum Total Water Phase Rate	m^3/d	1,000
Well Radius	m	0.086
Geometric Factor for the Well Element	unitless	0.249
Inflow Fraction (wfrac)	unitless	1.0
Well Skin Factor	unitless	0.0

Table 3.5.2.2 – SAGD Production Phase, Constraint Set-Up - Production Well

Parameter	Unit	Value or Parameter
Well Geometry	-	*j*-direction
Max Steam Constraint (*STEAM)	m^3/d	3.0
Minimum Bottom-Hole Pressure	kPa	1,000
Maximum Total Liquid Rate (water and oil phase)	m^3/d	1,000
Well Radius	m	0.086
Geometric Factor for the Well Element	unitless	0.249
Inflow Fraction (wfrac)	unitless	1.0
Well Skin Factor	unitless	0.0

The maximum steam constraint defined within this section approximates the sub-cool notation discussed within the introduction and is used in favour of the steam trapping mode within STARS™. The sub-cool constraint in this case is focused on producing a certain volume of live steam on a daily basis, as opposed to the steam trapping mode that is able to target a specific temperature difference between the injector and the producer. Operationally, it is easier to speak to the steam trapping mode, however, numerically the models converged better with the maximum steam constraint keyword. It should be noted that the instability in the steam trapping mode is the result of violating the temperature constraint that leads to liquid pooling above the producer well.

The maximum steam constraint value assigned to the simulations ($3m^3/d$) is comparable to the target sub-cool values as suggested with conventional liner systems (10-15^oC) and the steam trapping mode as mentioned prior.

The results are presented in **Table 3.5.2.3**, in which the maximum steam constraint run-time is comparable to steam trapping mode case of 10^oC. However, the production profiles presented in

Figure 3.5.2.1 show noticeable instability near the conclusion of the runs utilizing the steam trapping keyword for both 10^{o}C and 15^{o}C.

Table 3.5.2.3 – Comparison of Simulation Time for Different Sub-cool Model

Binary Model Association	**Shale Volume (%)**	**Dimensions *i, j, k* (m)**	**Maximum Steam Constraint Simulation Time (hh:mm:ss)**	**Maximum Temperature Constraint Simulation Time (hh:mm:ss)**	
			$3m^3/d$	**10^{o}C**	**15^{o}C**
Type-C	5	4, 25, 1	00:15:20	00:14:55	00:16:17
Type-D	5	2, 100, 1	00:07:06	00:06:15	00:07:44
Type-F	5	2, 25, 1	01:16:54	01:23:24	01:52:32

Figure 3.5.2.1 – Comparison of Production Profiles for Different Sub-cool Model

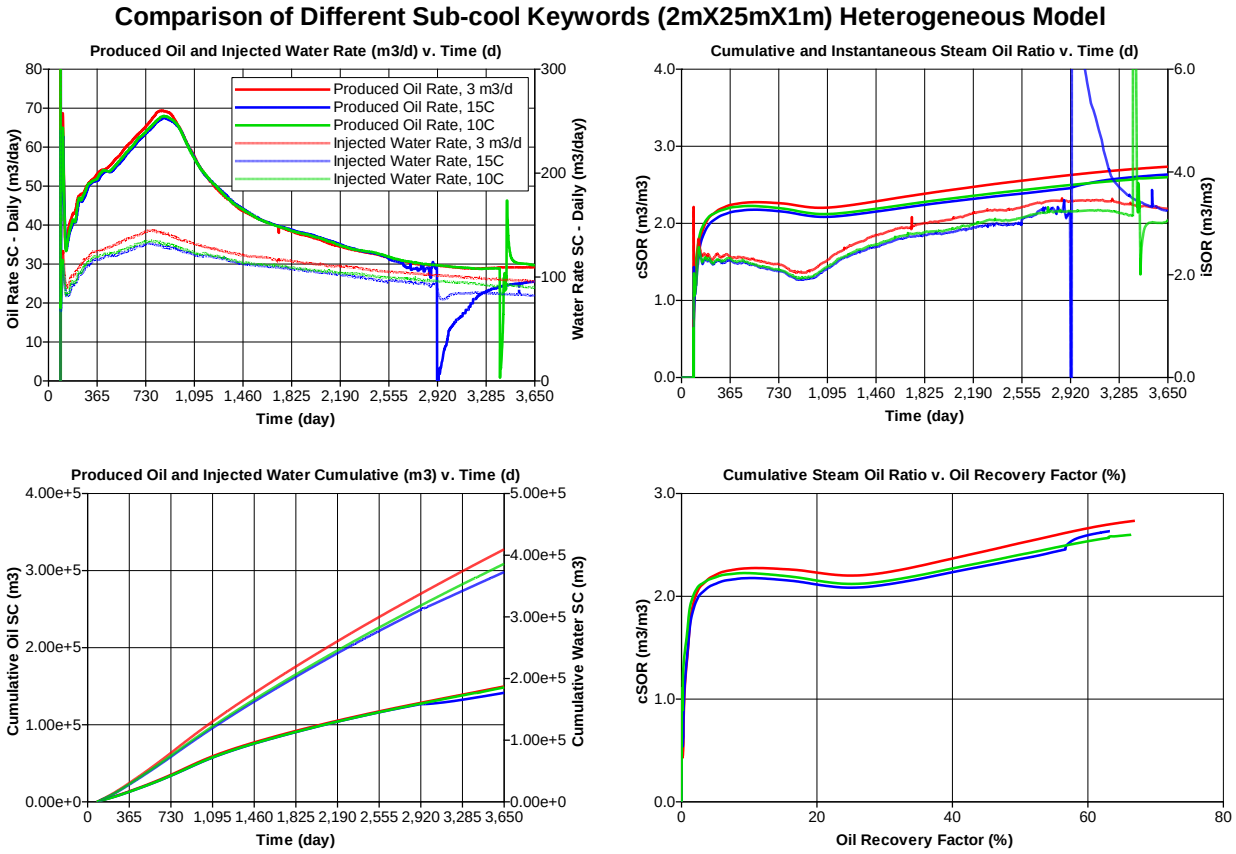

3.6 Key Performance Metrics

SAGD performance is measured by several metrics, and those metrics are important in terms of quantifying the efficiency of SAGD on a well pair basis. Examples are oil rate, cumulative oil production, produced water rate and cumulative water produced with respect to time. Another principle indicator for the SAGD process is the Steam-to-Oil Ratio (SOR). SOR can be represented in terms of the cumulative-SOR (cSOR) or instantaneous-SOR (iSOR). cSOR takes into consideration the cumulative volume of steam injected, on a CWE basis, and the cumulative volume of bitumen produced over the period the well pair is on-line. cSOR measurements within

industry include the carbon intensive circulation period. In the simulations done within this thesis, the circulation stage is modelled with block heaters and thus the actual amount of steam used in the circulation stage is not taken into account in this work-flow. iSOR takes into consideration the volume of steam injected, on a CWE basis, and bitumen produced for a given time period, typically a day.

SOR is an important key performance indicator because it provides insight into efficiency of steam usage for a period in time or lifetime of the well. For example, if steam injection is being increased to a particular tubing string and the downhole instrumentation suggests the heat is being displaced into the producer well because of a vertical barrier, then more heat will be recycled to surface. This indicates that the additional energy associated with the increased steam volume is not being used for chamber growth and will hurt thermal efficiency. This trend manifests itself as gradual increase in cSOR but with a more sudden increase in iSOR. Alternatively, if steam injection is being increased to a particular tubing string and the downhole instrumentation suggests that the pressure and temperature are stable, then it is likely that the incremental steam is being used to grow the chamber. This will often result in greater bitumen production and potentially a stabilization or reduction in SOR. Historically, industry has targeted cSOR of $3.0 m^3/m^3$ or less, however, due to the start-up of more marginal drainage areas within the McMurray formation, it is becoming increasingly more challenging target to achieve. The results of several SAGD projects in Alberta are listed in **Table 3.6.1**[36].

Table 3.6.1 – 2012 In-situ Progress Reports Published from the AER[36]

Company	Asset	Drainage Areas	Performance Metrics	
			cSOR (m^3/m^3)	iSOR (m^3/m^3)
Devon Canada Corp.	Jackfish - Phase 1	5 Well Pads (35 Well Pairs)	2.6	3.0
ConocoPhillips Canada Resources Corp.	Surmont – Phase 1	4 Well Pads (35 Well Pairs)	2.7	2.5
Statoil Canada Ltd.	Leismer Demonstration Project	4 Well Pads (22 Well Pairs)	2.9	2.4
Suncor Energy Inc.	MacKay River	7 Well Pads (70 Well Pairs)	2.5	2.3

In addition, for a representative Athabasca Oil Sands property with field bitumen production equal to 1,500m^3/d (representing approximately 10 well pairs) and a cSOR of 3.0m^3/m^3, the steam injection (CWE) requirement would be approximately 4,500m^3/d. Assuming a water cut equal to 75%, the produced water fraction in the emulsion stream is equal to approximately 4,500m^3/d. The aforementioned data is represented by an idealized type curve for a single well pair in **Figure 3.6.1**, in which the pair can potentially be online for approximately 20 years.

Figure 3.6.1 – Representative Type Well Injection and Production Profile

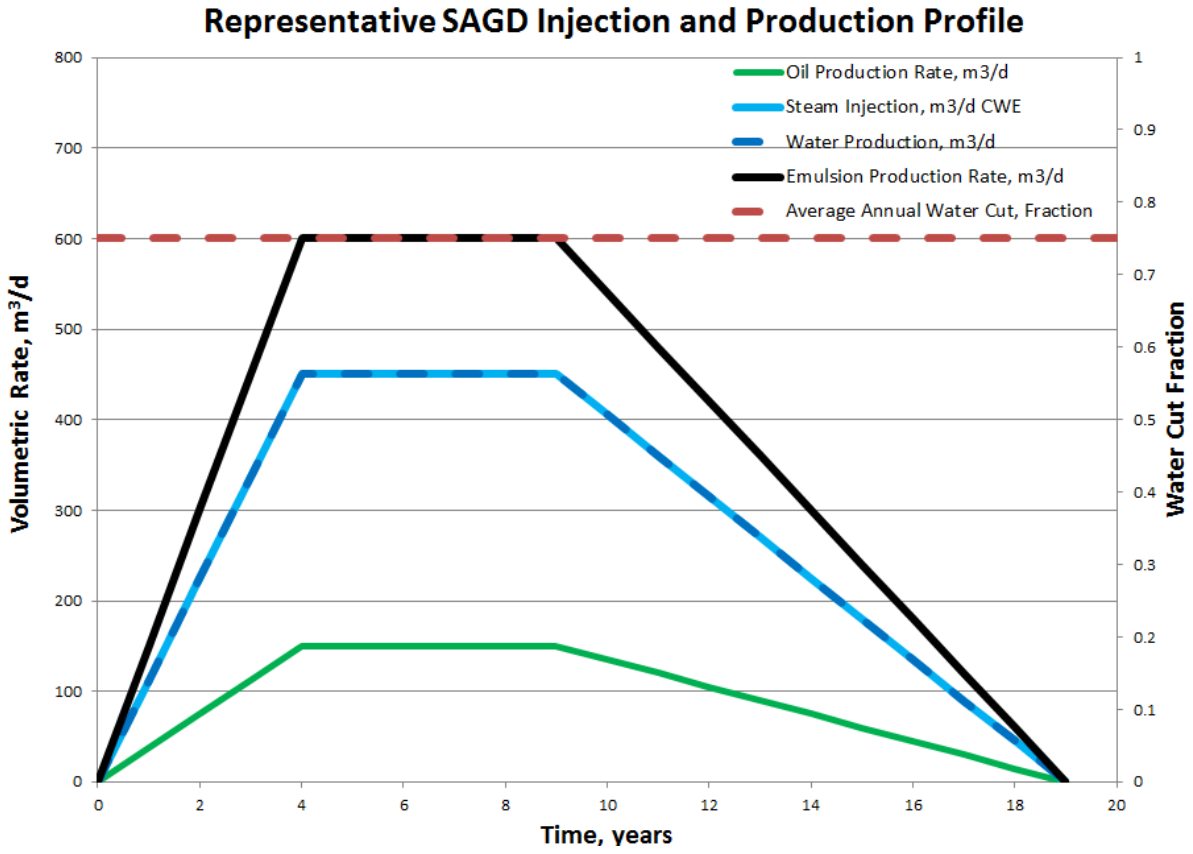

3.7 Binary-Geostatistical Models

Binary reservoir simulation models were generated by using CMG's Builder™ geostatistical object modelling tool (with a uniform probability distribution) to populate gridblocks with rectangular parallelepiped geological bodies. The object modelling tool was employed for a 3D distribution of shale bodies of specific dimensions and content. The fluvial depositional[37] model is appropriate for this choice of object modelling, and can often be linked to fining upward sequences which are very common within the McMurray formation.

To clarify the notation assigned to these models, a binary model consists of a discrete distribution representing one or another variable, in this case: Facies A (sand-dominated) or Facies B (shale-dominated). The values are binary from the perspective of the object modelling value (1 or 0, sand or shale). The petrophysical values assigned to each facies type are deterministic.

Table 3.7.1 – Depositional Quantities

Binary Model Association	**Coarse Dimensions *i, j, k* (m)**	**Fine Dimensions *i, j, k* (m)**	**Non-Reservoir Content (Percent by Volume)**
Type-A (Base Case)	4, 100, 1	1, 1, 1	1, 2, 3, 4, 5, 10, 15, 20
Type-B	4, 50, 1	1, 1, 1	1, 5, 10, 20
Type-C	4, 25, 1	1, 1, 1	1, 5, 10, 20
Type-D	2, 100, 1	1, 1, 1	1, 5, 10, 20
Type-E	2, 50, 1	1, 1, 1	1, 5, 10, 20
Type-F	2, 25, 1	1, 1, 1	1, 5, 10, 20

Figure 3.7.1 – Schematic Representing the Distribution of Facies for 1% Shale by Volume, Type-A

4m, 100m, 1m (*i, k*-direction)

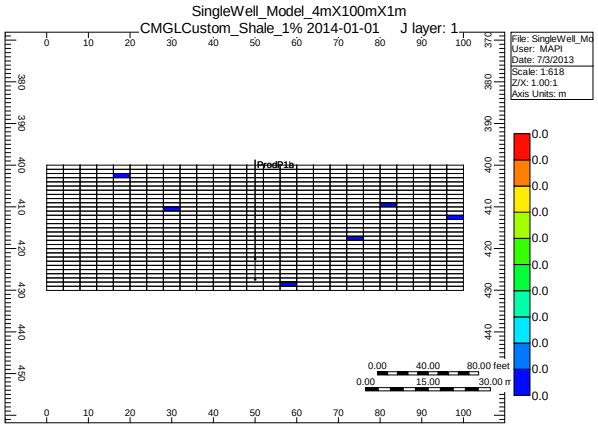

4m, 100m, 1m (*i, j*-direction)

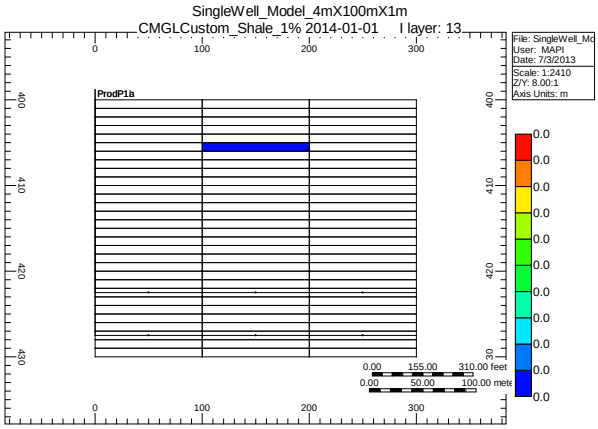

Table 3.7.2 – Builder™ Generated Geostatistical Model

Inputs	Units	Facies A	Facies B
		Sand-Dominated	**Shale-Dominated**
Object Modelling Value (Assignment)	unitless	1	0
Oil Saturation	fraction	0.80	0.00
Residual Oil Saturation	fraction	0.10	0.00
Water Saturation	fraction	0.20	0.00
Irreducible Water Saturation	fraction	0.10	0.00
Gas Saturation	fraction	0.00	0.00
Porosity	fraction	0.33	0.00
Shale Dimensions *(i, j, k)*	m	-	4, 100, 1
Shale Volume	fraction	0.00	(0.01, 0.20)
Permeability (*i-direction*)	mD	5,000	0.00
Permeability (*j-direction*)	mD	5,000	0.00
k_v/k_h	fraction	0.80	0.00
Permeability (*k-direction*)	mD	4,000	0.00

3.8 Facies-based Models

The statistical software package used to populate the petrophysical inputs for facies-generated models within Builder™ was Palisade's risk analysis tool, @RISK™ 5.0 Standard (Version 5.5)[38]. Risk analysis is utilized within industry to determine the frequency of occurrence of particular events and the magnitude of their outcome. However, risk and risk quantification can also be used to study the spread for a particular variable. Here, @RISK™ was used in two capacities: (1) to generate a discrete distribution for each facies type and (2) to generate a normal distribution for the petrophysical properties as a function of the facies type.

Four generic models were generated for the facies-based modelling approach: (1) Uniform Distribution model, (2) Fining Upwards model, (3) Coarsening Upwards model and (4) Channel

Deposition model. The coarsening upwards sequence can be found in a deltaic environment. Deltas prograde (build out) and form where rivers carry more sediment into the sea than marine erosion can carry away[39]. The fining upwards sequence can be found in a braided fluvial system environment and is defined as any body of water that is flowing but has insufficient discharge to carry its load of sediment. Here, the reservoir quality of a coarsening upwards sequence improves as you decrease depositional depth, whereas, the reservoir quality of the fining upwards sequence improves as you increase depth[40]. The uniform distribution model is defined as an area of decreased reservoir heterogeneity across the targeted interval and would be supported by logs showing continuous high resistivity and low gamma ray log readings. The channel depositional model is most closely related to the uniform depositional model, however, there is a greater distinction between base of pay (top of Devonian or basal McMurray) and top of pay (transition to roof or regional caprock)[41].

For the reservoir simulation models, an understanding of the depositional environments was coupled together with these four generate generic reservoir profiles to enable the ability of @RISK^{TM} to model a specific distribution. As a result, the final values selected for the petrophysical inputs (mean and standard deviation) were not specific to a particular location. The goal was to emphasize universality of the trends and the lack of uniformity observed within the reservoir. The facies-based models are also intended to be more representative of geological models of the Athabasca Oil Sands region.

The facies proportions were determined by using a RiskDiscrete model. A RiskDiscrete distribution has a number of outcomes equalling *n*. Each outcome has a particular value

assignment (x) and probability of occurrence or weight (p)[42]. The weight must be a value greater than or equal to zero. The RiskDiscrete formulation is given by:

$$f(x) = p_i \; for \; x = x_i \tag{3.8.1}$$

Figures 3.8.1 – 3.8.4 features the four different model configurations for the distribution of facies. The number associated with each facies type is the value and the probability of occurrence is a function of the vertical proportion curve for that particular distribution. The vertical proportion curves are defined per interval, with one interval representing the specified vertical reservoir layers. Due to the resolution of the images, the first figure is enlarged as the notation for the x-axis (facies type) and y-axis (probability of occurrence) is maintained for all the discrete distributions.

Figure 3.8.1 – Discrete Facies Distribution per Interval for the Uniform Distribution Model (Layers 1-30)

Layers 1-30

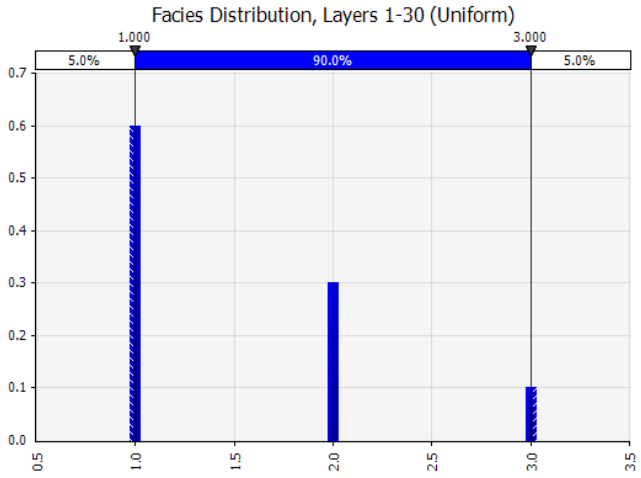

Figure 3.8.2 – Discrete Facies Distribution per Interval for the Fining Upwards Model (Layers 1-30)

Layers 1-10 **Layers 11-20** **Layers 21-30**

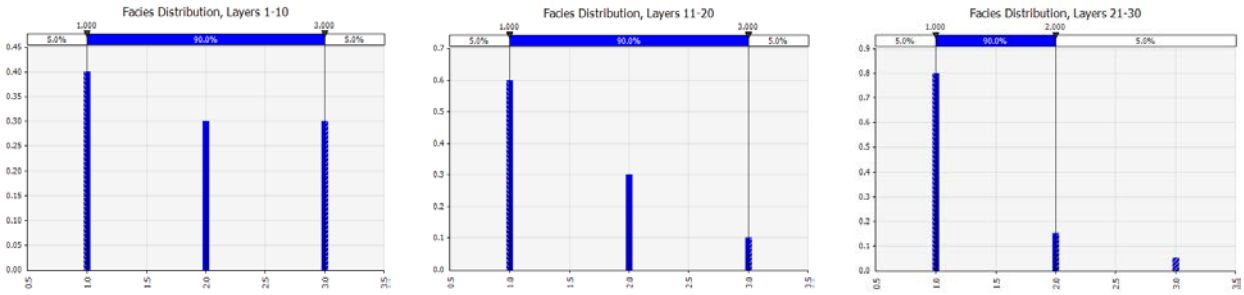

Figure 3.8.3 – Discrete Facies Distribution per Interval for the Coarsening Upwards Model (Layers 1-30)

Layers 1-10 **Layers 11-20** **Layers 21-30**

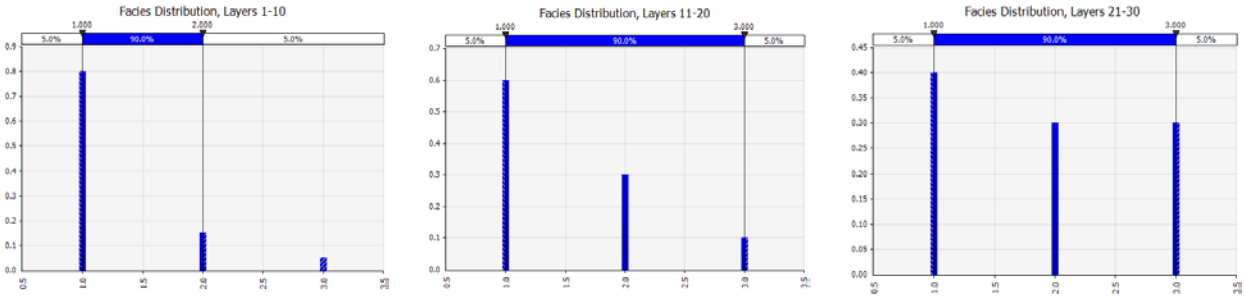

Figure 3.8.4 – Discrete Facies Distribution per Interval for the Channel Depositional Model (Layers 1-30)

Layers 1-5 **Layers 6-20** **Layers 21-25** **Layers 26-30**

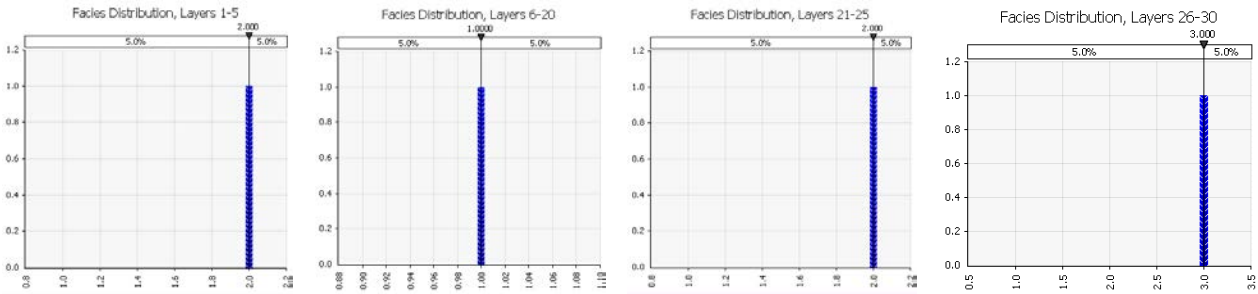

The petrophysical values were presented using a RiskNormal model given by:

$$f(x) = \frac{1}{\sqrt{2\pi}\sigma}\, e^{-\frac{1}{2}\left(\frac{x-\mu}{\sigma}\right)^2} \qquad (3.8.2)$$

A RiskNormal distribution is a typical Gaussian (normal) distribution curve. It is a symmetric continuous distribution which is unbounded on both sides ($-\infty < x < +\infty$) and is described by a mean (μ) and standard deviation (σ)[43]. All petrophysical parameters have a lower limit of 0.0 and the curves are truncated at that value to ensure no non-real values are generated.

Figure 3.8.5 – 3.8.7 highlights the RiskNormal distribution for oil saturation, porosity and vertical permeability per facies type. Based on the mean and standard deviation a unique value will be generated per gridblock representing that particular facies. Each numerical model will represent one particular realization based on the particular arrangement of values. Therefore, the purpose of the facie-based models was to generate a data-set that is more representative of geomodelling output for benchmark of the dynamic upscaling parameters. Due to the resolution

of the images, the first figure is enlarged as the notation for the x-axis (petrophysical value assignment) and y-axis (frequency of occurrence) is maintained for all the continuous distributions.

Figure 3.8.5 – Normal Oil Saturation Distribution per Facies

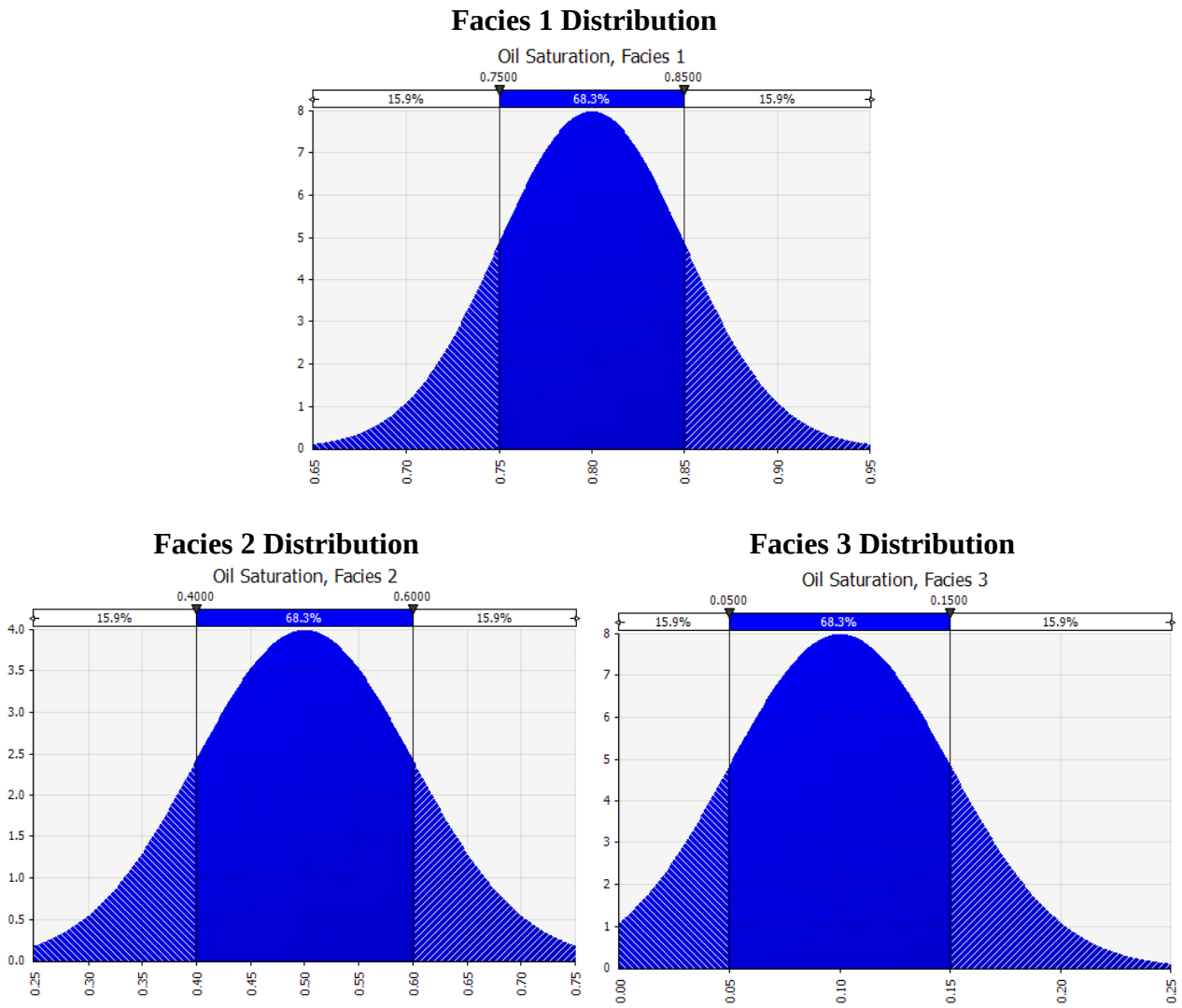

Figure 3.8.6 – Normal Porosity Distribution per Facies

Facies 1 Distribution **Facies 2 Distribution** **Facies 3 Distribution**

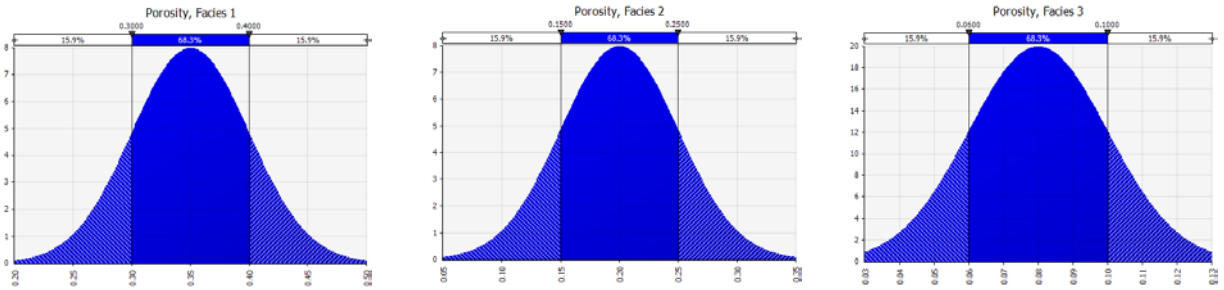

Figure 3.8.7 – Normal Vertical Permeability Distribution per Facies

Facies 1 Distribution **Facies 2 Distribution** **Facies 3 Distribution**

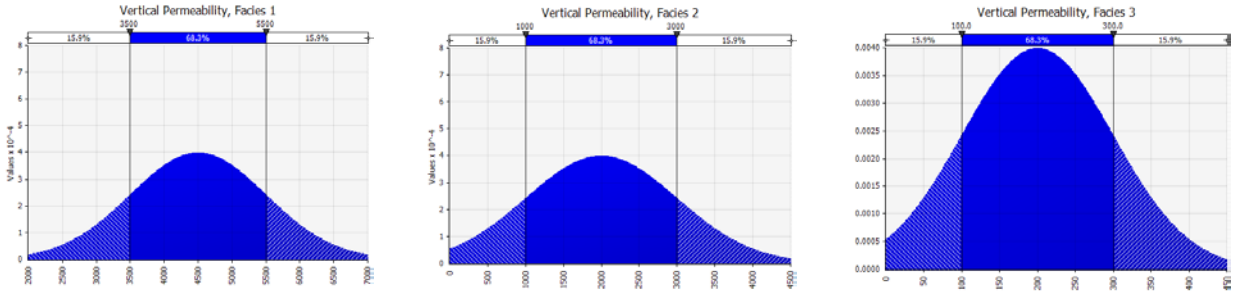

Given the distribution of oil saturation, the water saturation distribution is given by:

$$Sw = 1.0 - So, as\ Sg = 0.0 \tag{3.8.3}$$

The ratio of the vertical to horizontal permeability is constant and equal to 0.8. The values assigned for oil saturation, porosity, and vertical permeability for each facies type are stochastic in nature. Ideally, several realizations would be generated for each type to minimize anomalous distributions.

3.9 Vertical Proportion Curves

Vertical proportion curves provide an estimate as to the variation in facies amounts vertically within the reservoir interval. The vertical proportion curves for the given model are applied in each plane perpendicular the wellbore. The distribution of petrophysical values is controlled by the distributions described in the aforementioned sections. The aspect ratio notation refers to the length-to-width ratio of the shale layers with respect to the parallel and perpendicular flow direction. Therefore, for the base case models (4m, 100m, 1m), the aspect ratio is equal to 100m:4m or 25m/m.

Figure 3.9.1 – Vertical Proportion Curves for each Model Configuration

A. Uniform Distribution Model

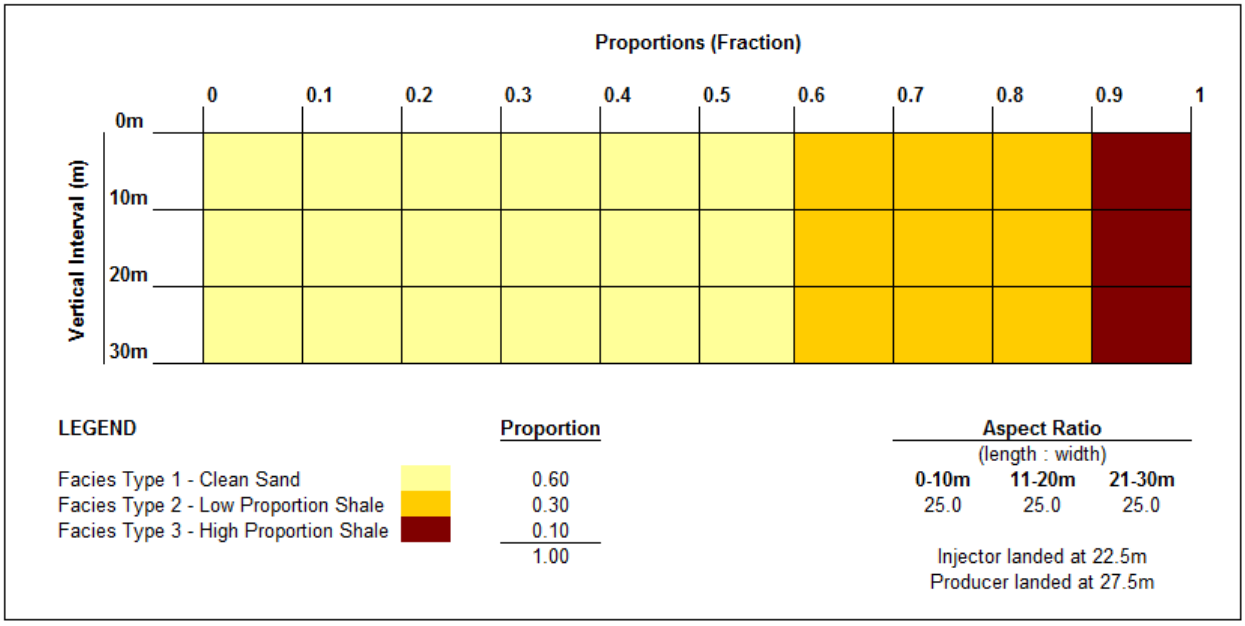

B. Coarsening Upwards Model

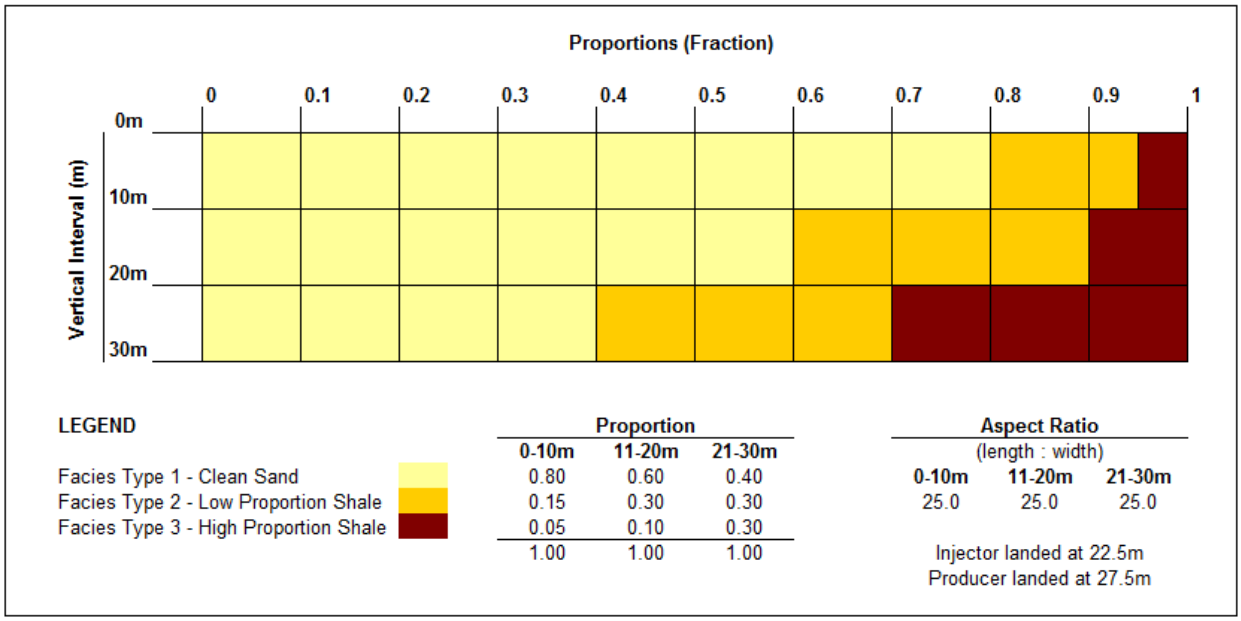

LEGEND

	Proportion			Aspect Ratio (length : width)		
	0-10m	11-20m	21-30m	0-10m	11-20m	21-30m
Facies Type 1 - Clean Sand	0.80	0.60	0.40	25.0	25.0	25.0
Facies Type 2 - Low Proportion Shale	0.15	0.30	0.30			
Facies Type 3 - High Proportion Shale	0.05	0.10	0.30			
	1.00	1.00	1.00			

Injector landed at 22.5m
Producer landed at 27.5m

C. Fining Upwards Model

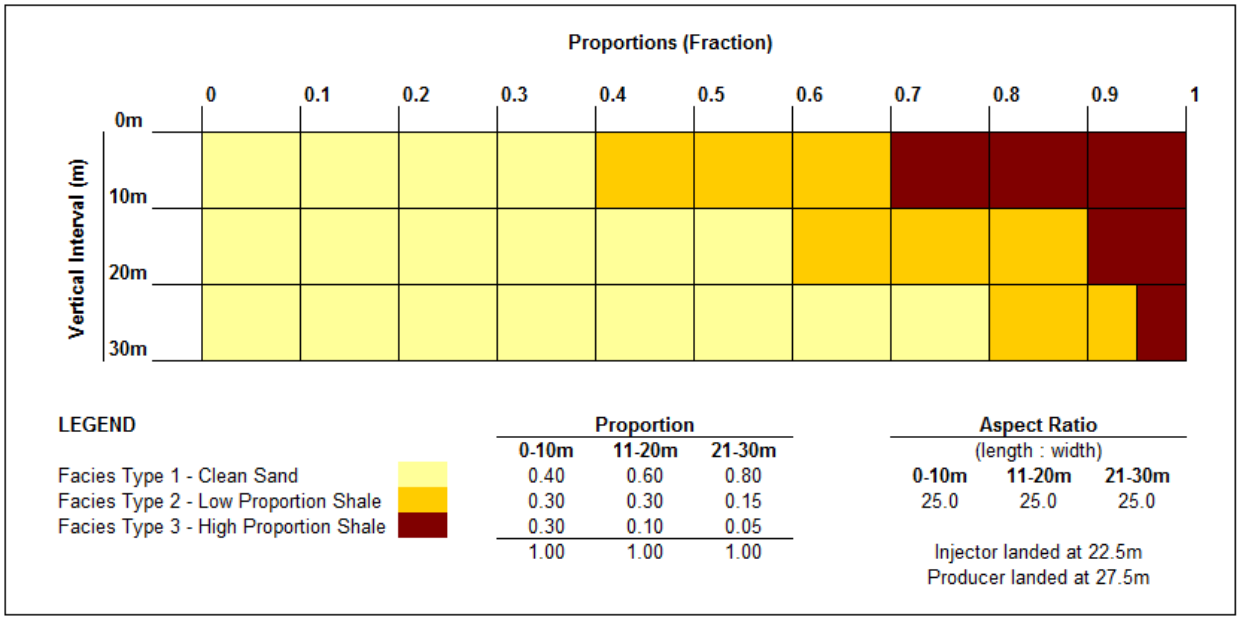

LEGEND

	Proportion			Aspect Ratio (length : width)		
	0-10m	11-20m	21-30m	0-10m	11-20m	21-30m
Facies Type 1 - Clean Sand	0.40	0.60	0.80	25.0	25.0	25.0
Facies Type 2 - Low Proportion Shale	0.30	0.30	0.15			
Facies Type 3 - High Proportion Shale	0.30	0.10	0.05			
	1.00	1.00	1.00			

Injector landed at 22.5m
Producer landed at 27.5m

D. Channel Depositional Model

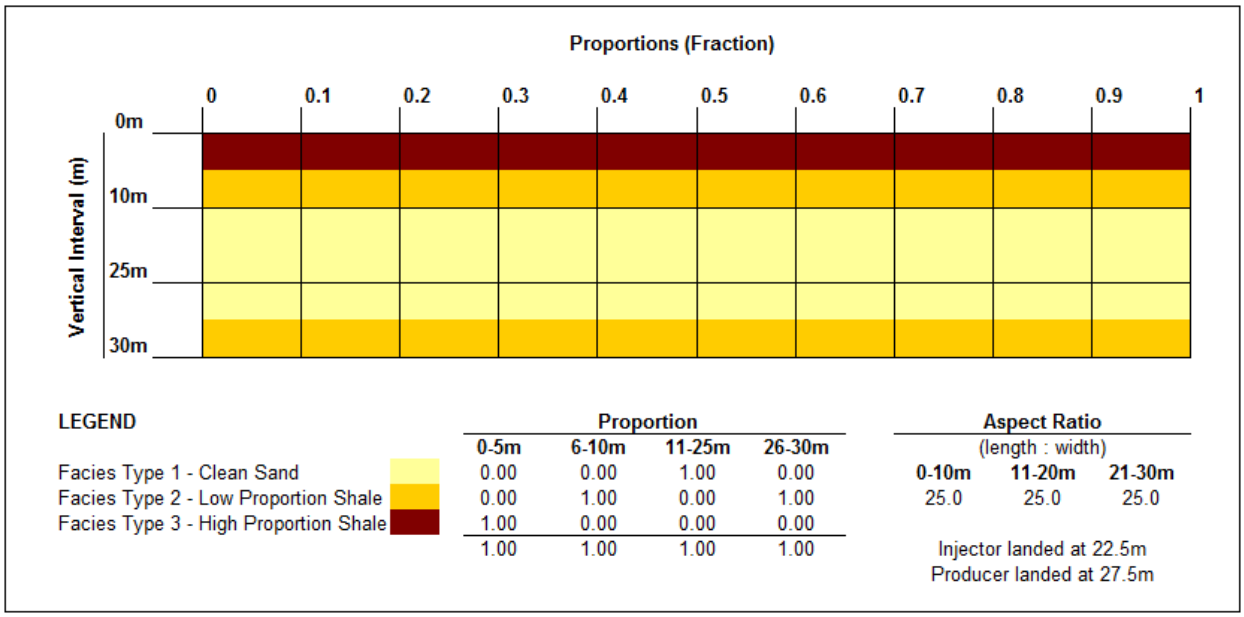

Table 3.9.1 – Standard Distribution Parameters

Inputs	Units	Facies 1		Facies 2		Facies 3	
		Mean (μ)	Deviation (σ)	Mean (μ)	Deviation (σ)	Mean (μ)	Deviation (σ)
Oil Saturation	fraction	0.80	0.05	0.50	0.10	0.10	0.05
Porosity	fraction	0.35	0.05	0.20	0.05	0.08	0.02
Vertical Permeability	mD	4,500	1,000	2,000	1,000	200	100

As an example of how the vertical proportion curves are populated within Builder™, the Channel Depositional model was selected to illustrate how the facies-based datasets are more representative of geological model exports than the binary models. The objective was to target more realistic realizations in which to benchmark the dynamic upscaling parameters.

Figure 3.9.2 – Builder™ Generated, Channel Depositional Model (4m, 100m, 1m)

Facies Distribution (*i, k*-direction)

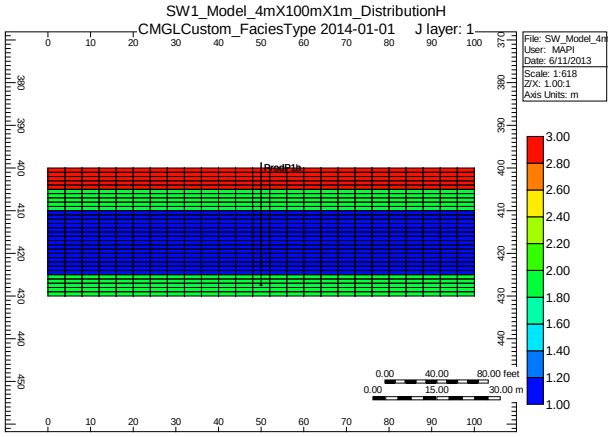

Facies Distribution (*i, j*-direction)

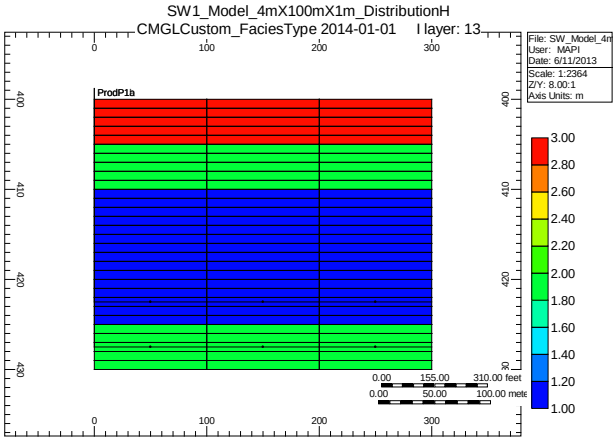

Vertical Permeability (*i, k*-direction)

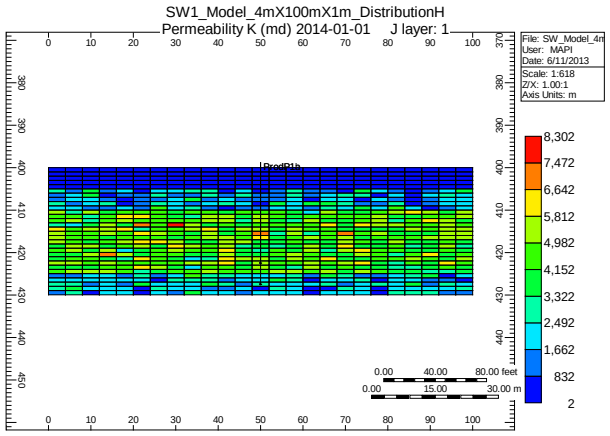

Vertical Permeability(*i, j*-direction)

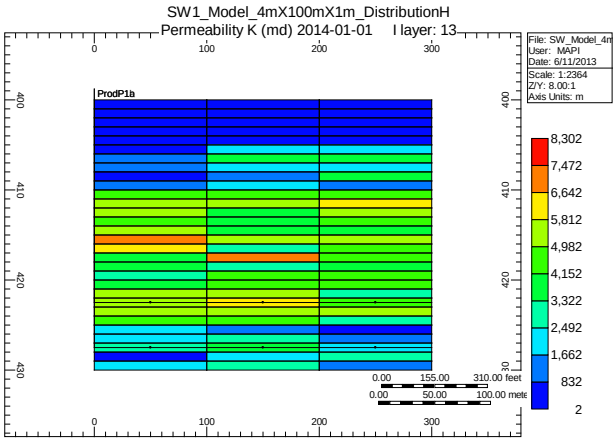

Horizontal Permeability (*i, k*-direction)

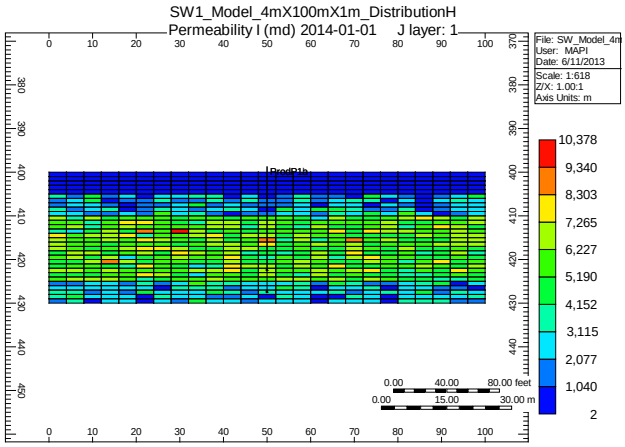

Horizontal Permeability (*i, j*-direction)

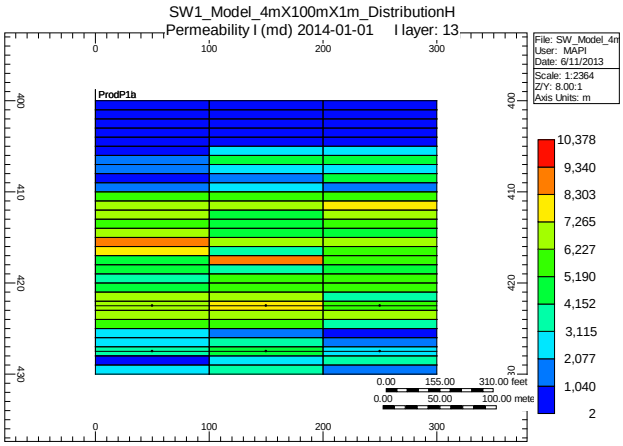

Porosity (*i, k*-direction)

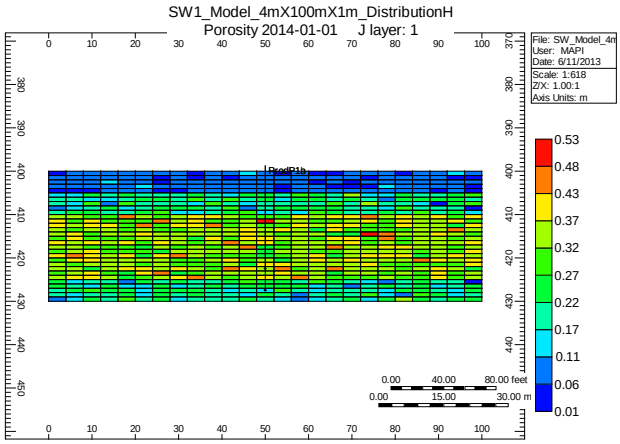

Porosity (*i, j*-direction)

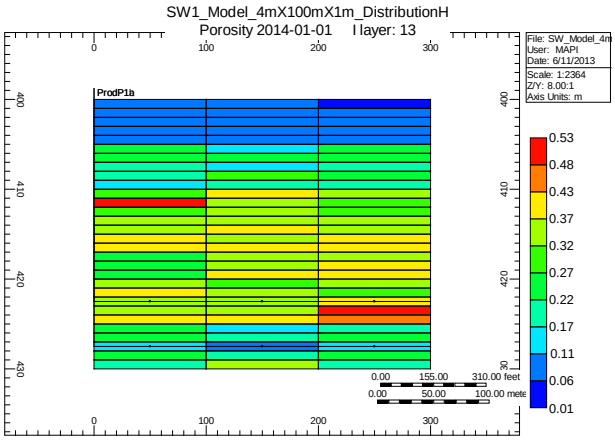

Oil Saturation (*i, k*-direction)

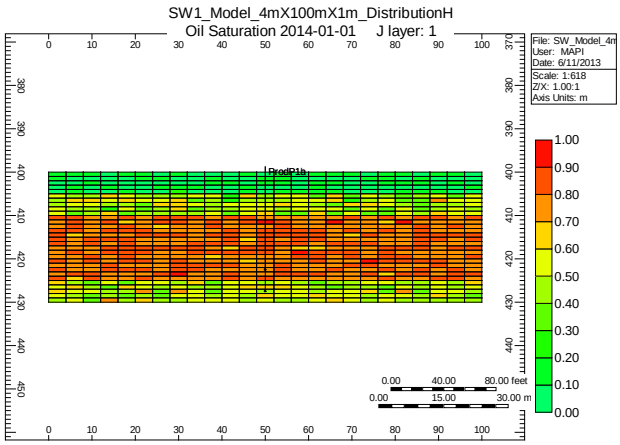

Oil Saturation (*i, j*-direction)

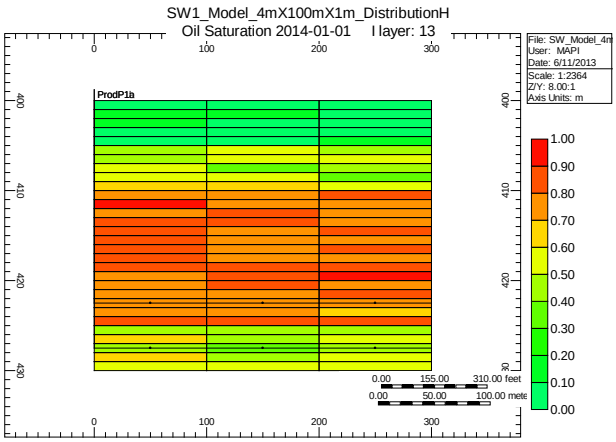

3.10 Dynamic Upscaling Concept

A coarse gridblock definition along the wellbore is a reasonable simplification provided the temperature gradient is small. However, with introduction of facies-based reservoir models with a variable magnitude of reservoir heterogeneities, large temperature gradients parallel the wellbore are often the norm rather than the exception. To capture the movement of temperature fronts in the SAGD well pair, it is necessary to refine the grid or introduce dynamic upscaling parameters in coarser models to more accurately model the movement of the temperature and

steam front due to the change in block volumes. This concept is different than what was proposed in **Sections 2.1** and **2.2**, in that the petrophysical values and realization are already finalized for export to the flow simulator and length scales are predetermined. Therefore, how does that combination of properties behave at different dimensions and block volumes?

The challenge is in determining the time to achieve the threshold (steam) temperature as well as the rate of mobilization from the larger gridblocks, especially as the chamber develops vertical and horizontally and growth occurs around the geological baffles, as indicated in **Figure 3.10.1**. Effectively, a smaller volume will heat faster and hydrocarbon will drain quicker than in a larger volume, even when the reservoir parameters are identical. There exists a relationship between the reduction in gridblock volume and the time to achieve the steam temperature and pressure.

Figure 3.10.1 – Schematic of Temperature Gradients within Varying Block Volumes at Time, t

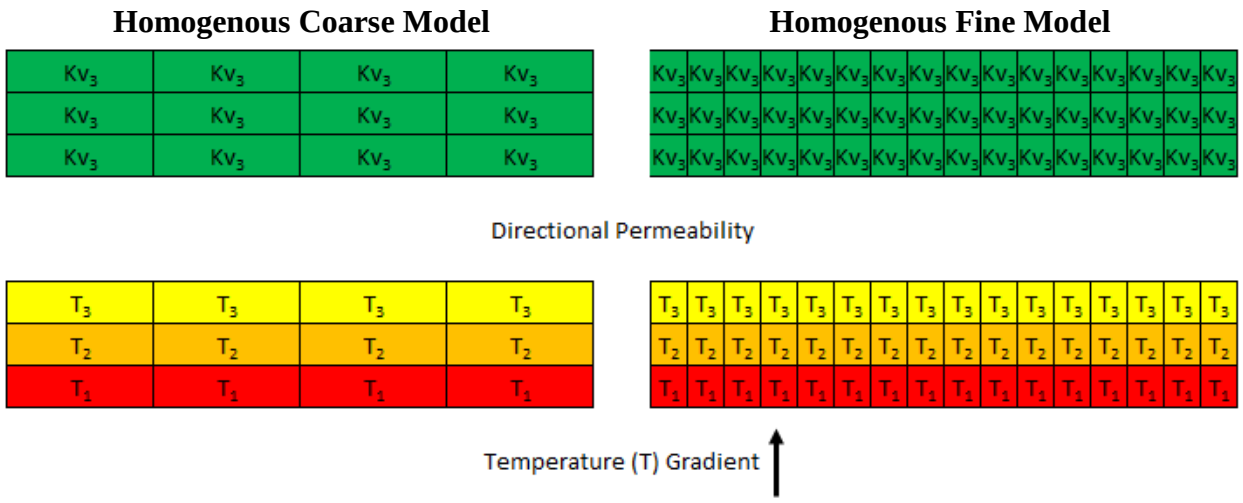

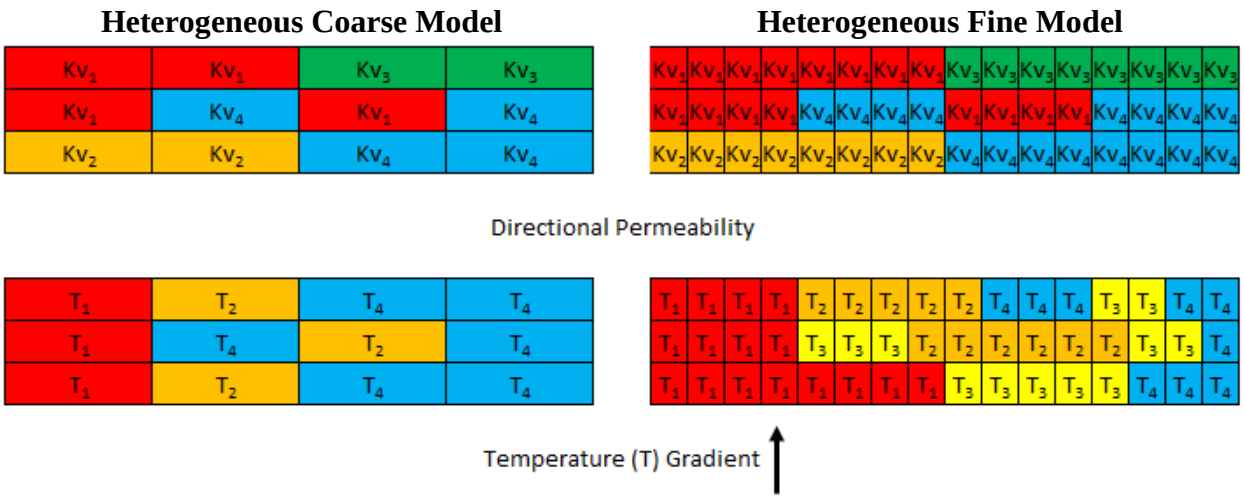

Based upon the analysis performed for this thesis, it is understood that temperature propagation within the model will be most similar in a homogenous environment despite the introduction of grid refinement. The coarse homogenous model will behave very closely to the fine homogenous model. As indicated in **Figure 3.10.1**, the rate of temperature migration is considered equivalent. This temperature signature has also been supported by the small differences observed in the production profiles for homogenous models of varying length scale, in that the rate of chamber growth and bitumen drainage is comparable. However, upon the introduction of variable reservoir quality and a higher fraction of heterogeneities, the temperature signature and nature in which the temperature propagates within the model is much different. The poorer reservoir quality can act as a baffle and delay heat development, especially as the grid refinement is varied. This phenomenon is further supported in **Figures 3.10.2** and **3.10.3**.

In successive sections, effort will be made to document the impact of reservoir heterogeneities and the impact of different block dimensions (volumes) on performance of SAGD chambers.

Figure 3.10.2 – Coarse Model Representation of Chamber Development (4m, 50m, 1m) Facies-based at 1 Year

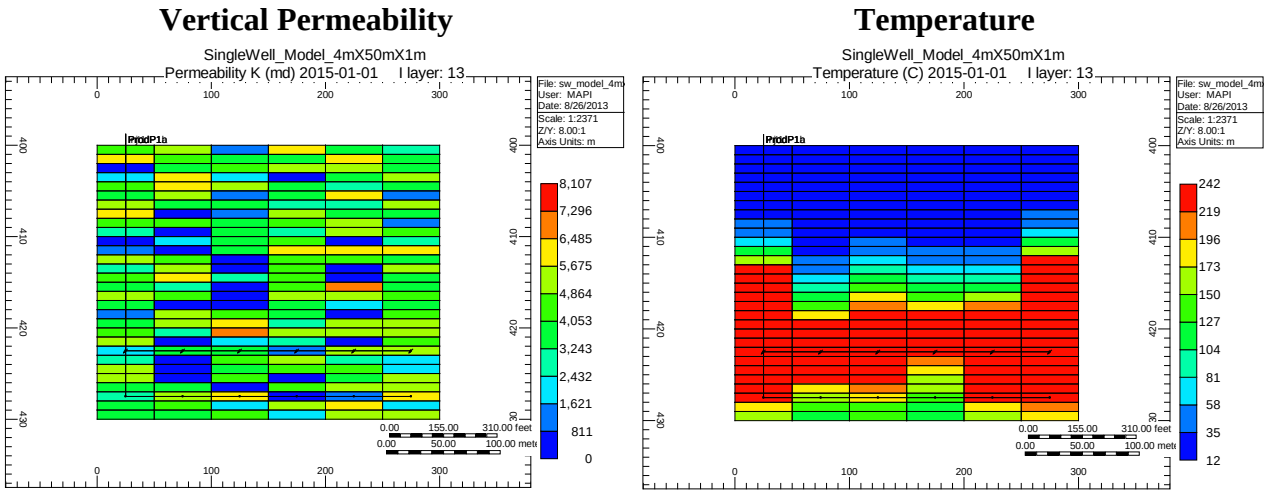

Figure 3.10.3 – Fine Model Representation of Chamber Development (4m, 50m, 1m) Facies-based at 1 Year

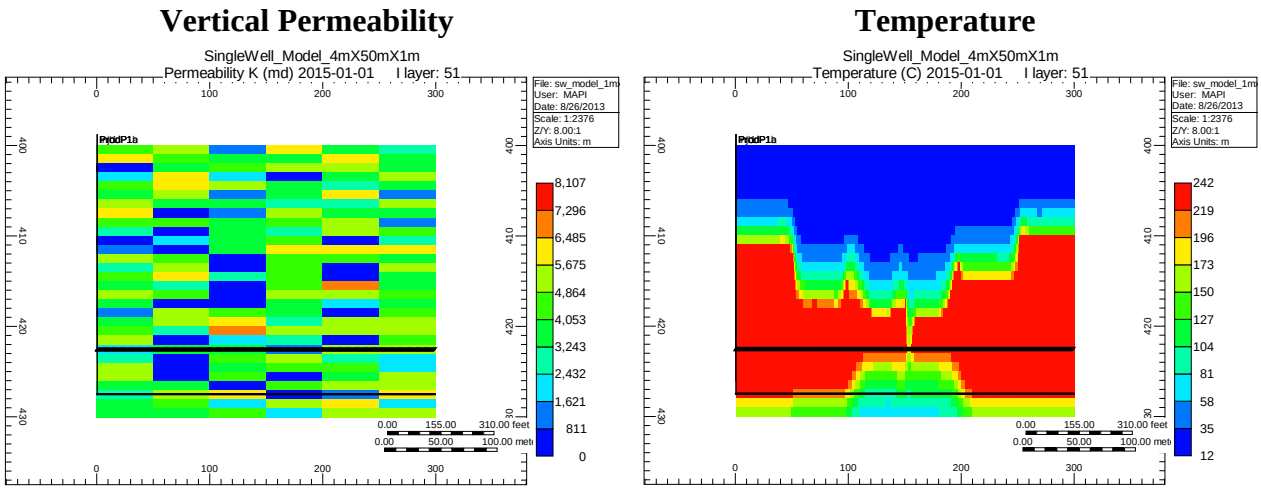

By manipulating the thermal conductivity and permeability values within the simulation, the hope is that rate of bitumen mobilization and the temperature gradient specific to that volume is achieved at comparable times. By achieving comparable performance at comparable times, we are increasing the likelihood that we are matching the performance. A schematic highlighting

that desired effect is presented in **Figure 3.10.4**. Alternatively, a one-dimensional (1D) heat equation could be solved to more rigorously capture the diffusion and advancement of heat on a block basis, in favour of the qualitative representation.

Figure 3.10.4 – Temperature Gradient within the Models at Time, t

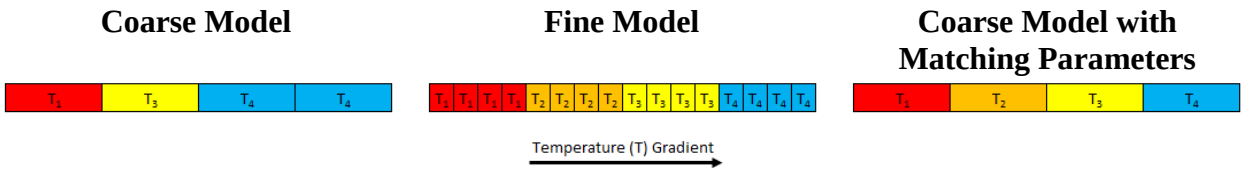

3.11 Impact of Reservoir Heterogeneities on SAGD Performance

One key observation early on during the analysis of simulation results was the relationship between reservoir heterogeneities and length scales. If the model was completely homogenous, being represented as a two-dimensional (2D) model, then the performances of the steam chamber and production profile were comparable. Fundamentally, different grid definitions will impact results, but as shown in **Figures 3.11.1** and **3.11.2**, the impact is less pronounced until reservoir heterogeneity is introduced. The primary differences were noted in the first few years of SAGD, in particular with respect to oil and water production rates. The energy required to achieve mobilization temperature in a gridblock is volume dependent. Therefore, most variation is expected during the first several years when the steam chamber-cold bitumen interface is growing most rapidly. This trend was observed despite different operational and petrophysical constraints, such as at different injection pressures and a spectrum of constant petrophysical values (such as, high, medium and low saturation, porosity and permeability profiles). Only upon

the introduction of variable reservoir quality did length scale effects begin to significantly impact performance. Even then the impact of the length scale can be absorbed into the impact of geology and potential productivity for that pair.

Figure 3.11.1 – Comparison of Homogenous Model of Different Length Scales (Coarse Model and Fine, Base Case Model), 0% Shale Content

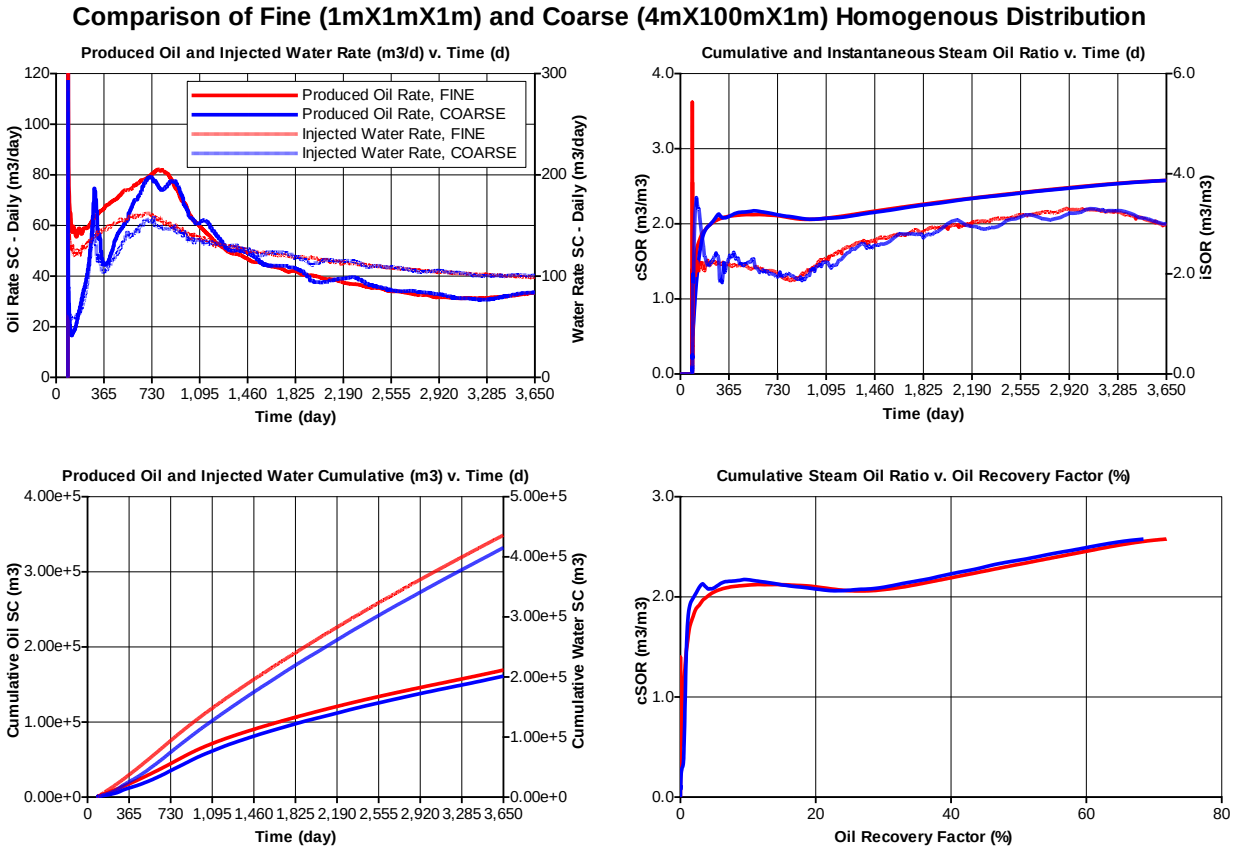

Figure 3.11.2 – Coarse Model, Chamber Conformance at 5 Years, Temperature

***i, k*-direction** ***i, j*-direction**

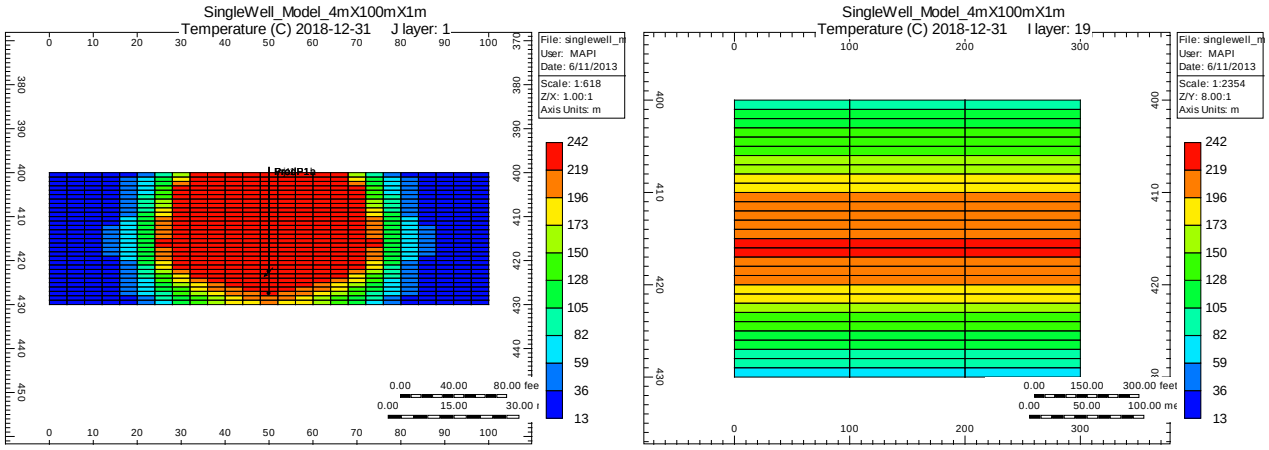

Figure 3.11.3 – Fine Model, Chamber Conformance at 5 Years, Temperature

***i, k*-direction** ***i, j*-direction**

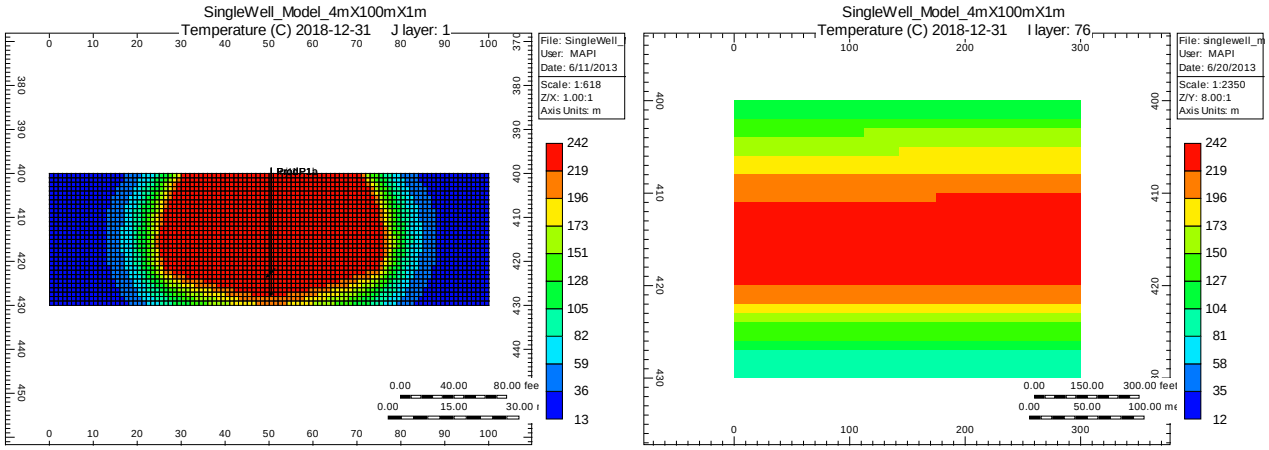

Figure 3.11.4 – Comparison of Heterogeneous Model of Different Length Scales (Coarse Model and Fine, Base Case Model), 10% Shale Content

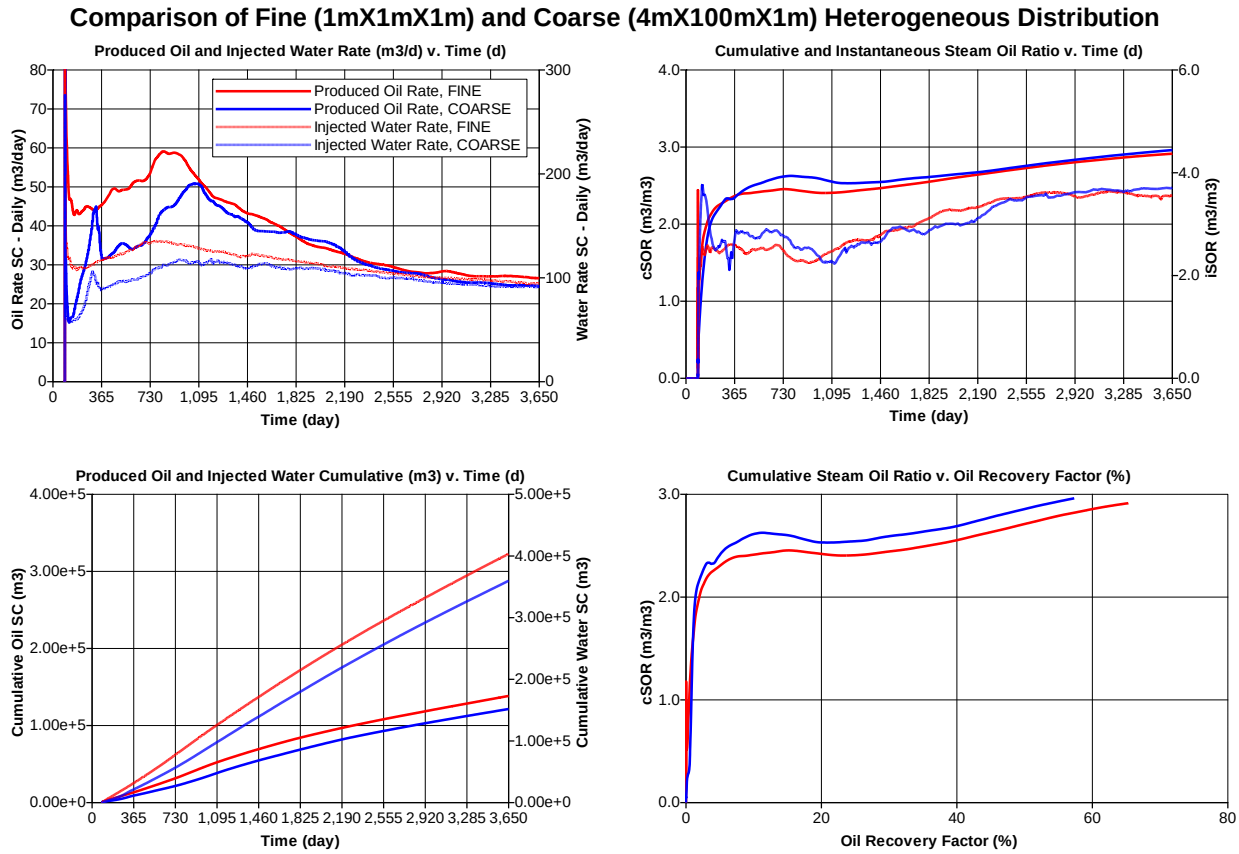

Figure 3.11.5 – Coarse Model, Chamber Conformance at 5 Years, Temperature

***i, k*-direction** ***i, j*-direction**

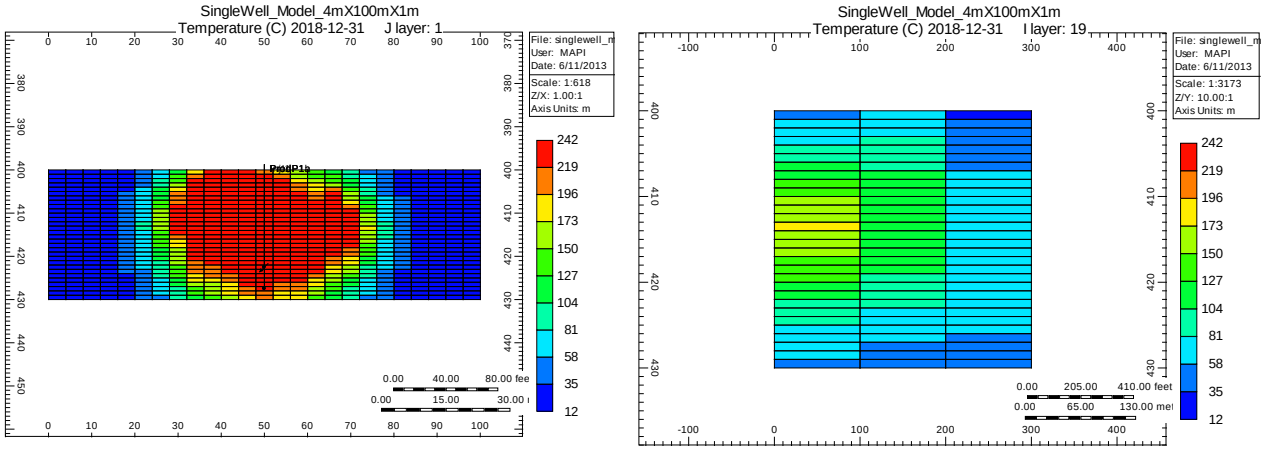

Figure 3.11.6 – Fine Model, Chamber Conformance at 5 Years, Temperature

***i, k*-direction** ***i, j*-direction**

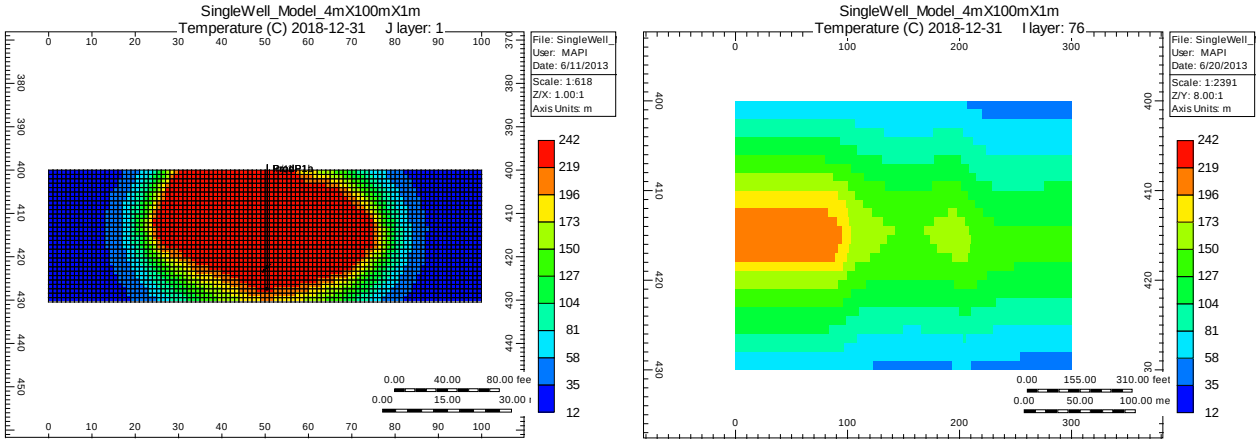

This observation is the foundation of the research documented in this thesis and the desire to seek an analytical solution to the noted differences. As identified in the **Section 1.1**, fine grid resolution is required to track temperature fronts in the reservoir. As a result, fine gridding is reserved for the gridblocks perpendicular to the wellbore and coarser gridblocks are an acceptable approximation parallel to the wellbore. However, as the degree of reservoir heterogeneity increases, the coarse gridding assumption parallel to the well is less valid as the temperature gradients in all dimensions are significant.

As an additional investigation the performance of a (2m, 25m, 1m) model was analyzed in the same capacity as the (4m, 100m, 1m) model above. The (2m, 25m, 1m) model typically represents the maximum degree of refinement acceptable for geoscience-engineering work-flows within industry. In many practical cases, finer gridding makes execution times excessive, especially for pad scale models consisting of up to 10 well pairs. As a result, the work presented

in this thesis was designed to evaluate the extremes for grid coarsening and its relative impact to understand the magnitude of influence.

Figure 3.11.7 – Comparison of Homogenous Model of Different Length Scales (Coarse Model and Fine, Base Case Model), 0% Shale Content

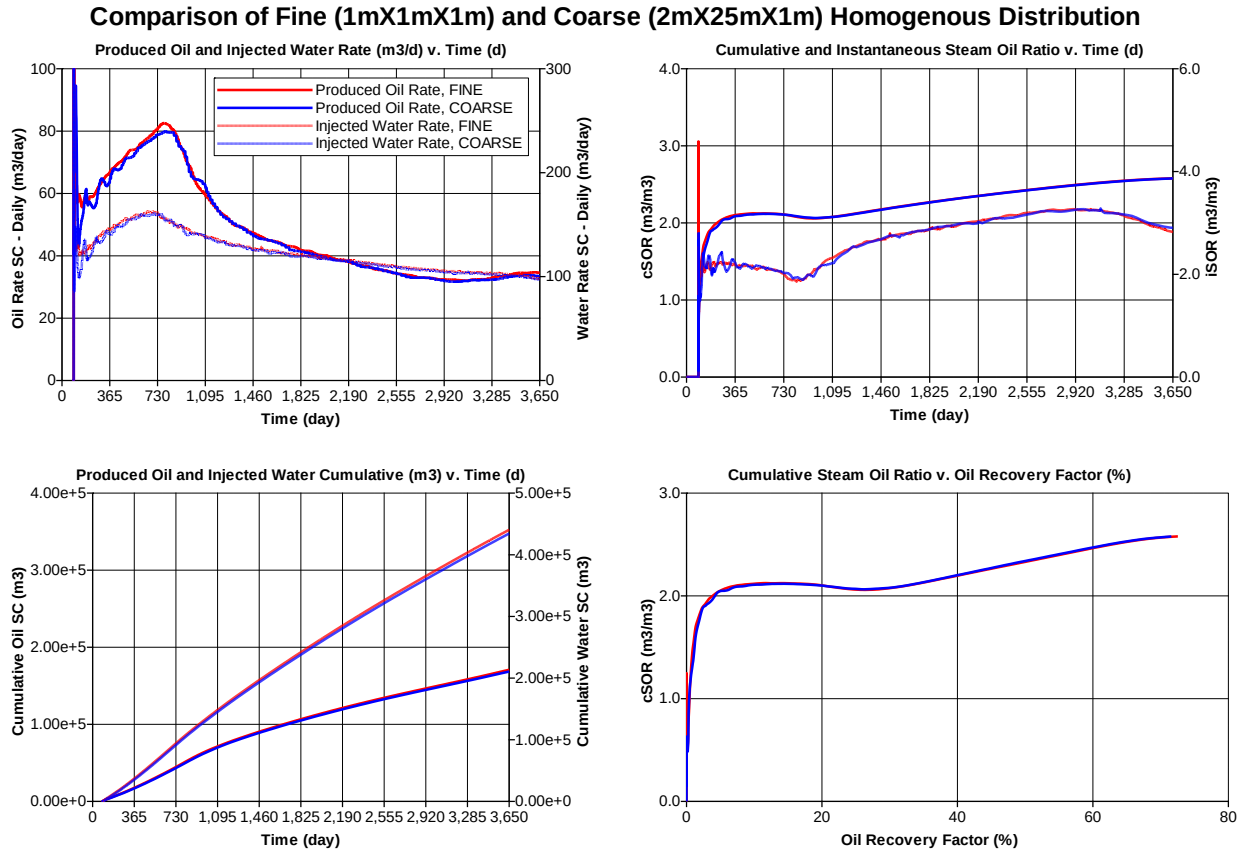

Figure 3.11.8 – Coarse Model, Chamber Conformance at 5 Years, Temperature

***i, k*-direction** ***i, j*-direction**

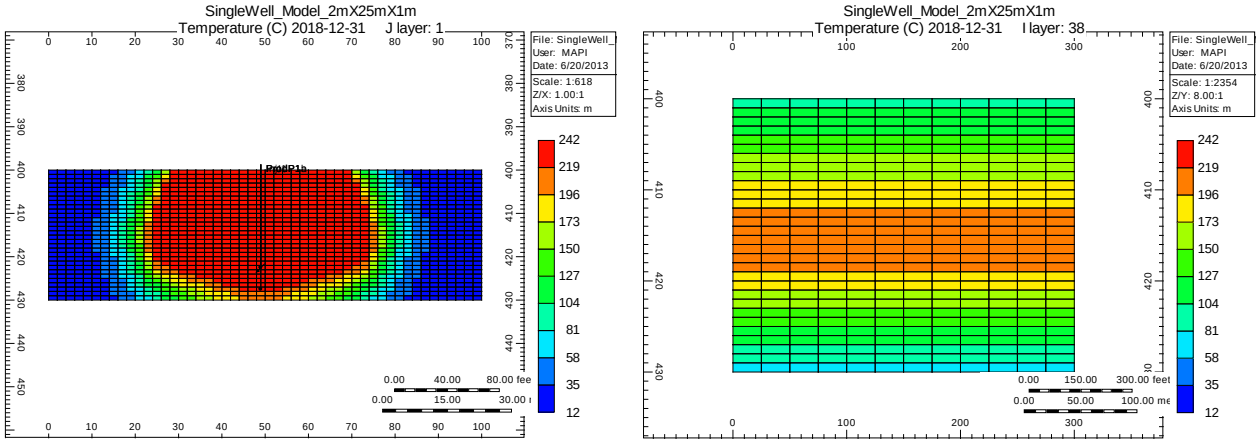

Figure 3.11.9 – Fine Model, Chamber Conformance at 5 Years, Temperature

***i, k*-direction** ***i, j*-direction**

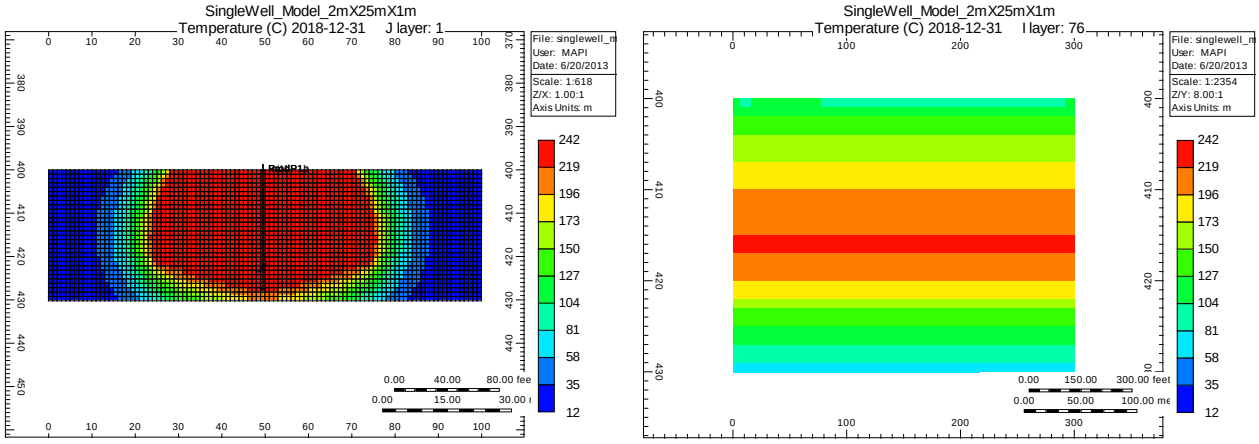

Figure 3.11.10 – Comparison of Heterogeneous Model of Different Length Scales (Coarse Model and Fine, Base Case Model), 10% Shale Content

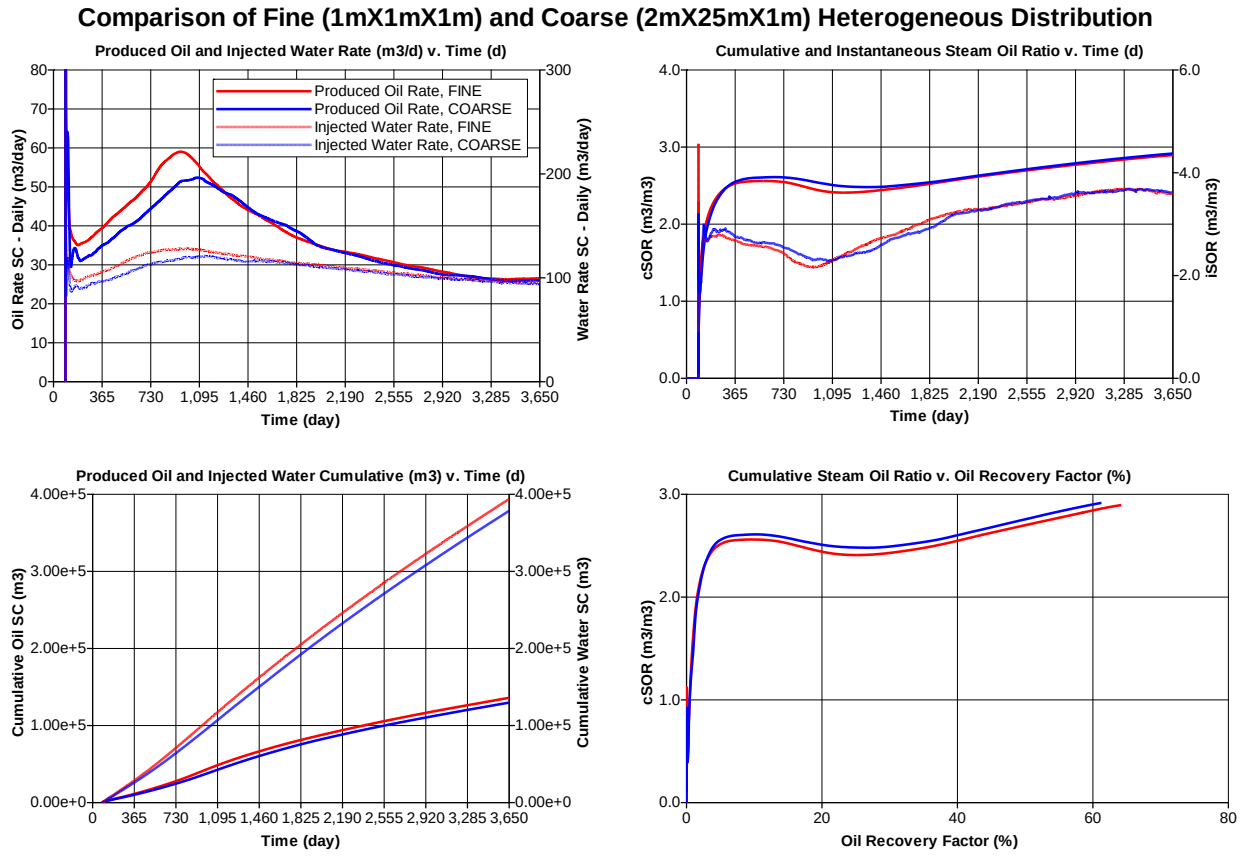

Figure 3.11.11 – Coarse Model, Chamber Conformance at 5 Years, Temperature

***i, k*-direction** ***i, j*-direction**

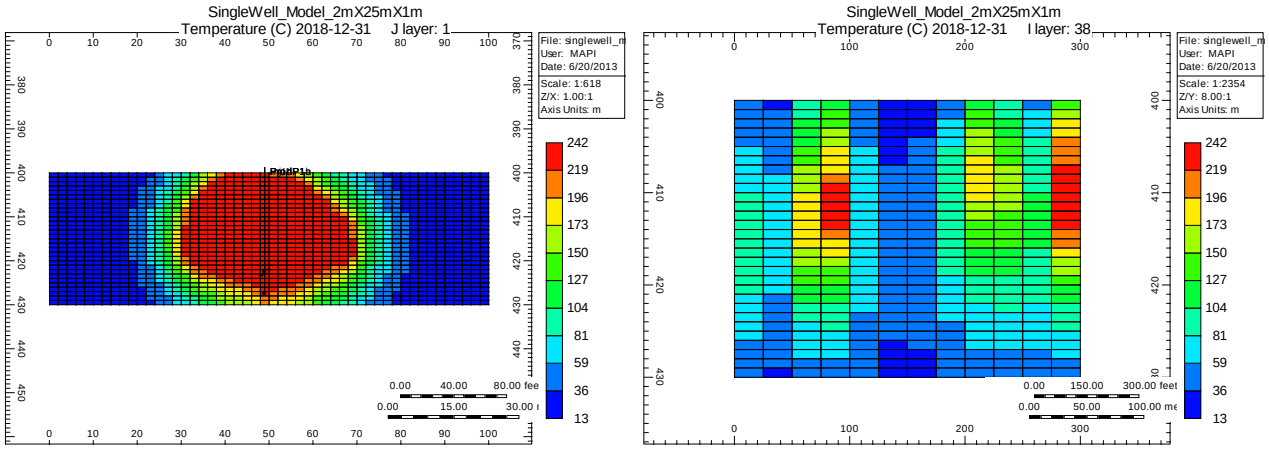

Figure 3.11.12 – Fine Model, Chamber Conformance at 5 Years, Temperature

***i, k*-direction** ***i, j*-direction**

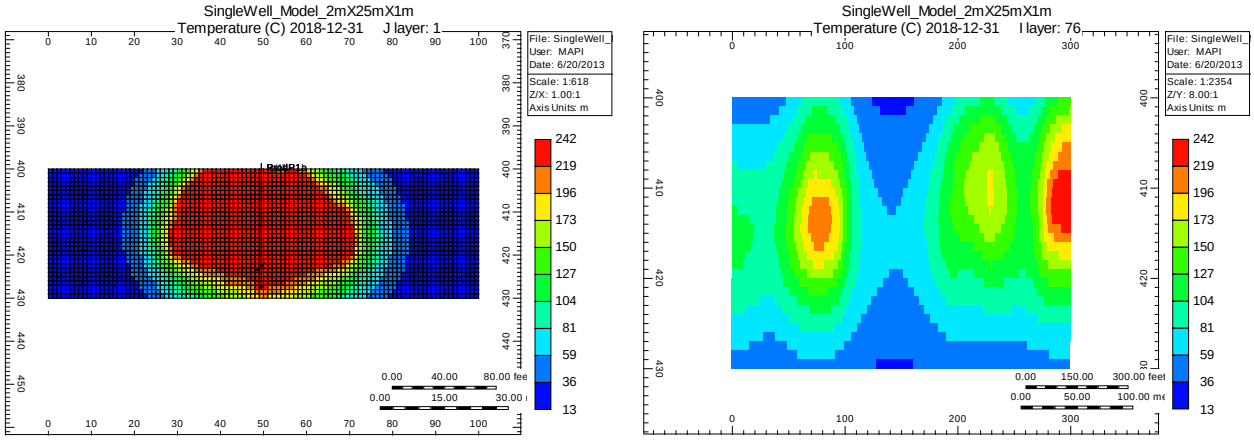

Table 3.11.1 – Comparison of Length Scales and Heterogeneity on Coarse Model Performance

Model Type		Objective Function (Equation 4.2.3.1), Original Error	
		Coarse Model (%)	Fine Model (%)
4m, 100m, 1m	0% Shale Content (Homogenous Properties)	4.77	Reference
	10% Shale Content (Heterogeneous Properties)	8.46	Reference
2m, 25m, 1m	0% Shale Content (Homogenous Properties)	1.10	Reference
	10% Shale Content (Heterogeneous Properties)	3.41	Reference

Table 3.11.2 – Comparison of Length Scales and Heterogeneity on Relative Performance

Model Type		Objective Function (Equation 4.2.3.1), Difference in Error as a function of Shale Content (%)
4m, 100m, 1m	0% Shale Content (Homogenous Properties)	3.69
	10% Shale Content (Heterogeneous Properties)	
2m, 25m, 1m	0% Shale Content (Homogenous Properties)	2.31
	10% Shale Content (Heterogeneous Properties)	

The objective function and 'Original Error' notation will be explained in more detail in **Sections 4.3** and **4.4**, respectively. The same relative effect is observed as previously mentioned, in that the different grid definitions will impact results, but it is more pronounced in the heterogeneous cases than the homogenous cases. However, at this point it is not known with confidence what controls the exact behaviour of models with different length scales and quantity of non-reservoir facies relative to the location within the model.

CHAPTER 4 – DYNAMIC UPSCALING: RESULTS

The two dynamic upscaling parameters that were selected for this study were permeability and thermal conductivity. The motivation for selecting these two parameters will be highlighted in detail in the following sections. However, to fully understand the impact of multipliers on simulation, a discussion on how some of these fundamental parameters can affect simulation processes is presented.

4.1 Dynamic Upscaling Parameters

Two critical phenomena that drive thermal recovery processes are fluid flow and heat transfer. Fundamental to SAGD is the mobilization of the bitumen followed by the production of the mobilized emulsion. Two key parameters that influence those events, and are linked to the gridblock size defined in the models, are permeability and thermal conductivity. By suggesting multipliers to these base values, an acceleration of heat and/or fluid flow can be induced.

It may not seem logical to apply such drastic corrections to the base values, however, the justification is three-fold. Firstly, geological models inherently have a high degree of uncertainty. Dependent on the well control in a given area, and the parameters for geostatistical simulation (channel directions, channel dimensions, variogram parameters) a high degree of ambiguity is assumed relative to the actual reservoir, with robust characterization a top challenge. Therefore, geoscience teams construct multiple realizations of a given area to try to capture the range of uncertainty in the geology. Secondly, most of the reservoir simulation models are limited in their

degree of grid refinement, as a function of software and hardware limitations, and so are the geological models. Therefore, the property of a gridblock represents the effective value of the property over the size of the gridblock. The actual distribution of values (within the gridblock) is smeared. In other words, the values assigned to gridblocks are approximate.

Finally, no history matching exercise is perfect but simply attempts to calibrate a model to represent reality. The objective of this report is not to focus so much on the magnitude of the parameter value, but rather which parameters are analyzed to offset the differences observed as a function of length scale and reservoir quality.

4.1.1 Permeability

Darcy's Law is the fundamental equation to describe fluid flow within porous medium[44]:

$$v_l^c = -\frac{k\, k_{rl}}{\mu_l}(\nabla \mathrm{p}_l - \gamma_l \nabla h) \tag{4.1.1.1}$$

A common representation of Darcy's Law in the horizontal flow direction is presented as:

$$q_l = \frac{k\, k_{rl}\, A}{\mu_l}\, \frac{p_1 - p_2}{L} \tag{4.1.1.2}$$

And a common representation of Darcy's Law while dominated by gravity is given by:

$$q_l = \frac{k\, k_{rl}\, A}{\mu_l}\, \rho_l g \tag{4.1.1.3}$$

There are several assumptions in Darcy's Law, such as the fluid is homogenous, single-phase, and Newtonian. However, it is a fundamental component of all reservoir simulation models as it describes the convective velocity of the system and is associated with the movement of the entire phase, such as a liquid (v_l^c).

Therefore, Darcy's Law and permeability have a significant impact upon steam chamber growth and bitumen production within SAGD. Fundamentally, permeability is defined as a rock's ability to transmit fluids. In this sense, permeability is often considered as absolute permeability, and is in the absence of other fluids within the reservoir. Effective permeability is the flow of the given fluid in the presence of other immiscible fluids. Consequently, the relative permeability of a given fluid is the relationship of the effective permeability divided by the absolute permeability, as indicated by:

$$k_{rl} = \frac{k_{eff}}{k_{abs}} \tag{4.1.1.4}$$

Relative permeability plots are required to be defined in the reservoir input section of the STARS™ data-set and shows the relative permeability of a fluid to another fluid at a given saturation. The reservoir system is considered to be water-wet and is reflected in the permeability curves.

Figure 4.1.1.1 – Normalized Relative Permeability Curves

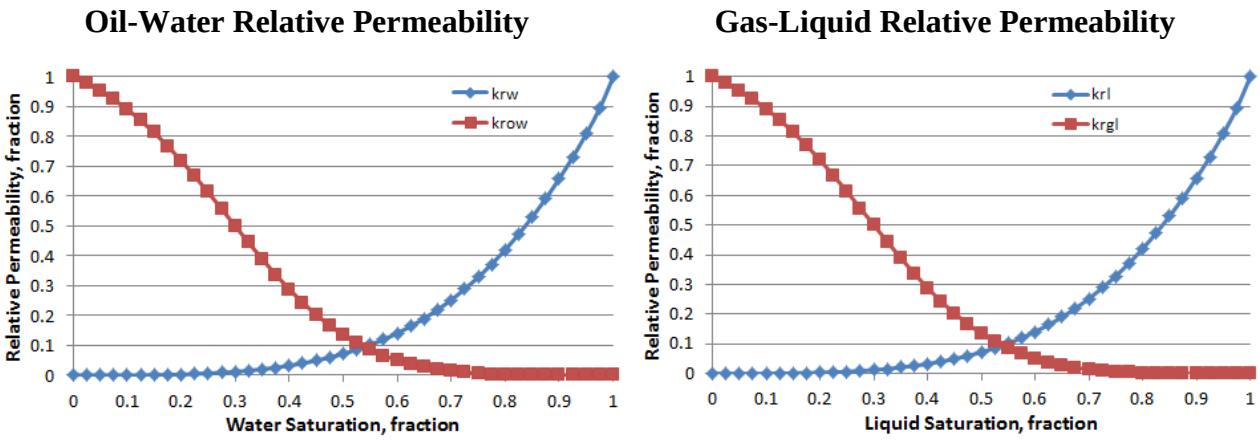

For the purpose of matching the coarse reservoir models to the fine reservoir models, the in-situ permeability (represented as the absolute permeability) was manipulated, but did not influence the relative permeability curves. The effective permeability and absolute permeability can be thought of as being scaled together, to maintain the relative permeability values. While a normalized relative permeability curve was generated, the irreducible water saturation (Sw_{irr} = 0.10) and residual oil saturation (So_r = 0.10) were defined on a gridblock basis, but constant and independent of facies type. The motivation for modifying the absolute permeability was to accelerate fluid transfer within the blocks, but not the relationship between flows of different fluids.

The transmissibility of the system takes into consideration the relationship of permeability and gridblock dimensions, as seen by **Equation 4.1.1.5**. As a result, the expectation is that the modification to the gridblocks dimensions is impacting the transmissibility of the system despite the same defined permeability. In response to a change in grid dimensions, by manipulating the

permeability in the coarse model the goal is to achieve comparable interface transmissibility to the fine model. The mobility is defined by:

$$\lambda = \frac{k}{\mu B} \tag{4.1.1.5}$$

The transmissibility, in the x-direction, is given by:

$$T = \frac{kA}{\mu B \Delta x} = \frac{\lambda A}{\Delta x} \tag{4.1.1.6}$$

4.1.2 Heat Transfer – Thermal Conductivity

Fourier's Law of heat conduction states that the heat transfer rate is proportional to a temperature difference in the direction of heat flow with the thermal conductivity constant of the material and area[45]:

$$q = -kA \frac{dT}{dx} \tag{4.1.2.1}$$

Where k is the thermal conductivity constant, A is the cross-sectional area open to heat transfer, and dT/dx is the temperature gradient. Dr. Roger Butler describes two major mechanisms for heat transfer within thermal recovery processes: thermal conduction and convective fluid transport[46]. On its own, thermal conduction is inadequate to transfer heat to large reservoir volumes. However, it is most effective at the bitumen-chamber interface. Therefore, it is a combination of convective flows and thermal conductivity that permit continual development of a SAGD chamber. However, in the majority of analysis performed on transfer of heat at the bitumen-chamber interface, it was concluded that the primary mode of heat transfer in SAGD is

conduction[47-53], especially when the chamber temperature is assumed constant. It can be enhanced in several capacities, which include: (1) increasing the thermal conductivity of the oil sands, and (2) maximizing the heat transfer surface area by voiding the reservoir faster. The focus here is to analyze temperature and chamber development as a function of heat transfer at the bitumen-steam interface and how the process is affected by varying reservoir quality and grid dimensions. Therefore, the enhancements mentioned above can be accomplished with modification to thermal conductivity and permeability.

A summary of thermal properties is presented **Figure 4.1.2.1**, which form the base case values that will be manipulated with the multipliers. **Appendix B** captures the necessary syntax that is required to manipulate these base values within the simulation software.

Table 4.1.2.1 – Thermal Properties within STARS™ for a Single Rock Type [54]

Thermal Conductivity Keyword	Description	Units	Value
PRPOR	Reference Pressure	kPa	2,000
CPOR	Effective Formation Compressibility	kPa^{-1}	1.45E-6
ROCKCP	Rock Heat Capacity	J/m^3-^oC	2.35E+6
THCONR	Thermal Conductivity of Reservoir Rock	J/m-day-^oC	2.74E+5
THCONW	Thermal Conductivity of Water Phase	J/m-day-^oC	5.35E+4
THCONO	Thermal Conductivity of Oil Phase	J/m-day-^oC	1.15E+4
THCONG	Thermal Conductivity of Gas Phase	J/m-day-^oC	2,892
THCONMIX	Rule Used to Mix Thermal Conductivities of Rock and Phases	-	SIMPLE
HLOSST	Overburden Temperature	^oC	12
HLOSSTDIFF	Critical Temperature Difference	^oC	1.0
HLOSSPROP	Directional Dependency for Heat-loss	-	-
HLOSSPROP, OVERBUR	Heat-loss Properties to the Outer Gridblock Faces at the Reservoir Top	-	-
HLOSSPROP, OVERBUR (*dnurol)*	Volumetric Heat Capacity of Formation Adjacent to the Reservoir in the Indicated Direction	J/m^3-^oC	2.35E+6
HLOSSPROP, OVERBUR (*hconl)*	Thermal Conductivity of Formation Adjacent to the Reservoir in the Indicated Direction	J/m-day-^oC	1.50E+5
HLOSSPROP, UNDERBUR	Heat-loss Properties to the Outer Gridblock Faces at the Reservoir Bottom	-	-
HLOSSPROP, UNDERBUR (*dnurol)*	Volumetric Heat Capacity of Formation Adjacent to the Reservoir in the Indicated Direction	J/m^3-^oC	2.35E+6
HLOSSPROP, UNDERBUR (*hconl)*	Thermal Conductivity of Formation Adjacent to the Reservoir in the Indicated Direction	J/m-day-^oC	1.50E+5

4.2 History Matching Process

The determination of dynamic parameter values for application with the coarse model was performed within CMOST™. CMOST™ states that a Global Objective Function (GOF) is required for History Matching (HM) and is always the weighted average of all the Local

Objective Functions (LOF). The LOF, as it relates to History Matching Error (HME), is the relative difference between the simulation results and the historical data (fine model, reference case). The weighted average formulation will average all values using the weight assigned for each LOF. For the purpose of this report, the weight is equally assigned to all three parameters of interest: (1) cumulative oil production, (2) cumulative water production and (3) cumulative steam injection.

$$GOF = \frac{\sum w_i \, LOF_i}{\sum w_i} \tag{4.2.3.1}$$

Therefore, the GOF or Objective Function (OF), as tabulated in this report, is given by the following equation and represented on a percentage basis:

$$OF\ (\%) = \frac{1}{3}\left(HME_{Cumulative\ Oil\ Production} + HME_{Cumulative\ Water\ Production} + HME_{Cumulative\ Steam\ Injected}\right) \tag{4.2.3.1}$$

Further details of History Matching Error (HME) calculation is outlined in the CMOST™ data-manual.

The process that was involved to configure CMOST™ is outlined below and requires several steps. First, the coarse and fine models had to be simulated to completion, which corresponded to 10 years of simulation time. Based upon the characteristics of the production profiles, 10 years was sufficient to capture the ramp-up, plateau and decline periods for each well pair. The fine model production data or reference historical data was then exported and loaded into a Field History File (.FHF) as required by CMOST™. Second, the original coarse data file had to be

conditioned to include the necessary CMOST™ keywords to run a range of values for a given parameter.

As no grid refinement occurs in the *k*-direction, no justification exists to manipulate the permeability and thermal conductivity in that direction. The remaining inputs for a CMOST™ task file (.CMT) are highlighted below and in the order they are required within the software. Supplemental information is presented in **Appendix B**.

4.2.1 Parameters

The parameters section is devoted to allowing the user to define different value ranges for each parameter that will later be used to substitute into the master data-set (.CMM).

Table 4.2.1.1 – Parameter Inputs

Parameter Name	Default Multiplier	Value Generator Method	Minimum Multiplier	Maximum Multiplier	Number of Values
PERM, *i*	1	Arithmetic Sequence	1	2.5	25
PERM, *j*	1	Arithmetic Sequence	1	10	25
TH, *i*	1	Arithmetic Sequence	1	5	25
TH, *j*	1	Arithmetic Sequence	1	15	25

4.2.2 Optimization Method

Four different optimization methods exist for use in CMOST™: (1) Brute force, (2) Random search, (3) Particle Swarm Optimization (PSO) and (4) CMG Designed Exploration Controlled Evolution (DECE) Optimization[55]. The method employed for all models was the CMG DECE

Optimization Method as it is well-suited for engineering-related problems. This is due to the need to run multiple models with multiple configurations, while focusing on practicality with respect to execution speed. The DECE method is configured to successively eliminate parameter values until the best possible solution set remains. The strength of the DECE method allows it to identify the cause of the improvement or deterioration of a solution. The results of all simulation runs are analysed and used by the algorithm. Finally, it tends to converge faster than other optimization methods, particularly the PSO method. Considering all these factors, it was identified as an appropriate choice for the purpose of this study.

4.2.3 Objective Function

An objective function (weighted average of objective terms) is an expression of a single or multiple quantities that is designed to achieve a certain goal, which is often a minimum or maximum value. For example, the purpose of the history matching exercise for this report is to minimize the error between the historical data (fine gridded models) with the simulated data (coarse gridded models). As previously mentioned, the quantities that were targeted were cumulative production values: (1) cumulative oil production, (2) cumulative water production and (3) cumulative steam injection. The weighting assigned to each parameter was identical because the target is to minimize the 'Total Error' for the history match while honouring all three parameters with equal importance. This preference was also honoured with the influence matrix.

4.2.4 Influence Matrix

The influence matrix is a feature that permits the DECE method insight into which parameters will impact the objective function the greatest. The aim is to improve convergence times of the

runs. The CMG Manual states that the more likely a parameter is to affect the OF, the higher the value should be, with a maximum value assignment of 1.0. As engineering judgment is required to pre-identify the impact upon certain parameters to the objective function, it was concluded that the possibility of influence for all parameters should be held constant and uniform, so as not to introduce a basis based upon the conclusions of select models. Since no sensitivity analysis was performed to evaluate of the impact of the certain variables, no basis was formed to make such decisions. In addition, the number of parameters is relatively small, given some history matching exercises, so the DECE method was given control over the extent of influence. As indicated in **Table 4.2.4.1**, the influence matrix is configured in the following manner, with the value '1' representing 'Definitively Yes (1.0)' possibility of influence.

Table 4.2.4.1 – Influence Matrix

	Cumulative Oil Produced	**Cumulative Water Produced**	**Cumulative Steam Injected**
PERM, *i*	1	1	1
PERM, *j*	1	1	1
TH, *i*	1	1	1
TH, *j*	1	1	1

4.2.5 Constraints

No constraints on the optimization parameters were employed during the history matching exercise. The purpose of the constraints is to prevent unnecessary simulation runs and allow the user to change objective function values if constraints are violated. However, based upon the parameter ranges provided in the 'Parameter' section the use of hard or soft constraints was not employed.

4.2.6 Run Configurations

Configuration of the CMOST™ engine is an important step for processing of simulation runs. Due to the hardware and software constraints imposed upon the user, all jobs were run locally using a single processor. The criteria defined for an optimal solution was when the best solution set differed by less than 1% of the original. Of the optimal solutions, the data-decks of the top three results were kept for organization and presentation of the raw data.

4.3 Comparison of Preliminary Results

After post-processing the preliminary data, it was noted that the application of dynamic upscaling parameters with the coarse model generated a strong match to the fine model. As highlighted in the following section, and quantified in **Table 4.3.1**, the improvement to the cumulative production characteristics is significant. For the information presented below, the percentage improvement is approximately 75% of the 'Original Error.'

Table 4.3.1 – Binary Model Results, 5% Shale Distribution (Model A)

Ranking	CMOST Job ID	Objective Function		Cumulative Oil Produced		Cumulative Water Produced		Cumulative Steam Injected	
		Original Error (%)	Final Error (%)	Original Error (%)	Final Error (%)	Original Error (%)	Final Error (%)	Original Error (%)	Final Error (%)
1	600	7.43	1.82	8.46	2.34	7.20	1.66	6.63	1.47
2	404	7.43	1.83	8.46	2.41	7.20	1.62	6.63	1.46
3	580	7.43	1.83	8.46	2.40	7.20	1.63	6.63	1.47

The method of error calculation is an important process, so it is valuable to discuss the various details. The 'Original Error' is the error between the coarse and fine models prior to application of matching parameters, as computed by CMOST™. The 'Final Error' is the error between the coarse and fine models when applying the matching parameters as suggested by the 'best job' scenarios to the base coarse model. This is the primary output of the CMOST™ results file (.CMR). The 'Delta Error' can be thought of the improvement in result by applying the matching parameters. If a model distribution gives a small 'Delta Error', then the parameter values were less successful in mitigating the impact of the variation in gridding and reservoir properties relative to a large 'Delta Error'. However, inherently, the matching parameters can only improve the base model a certain percentage and a perfect 'Final Error' can never be obtained.

The same rules apply for cumulative oil produced, cumulative water produced and cumulative steam injected error notation. Also, the CMOST™ Job ID varies from one history matching exercise to another, as it represents the particular run that achieved that solution, which is to be expected to vary in such a process. For example, in the aforementioned model, the 'best job' or 'best case' was achieved after the 600th simulation.

Table 4.3.2 – Binary Model Results, 5% Shale Distribution (Model A)

Ranking	CMOST Job ID	Objective Function	Cumulative Oil Produced	Cumulative Water Produced	Cumulative Steam Injected
		Delta Error (%)			
1	600	5.61	6.12	5.54	5.16
2	404	5.60	6.05	5.58	5.17
3	580	5.60	6.04	5.57	5.16

The matching parameters generated by CMOST™ are highlighted in **Table 4.3.3**, in which the multiplier values were selected from the range provided in the parameters section of the CMOST™ task file.

Table 4.3.3 – Matching Parameters Assigned by CMOST™, 5% Shale Distribution (Model A)

Ranking	CMOST Job ID	PERM, *i*	PERM, *j*	TH, *i*	TH, *j*
1	600	1.56	8.13	1.00	7.42
2	404	1.56	9.25	1.00	13.83
3	580	1.56	9.63	1.00	10.92

An obvious observation in the result between Job ID 600 and 404 is that almost a nominal change in the 'Delta Error' results despite significant changes in the PERM, j and TH, j multipliers. Approximately a 12% reduction in PERM, j and a 46% reduction in TH, j resulted in a ~0.01% improvement to the match. In this way, the values generated by any particular case should not been seen as absolute but a guideline in terms of predicting matching success.

The application of the results as indicated above is presented as a production profile in **Figure 4.3.1** and visually in **Figures 4.3.2 – 4.3.4**.

Figure 4.3.1 – Production Profile of Coarse Model, Fine Model and Matched Coarse Model Performance, 5% Shale Distribution (Model A)

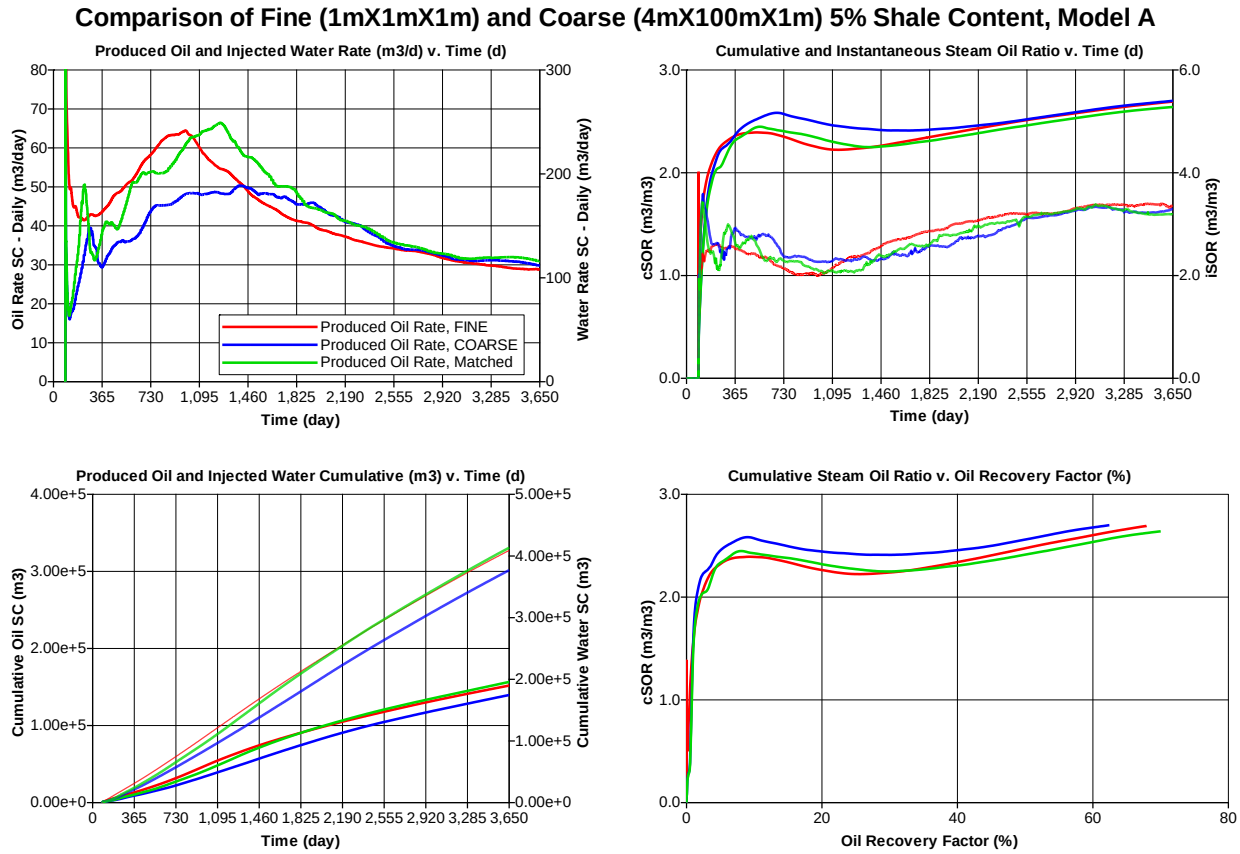

Figure 4.3.2 – Coarse Model, Chamber Conformance at 5 Years, Temperature

***i, k*-direction** ***i, j*-direction**

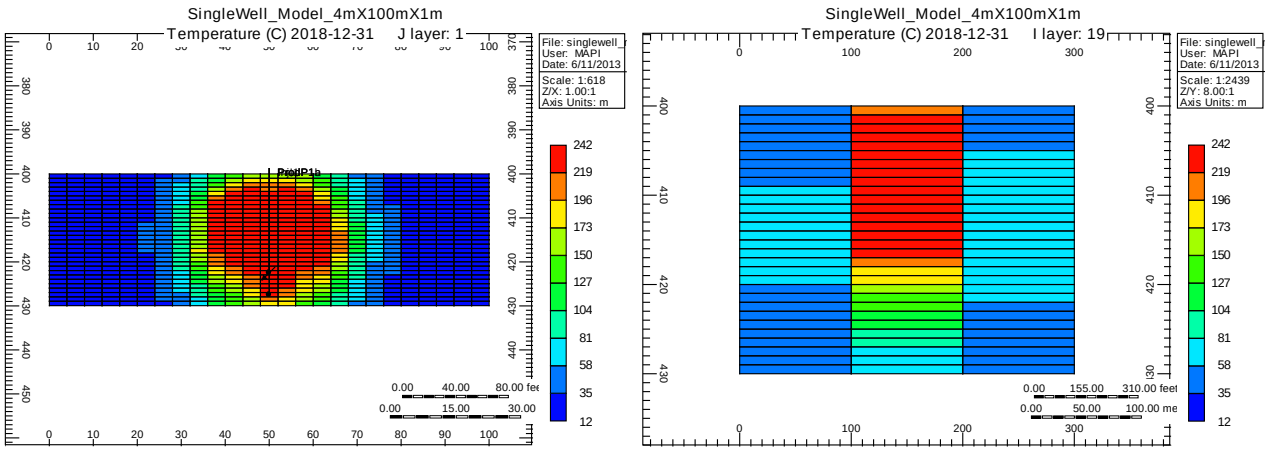

Figure 4.3.3 – Fine Model, Chamber Conformance at 5 Years, Temperature

***i, k*-direction** ***i, j*-direction**

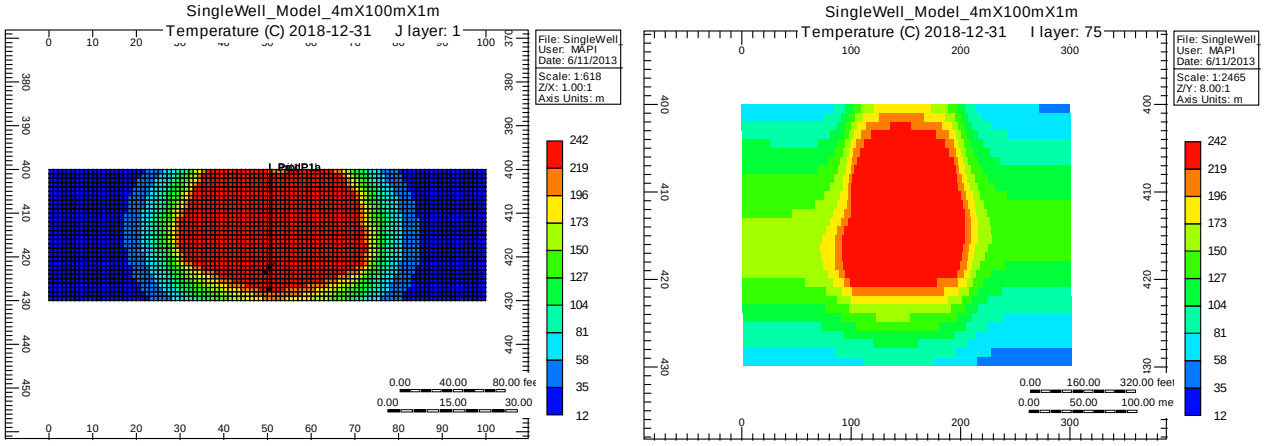

Figure 4.3.4 – Matched Model, Chamber Conformance at 5 Years, Temperature

***i, k*-direction** ***i, j*-direction**

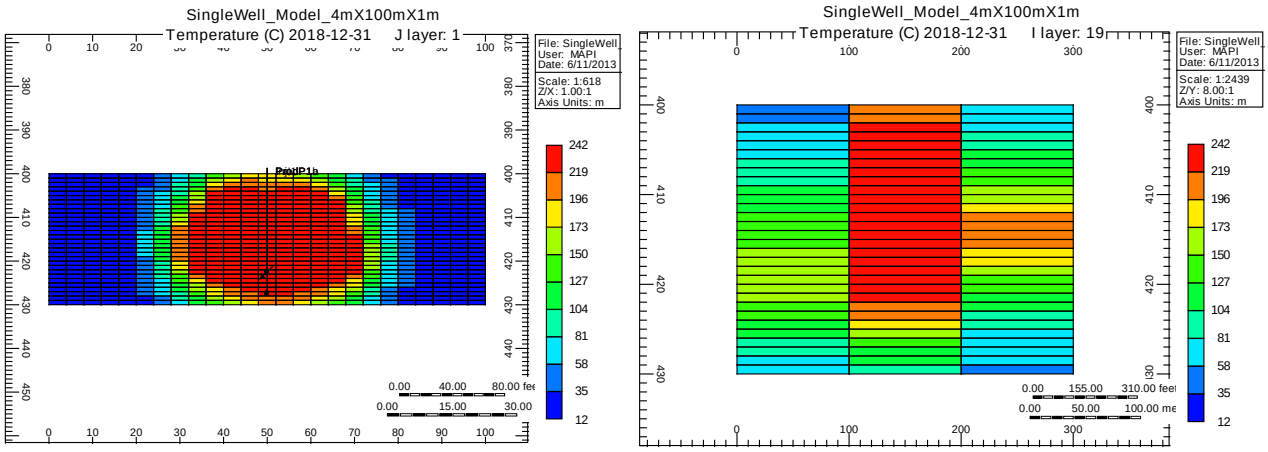

4.4 Non-Unique Solutions

During the course of the analysis, it was also observed the DECE optimization method was capable of generating non-unique solutions for the same model distributions. Based upon how the process searches for the optimal solution, it is possible this phenomenon could occur. For example, the distribution emphasised in the prior section was analysed with two separate history-matching runs. Based upon those two unique runs, a different set of output was generated. The optimal ‘best job’ values and the third ‘best job’ values were the same, but the second ‘best job’ values were different. Additionally, for another distribution, while the third ‘best job’ of the first unique solution was the second ‘best job’ from the second solution set the remaining results were different.

However, for both sets of distributions the ‘Delta Error’ generated for each solution set were the same. To iterate **Section 4.3**, it can be further concluded that different combinations of the parameters can generate comparable, if not identical results. This is an important conclusion prior to the organization and analysis of the data. The user can manipulate some of the results, as long as the improvement to the base models is maximized.

Tables 4.4.1 – 4.4.2 summarizes the variation in history matching runs as mentioned above. The rows that are highlighted in red represent those solutions that are the same in terms of error assignment. Whereas, **Tables 4.4.3 – 4.4.6** highlight the exact same issue with a different percentage shale distribution for a different set of runs.

Table 4.4.1 – Alternative Binary Model Results, 5% Shale Distribution (Model A)

Ranking	CMOST Job ID	Objective Function		Cumulative Oil Produced		Cumulative Water Produced		Cumulative Steam Injected	
		Original Error (%)	Final Error (%)	Original Error (%)	Final Error (%)	Original Error (%)	Final Error (%)	Original Error (%)	Final Error (%)
1	881	7.43	1.82	8.46	2.34	7.20	1.66	6.63	1.47
2	906	7.43	1.83	8.46	2.55	7.20	1.50	6.63	1.43
3	800	7.43	1.83	8.46	2.40	7.20	1.63	6.63	1.47

Table 4.4.2 – Alternative Matching Parameters Assigned by CMOST™, 5% Shale Distribution (Model A)

Ranking	CMOST Job ID	PERM, *i*	PERM, *j*	TH, *i*	TH, *j*
1	881	1.56	8.13	1.00	7.42
2	906	1.63	8.88	1.00	9.17
3	800	1.56	9.63	1.00	10.92

Table 4.4.3 – Binary Model Results, 1% Shale Distribution (Unique Solution #1)

Ranking	CMOST Job ID	Objective Function		Cumulative Oil Produced		Cumulative Water Produced		Cumulative Steam Injected	
		Original Error (%)	Final Error (%)	Original Error (%)	Final Error (%)	Original Error (%)	Final Error (%)	Original Error (%)	Final Error (%)
1	826	5.26	1.40	5.41	1.59	5.34	1.38	5.02	1.23
2	950	5.26	1.40	5.41	1.54	5.34	1.43	5.02	1.25
3	707	5.26	1.41	5.41	1.58	5.34	1.40	5.02	1.24

Table 4.4.4 – Matching Parameters Assigned by CMOST™, 1% Shale Distribution (Unique Solution #1)

Ranking	CMOST Job ID	PERM, *i*	PERM, *j*	TH, *i*	TH, *j*
1	826	1.13	8.13	1.17	2.17
2	950	1.13	8.13	1.17	5.67
3	707	1.13	3.63	1.17	6.25

Table 4.4.5 – Binary Model Results, 1% Shale Distribution (Unique Solution #2)

Ranking	CMOST Job ID	Objective Function		Cumulative Oil Produced		Cumulative Water Produced		Cumulative Steam Injected	
		Original Error (%)	Final Error (%)	Original Error (%)	Final Error (%)	Original Error (%)	Final Error (%)	Original Error (%)	Final Error (%)
1	655	5.26	1.40	5.41	1.59	5.34	1.38	5.02	1.23
2	623	5.26	1.41	5.41	1.58	5.34	1.40	5.02	1.24
3	659	5.26	1.41	5.41	1.63	5.34	1.37	5.02	1.24

Table 4.4.6 – Matching Parameters Assigned by CMOST™, 1% Shale Distribution (Unique Solution #2)

Ranking	CMOST Job ID	PERM, *i*	PERM, *j*	TH, *i*	TH, *j*
1	655	1.13	3.25	1.17	6.25
2	623	1.13	3.63	1.17	6.25
3	659	1.13	3.25	1.17	7.42

Figure 4.4.1 – Production Profile of Coarse Model, Fine Model and Matched Coarse Models Performance for both Unique Solution Sets, 1% Shale Distribution (Optimal 'Best Job')

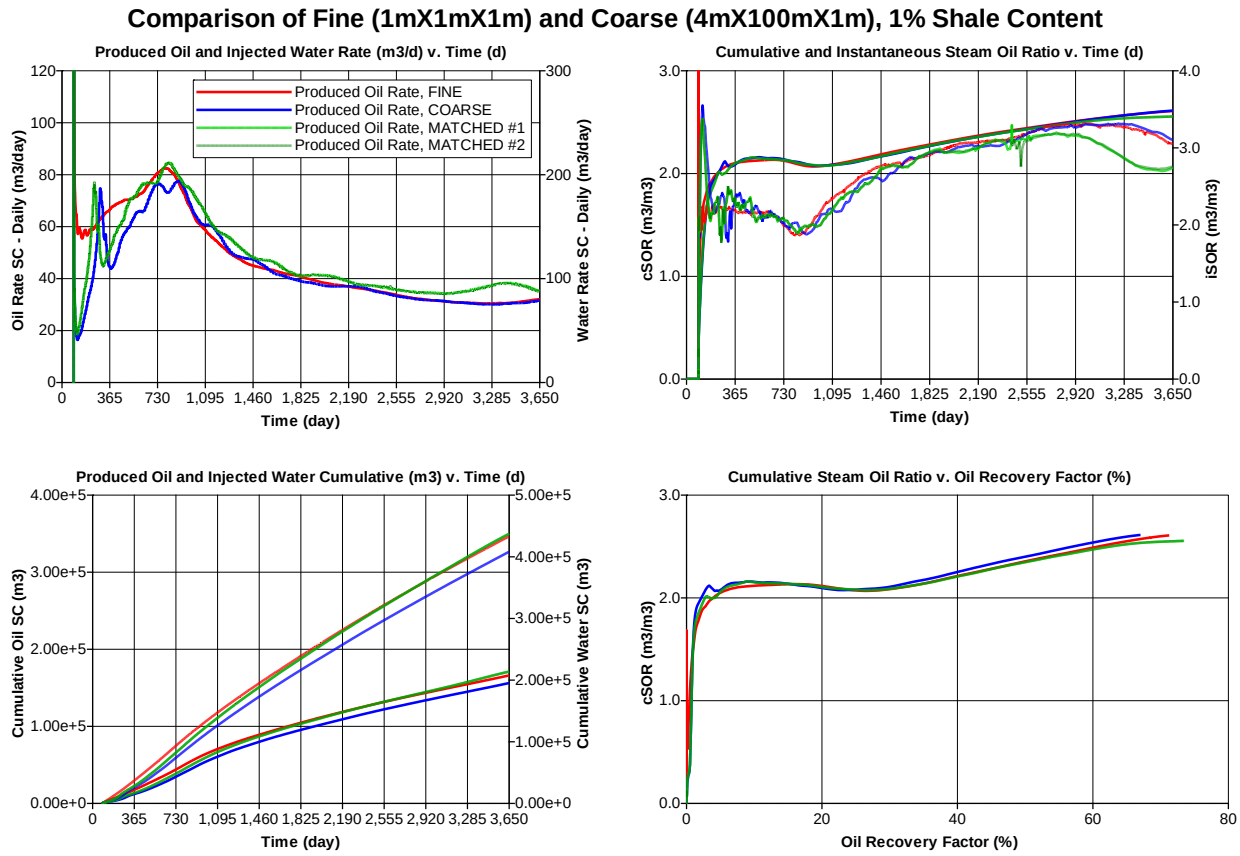

Despite different solution sets resulting in a different combination of parameter values, the impact to the 'Final Error' is nominal, as well as the improvement to the production profile. While the production profiles are not identical for different parameter values of the same 'Final Error', the cumulative profiles are effectively identical and all work to minimize the 'Final Error.'

4.5 Organization of Raw Data

After successful completion of all the simulation runs, the raw data was organized and the extensive exercise of post-processing begun. Several approaches were conceived to best represent the data without biasing or influencing the results. The objective was to analyze the impact of different length scales for altered petrophysical arrangements to determine if an analytical relationship could be generated to more accurately track temperature fronts in the reservoir. Ideally, the history matching exercise would also indirectly serve as a sensitivity analysis from the perspective that multiple runs with different inputs would enable the user to identify if one parameter was being weighted more heavily than other, which would be assumed to have the biggest impact upon performance. This would also be achieved by introducing no influence on parameter selection, and weighting their potential contribution equally.

Firstly, a linear relationship was generated to ensure that an increase in reservoir heterogeneities for a given grid dimension, resulted in an increase to 'Original Error'. This behaviour can also be assumed for 'Delta Error' provided that an increase in reservoir heterogeneity would allow more opportunity for improvement and only those models with the greatest 'Original Error' could be improved the greatest. That data is depicted in **Figure 4.5.1**.

Figure 4.5.1 - Relationship between Shale Content by Volume and Error Correlations for Binary Model, (4m, 100m, 1m)

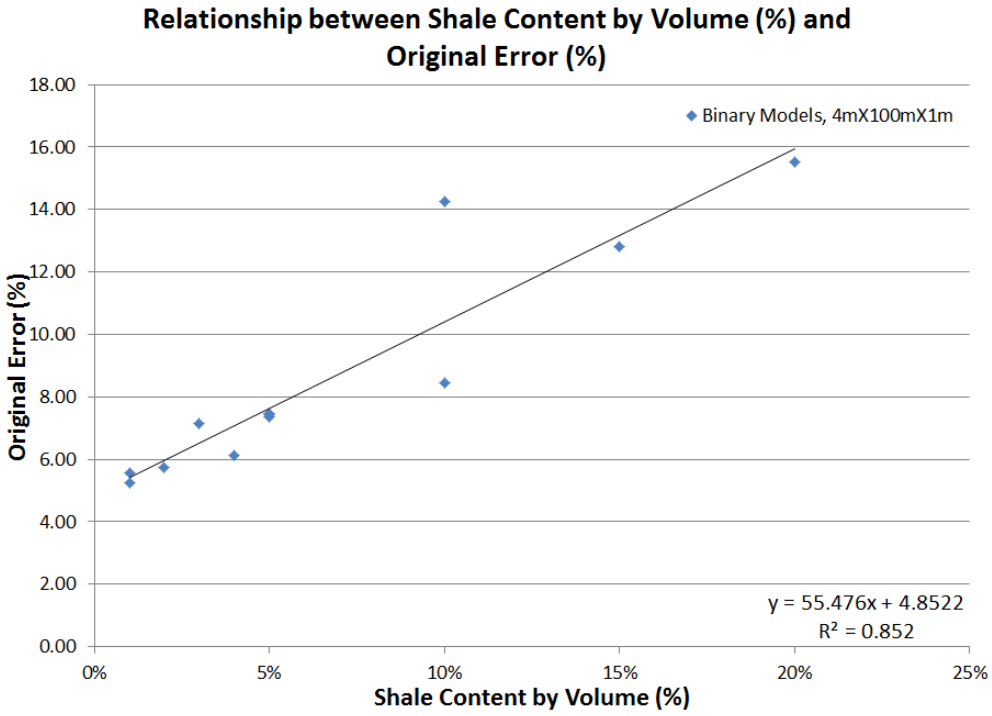

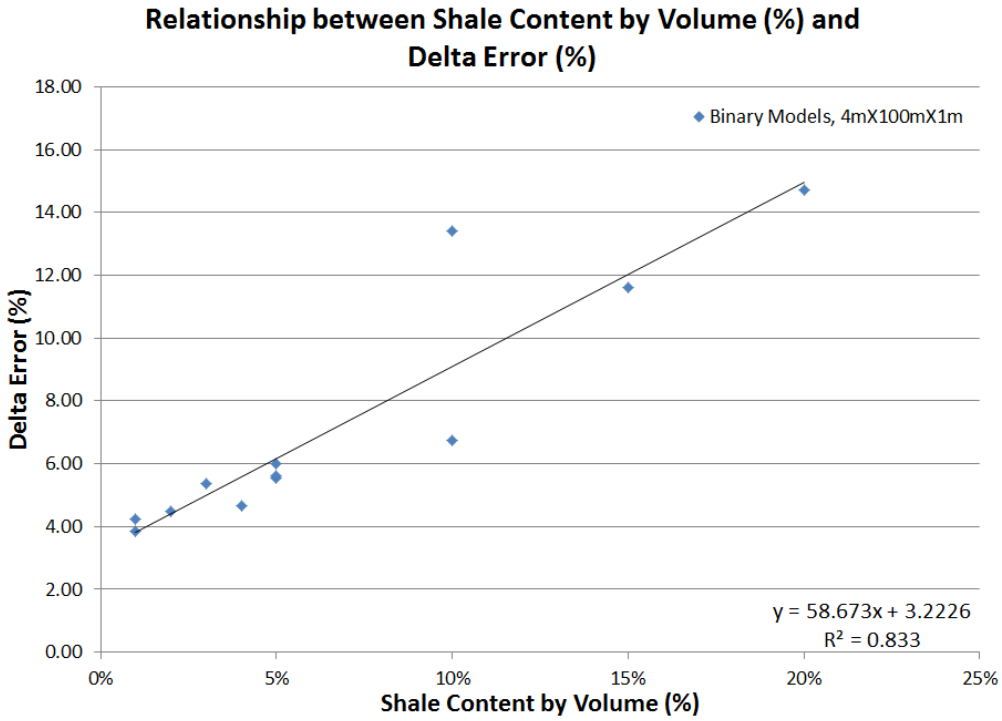

Secondly, cross-plots were generated for each parameter and their corresponding value with respect to 'Original Error' and 'Delta Error' was organized. Those results are summarized in **Figures 4.5.2** and **4.5.3** for the (4m, 100m, 1m) binary set of models. Data was organized for the other binary gird dimensions as well as the facies-based models, however, for ease of presentation and discussion only the (4m, 100m, 1m) cases are presented. The conclusions for the (4m, 100m, 1m) cases are applicable to the other type models.

Figure 4.5.2 – Cross-Plot of Parameter Values and 'Original Error' (%)

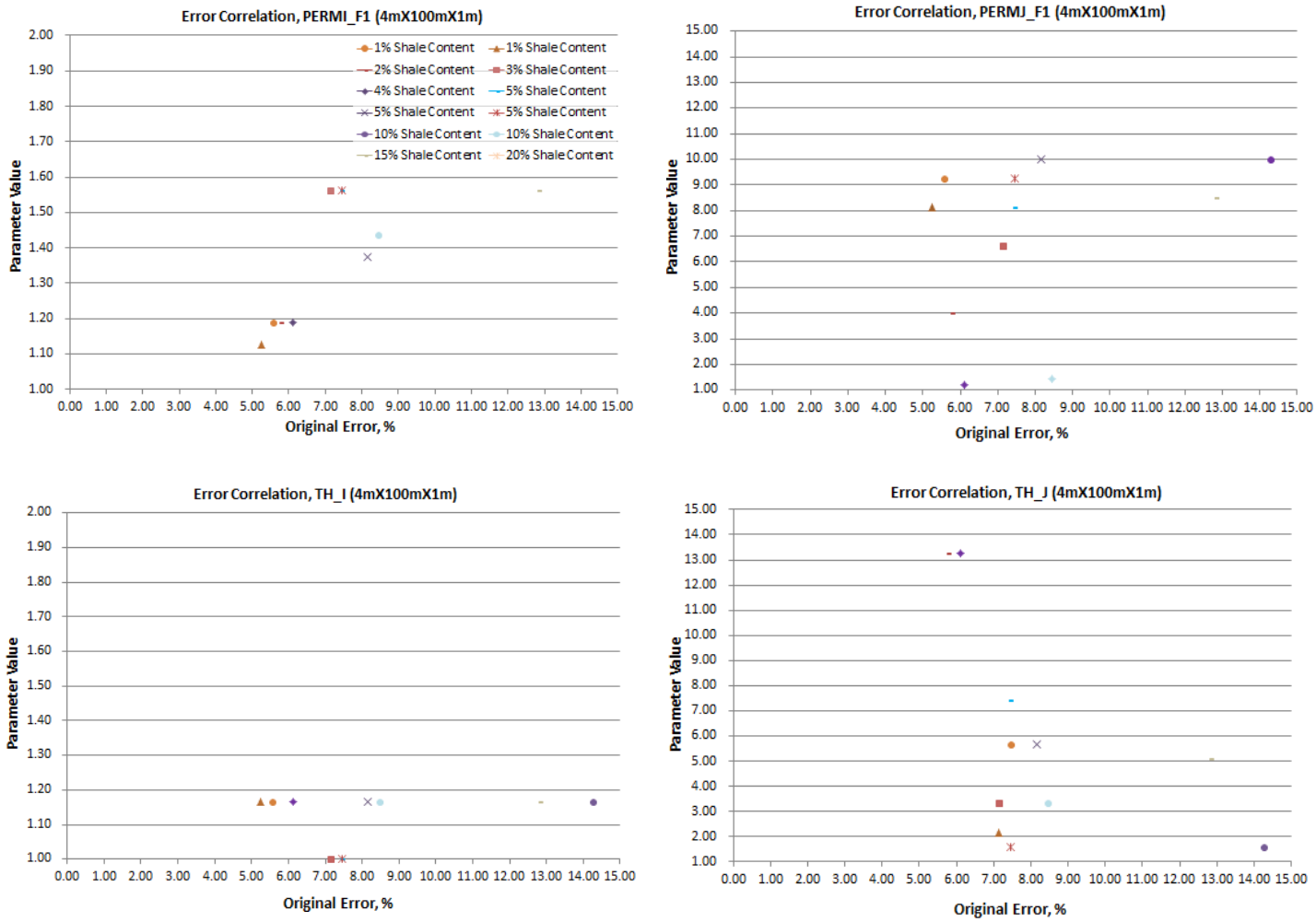

Figure 4.5.3 – Cross-Plot of Parameter Values and 'Delta Error' (%)

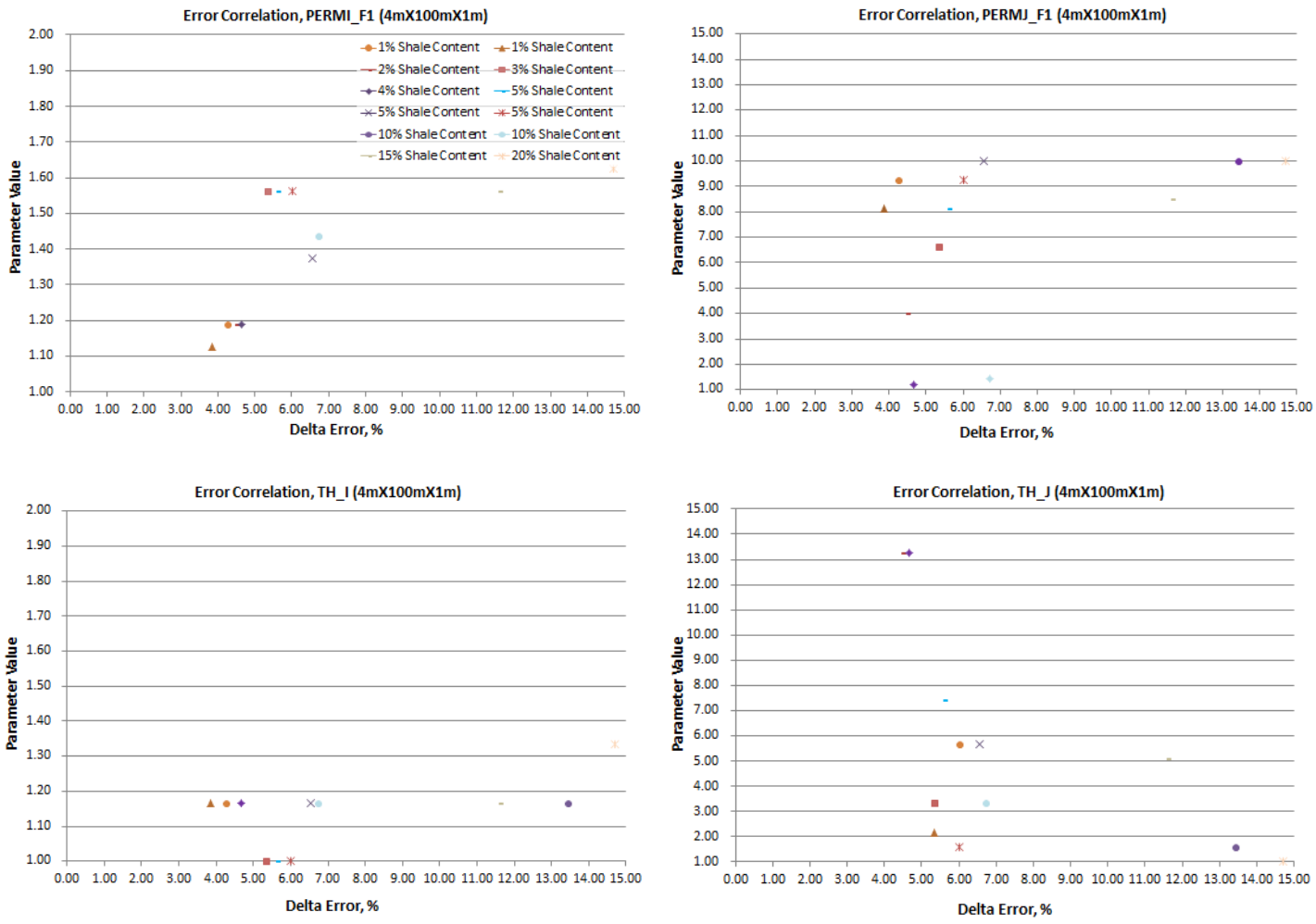

The principal challenge with this approach is it only partially takes into consideration the location of the reservoir heterogeneities relative to the injector and producer well. Therefore, there is some scatter present in the results that is difficult to build a correlation around. For example, the 'Original Error' plots have an instance of high reservoir quality (1% Shale Content) showing significantly more aggressive multipliers than a low reservoir quality case (10% Shale Content). This result is supported in **Table 4.5.1**.

Table 4.5.1 – Outliers in the 'Original Error' Cases (4m, 100m, 1m)

Type-A Binary Model Association	Original Error (%)	Parameters			
		PERM, *i*	**PERM, *j***	**TH, *i***	**TH, *j***
1% Shale Content	7.46	1.19	5.67	1.17	9.25
10% Shale Content	12.82	1.44	3.33	1.17	4.75

Additionally, the 'Delta Error' plots for the same parameters show a different observation. For a smaller magnitude of parameter values, a larger improvement in 'Delta Error' occurs, with the effect normalized by the Percent Improvement from 'Original Error' reference. This result is supported in **Table 4.5.2**.

Table 4.5.2 – Outliers in the 'Delta Error' Cases (4m, 100m, 1m)

Type-A Binary Model Association	Delta Error (%)	Percent Improvement from Original Error (%)	Parameters			
			PERM, *i*	**PERM, *j***	**TH, *i***	**TH, *j***
1% Shale Content	4.25	43.0	1.19	5.67	1.17	9.25
10% Shale Content	6.73	47.5	1.44	3.33	1.17	4.75

In general, there is no discernible trend between the 'Original Error' and the matching parameters. In that, the 'best job' values assigned do not offer any indication of which configurations have the most or least significant variation from the coarse to the fine models. However, the 'Delta Error' plots provide a clearer trend. The 'Delta Error' plots are effective in showing that an increase in parameter magnitude has a more significant impact upon reducing

the error between the coarse and fine models. There is a dependency of the magnitude of the parameters on matching the models, even if it is not understood which models are most likely to see certain values. Therefore, the goal moving forward is to refine this approach in order to enhance the relationship between parameter value and reservoir quality with gridding dependency.

Due to the petrophysical values assigned to the shale (Facies B) in the binary models or high proportion shale (Facies 3) in the facies-based models, no models have any inter-well gridblocks of these properties. As the occurrence of those facies types would prevent chamber development in that particular plane, and the overall performance would be independent of the distribution within the rest of the model. However, proximity of these reservoir facies relative to the well pair (such as, proximity above the injector well) will have significant impact on chamber signature and ultimate recovery. For example, if we review the coarsening upwards and fining upwards models generated in the facies-based exercise, the reservoir quality of a coarsening upwards sequence improves as you decrease depositional depth, whereas, the reservoir quality of the fining upwards sequence improves as you increase depth. Therefore, it is expected that the performance of the fining upwards model will tend to be better than the coarsening upwards model, as the best reservoir quality is closer to the well pair where the need to establish communication is of paramount importance for future chamber growth. Consequently, the poorer reservoir quality is closer to the overburden of the model which would only affect the later portion of the production profile. While the models may have the identical proportions of reservoir facies, the location alone will be the overriding factor for performance. The relative

performance of the coarse and fine model will be captured with respect the 'Original and Final Error', however, it is for that unique case.

Therefore, it can be concluded that the relationship of the fine model to the coarse models performance will vary with respect to the location of these heterogeneities within the model, despite identical proportions. For example, the performance of two models of identical proportions but distributed differently as presented in **Figures 4.5.4 – 4.5.7.** Upon review of the steam signatures and production profiles, it is easy to appreciate the spatial impact.

Figure 4.5.4 – Production Profile of Coarse and Fine Model Performance, 5% Shale Distribution (Model #1)

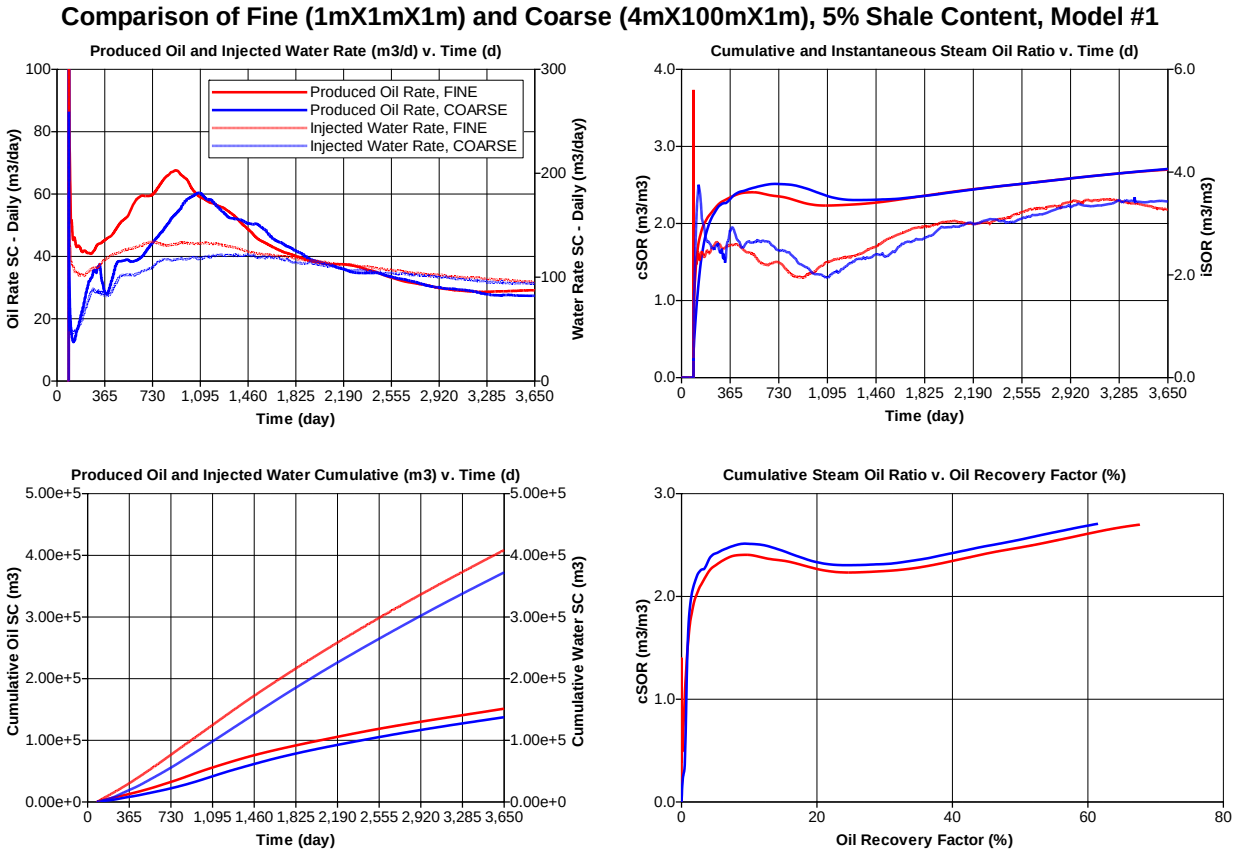

Figure 4.5.5 – Production Profile of Coarse and Fine Model Performance, 5% Shale Distribution (Model #2)

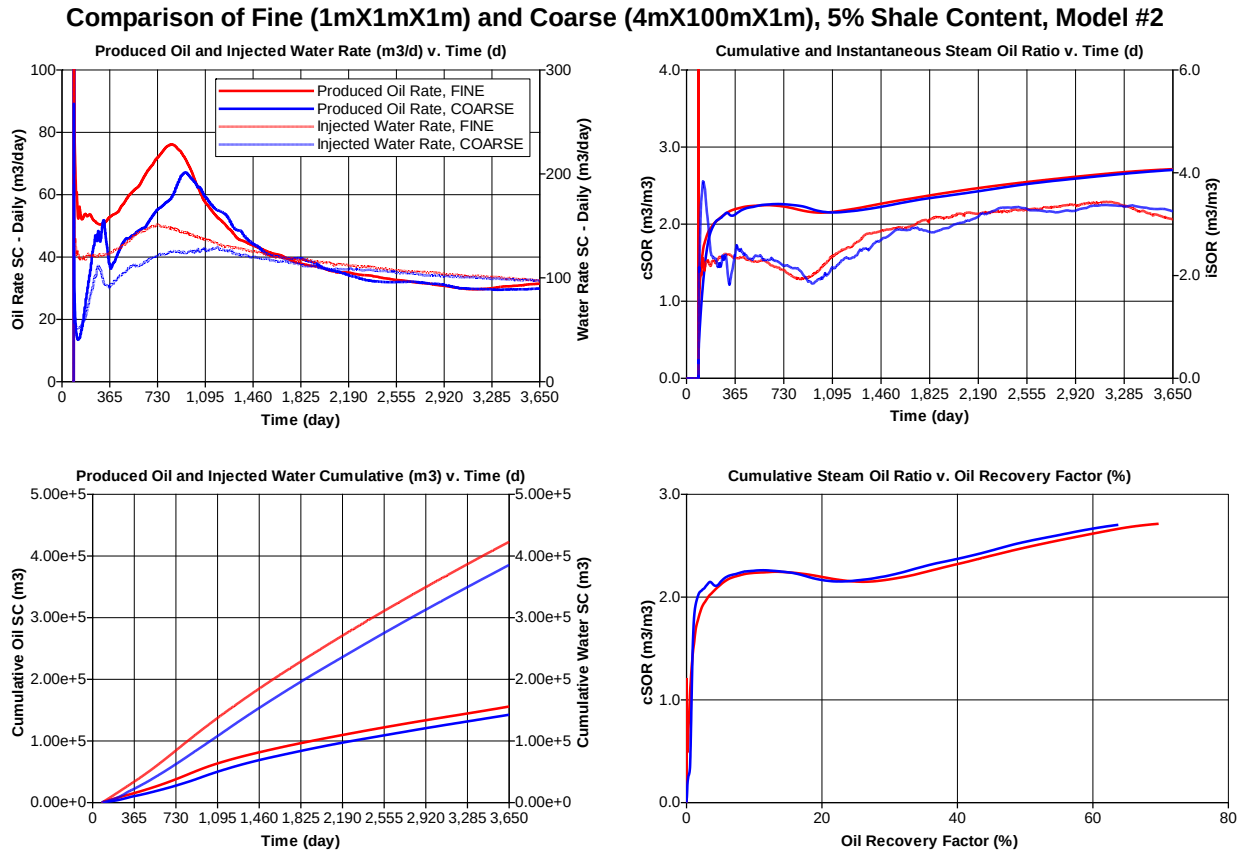

Figure 4.5.6 – Production Profile of Coarse Model #1 and Coarse Model #2 Performance (5% Shale Distribution)

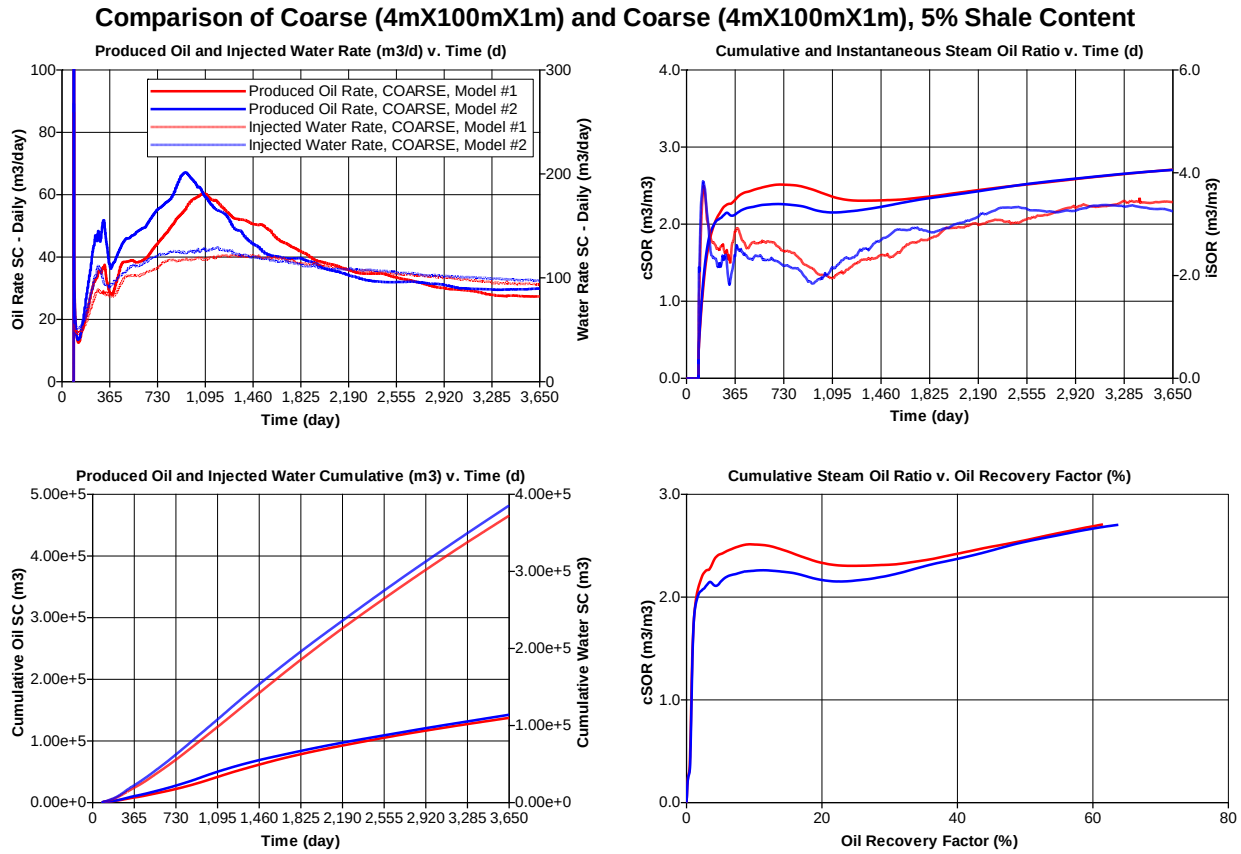

Figure 4.5.7 – Production Profile of Fine Model #1 and Fine Model #2 Performance (5% Shale Distribution)

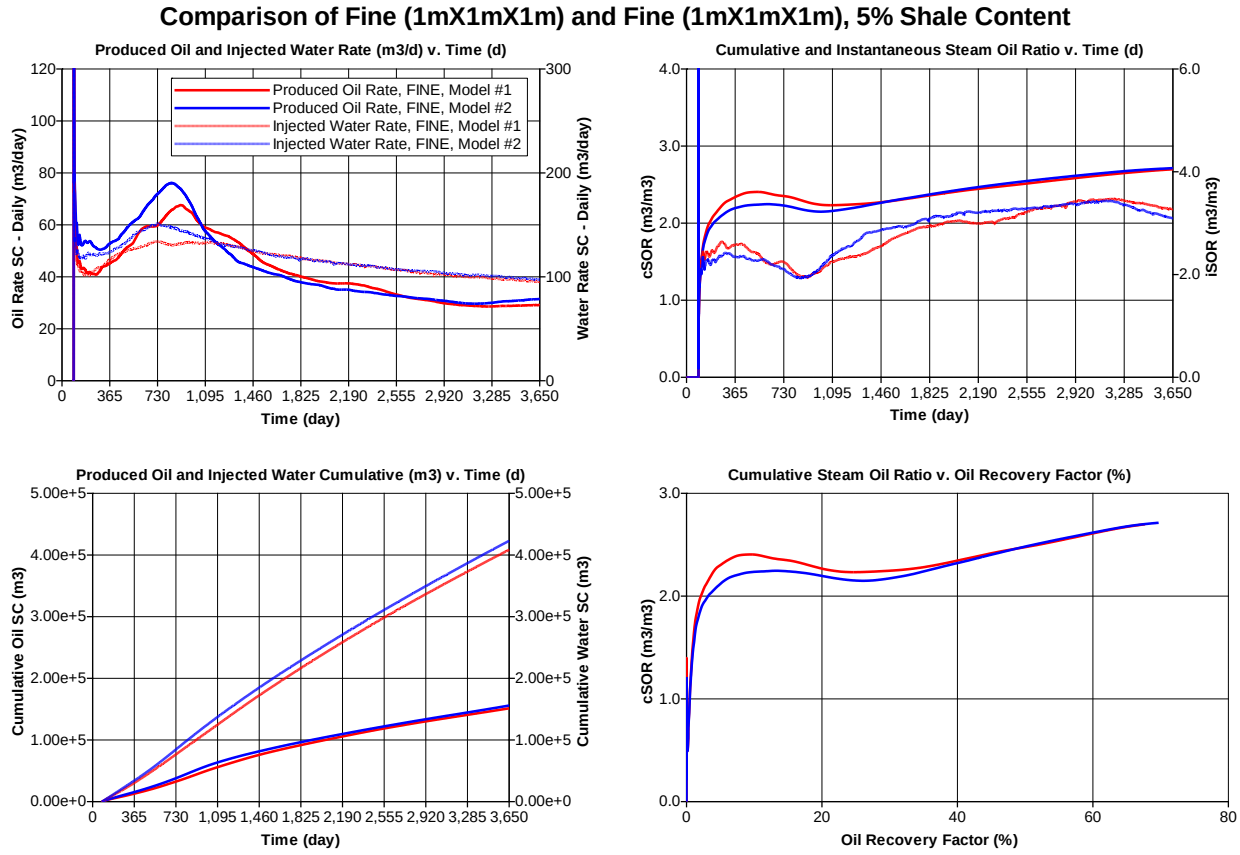

Table 4.5.3 – Binary Model Results, 5% Shale Distribution (Model #1), 'Original and Final Error'

Ranking	CMOST Job ID	Objective Function		Cumulative Oil Produced		Cumulative Water Produced		Cumulative Steam Injected	
		Original Error (%)	Final Error (%)	Original Error (%)	Final Error (%)	Original Error (%)	Final Error (%)	Original Error (%)	Final Error (%)
1	558	7.46	1.46	7.98	1.90	7.42	1.23	6.99	1.24
2	744	7.46	1.46	7.98	1.64	7.42	1.42	6.99	1.33
3	823	7.46	1.46	7.98	1.91	7.42	1.23	6.99	1.25

Table 4.5.4– Binary Model Results, 5% Shale Distribution (Model #1), 'Delta Error'

Ranking	CMOST Job ID	Objective Function	Cumulative Oil Produced	Cumulative Water Produced	Cumulative Steam Injected
		Delta Error (%)			
1	558	6.00	6.08	6.19	5.75
2	744	6.00	6.34	6.00	5.66
3	823	6.00	6.07	6.19	5.74

Table 4.5.5 – Matching Parameters Assigned by CMOST™, 5% Shale Distribution (Model #1)

Ranking	CMOST Job ID	PERM, *i*	PERM, *j*	TH, *i*	TH, *j*
1	558	1.56	9.25	1.00	1.58
2	744	1.50	10.00	1.00	14.42
3	823	1.56	9.25	1.00	2.75

Table 4.5.6 – Binary Model Results, 5% Shale Distribution (Model #2)

Ranking	CMOST Job ID	Objective Function		Cumulative Oil Produced		Cumulative Water Produced		Cumulative Steam Injected	
		Original Error (%)	Final Error (%)	Original Error (%)	Final Error (%)	Original Error (%)	Final Error (%)	Original Error (%)	Final Error (%)
1	648	7.35	1.82	7.36	2.12	7.57	1.75	7.10	1.58
2	538	7.35	1.82	7.36	2.15	7.57	1.73	7.10	1.58
3	627	7.35	1.82	7.36	2.14	7.57	1.74	7.10	1.58

Table 4.5.7 – Binary Model Results, 5% Shale Distribution (Model #2)

Ranking	CMOST Job ID	Objective Function	Cumulative Oil Produced	Cumulative Water Produced	Cumulative Steam Injected
		Delta Error (%)			
1	648	5.53	5.24	5.82	5.52
2	538	5.53	5.21	5.84	5.52
3	627	5.53	5.22	5.83	5.52

Table 4.5.8 – Matching Parameters Assigned by CMOST™, 5% Shale Distribution (Model #2)

Ranking	CMOST Job ID	PERM, *i*	PERM, *j*	TH, *i*	TH, *j*
1	648	1.31	8.50	1.17	11.50
2	538	1.31	10.00	1.17	12.67
3	627	1.31	9.63	1.17	10.33

Table 4.5.9 – 'Best Job' Matching Parameters Assigned by CMOST™

Model	CMOST Job ID	PERM, *i*	PERM, *j*	TH, *i*	TH, *j*
#1	558	1.56	9.25	1.00	1.58
#2	648	1.31	8.50	1.17	11.50

Fundamentally, these are very similar models yet the matching values proposed by CMOST™ vary significantly for thermal conductivity in the *j*-direction. The other values are fairly comparable, however, the difference in value for the thermal conductivity parallel the wellbore is significant. While noted here for the first time, this observation is a re-occurring trend within the analysis portion of the report that the thermal conductivity in the *j*-direction often has the most variation. A review of the results reported in **Sections 4.3** and **4.4** supports this conclusion. The values generated for those versions of binary models with 5% shale distribution are comparable to above.

Table 4.5.10 – 'Best Job' Matching Parameters Assigned by CMOST™

Model	CMOST Job ID	PERM, *i*	PERM, *j*	TH, *i*	TH, *j*
A	600	1.56	8.13	1.00	7.42

Figure 4.5.8 – Vertical Permeability Distribution of Binary Models (*i*, *k*-direction), 5% Shale Content

Model #1 **Model #2** **Model A**

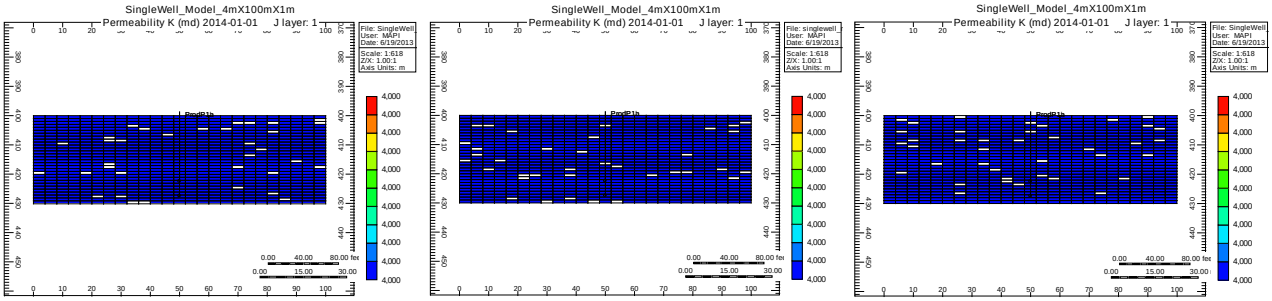

Figure 4.5.9 – Vertical Permeability Distribution of Binary Models (*i*, *j*-direction), 5% Shale Content

Model #1 **Model #2** **Model A**

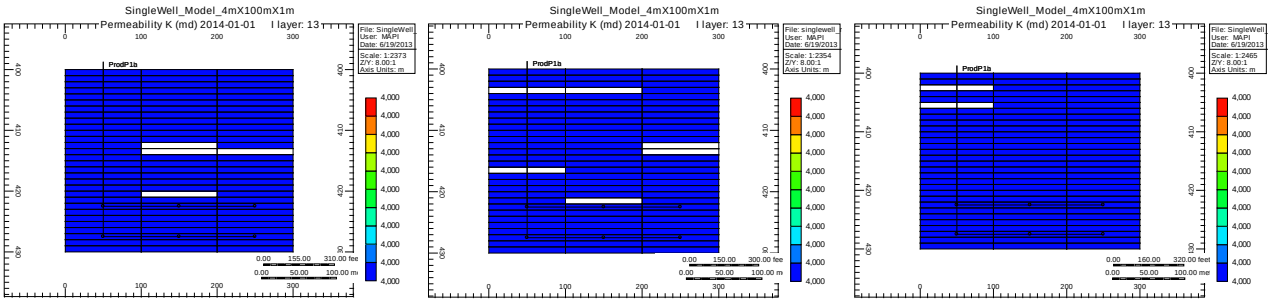

Figure 4.5.10 – Production Profile of Coarse Model #1, Model #2 and Model A Performance (5% Shale Distribution)

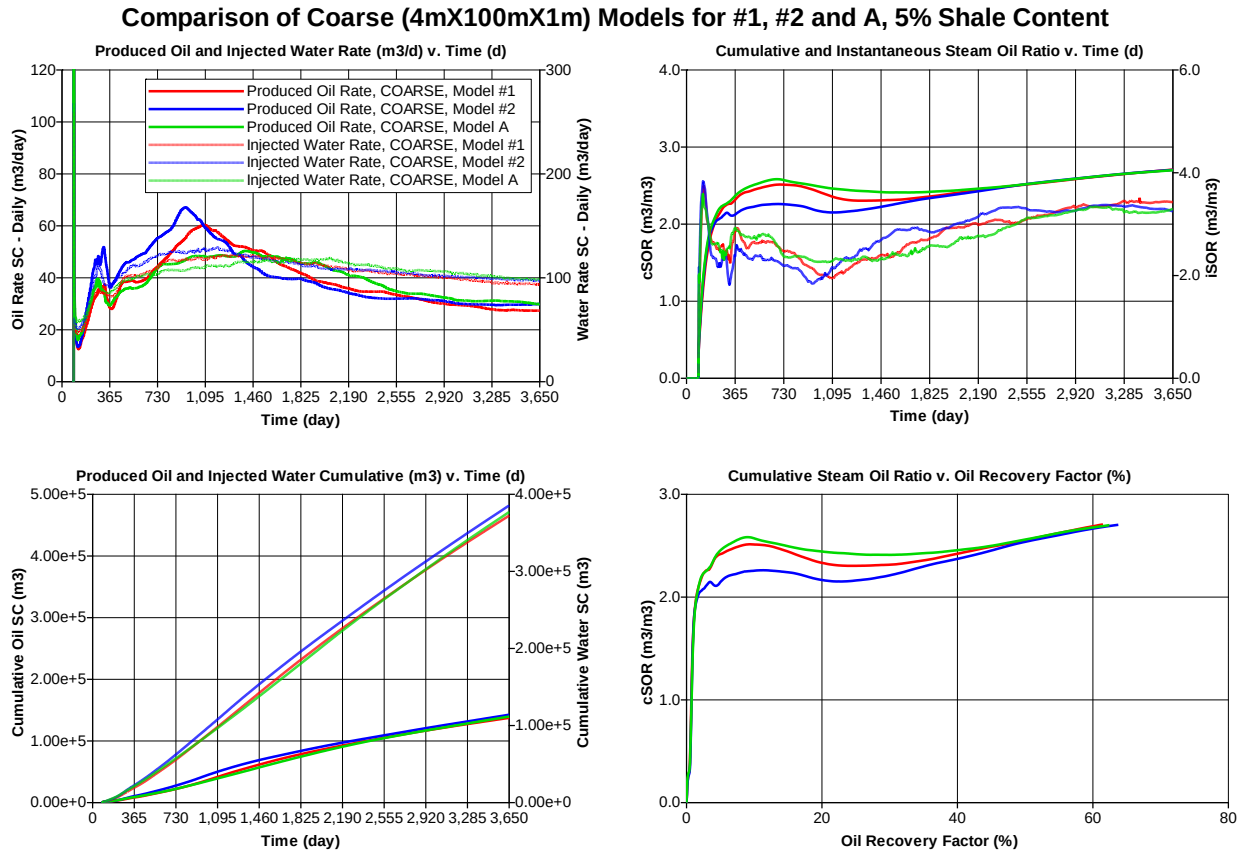

As observed in **Figures 4.5.4 – 4.5.7**, the distribution of non-reservoir relative to reservoir rock will impact early SAGD development. The impact to the rate of chamber growth will manifest itself by calling for more or less aggressive multipliers to offset the presence of those non-reservoir gridblocks. However, the exact choice of those multiplier values is not expertly known. Therefore, an additional technique to process the numerical results needs to be developed to confirm the quantity of reservoir heterogeneities and impact of the location. In developing a secondary approach for analyzing the data, the hope is additional observations will become apparent. CMG has recently developed a tool that can analyze several realizations of a static

reservoir model and provide an indication of productivity. CMG refers to this tool as the SAGD Productivity Index (SPI).

4.6 Normalization of Length Scale Impact

As described in **Section 3.11**, the concept of length scale relative to facies proportions was introduced. Given the magnitude of various parameters and the impact of reservoir heterogeneities relative to well placement, the following two concepts can be revisited:

- To what extent is reservoir quality over-riding the impact of length scales?
- To what extent do length scales drive reservoir performance?

To iterate **Tables 3.11.1** and **3.11.2**, the following result was proposed for two binary models.

Table 3.11.1 – Comparison of Length Scales and Heterogeneity on Coarse Model Performance

Model Type		**Objective Function, Original Error**	
		Coarse Model (%)	**Fine Model (%)**
4m, 100m, 1m (Type-A)	0% Shale Content (Homogenous Properties)	4.77	Reference
	10% Shale Content (Heterogeneous Properties)	8.46	Reference
2m, 25m, 1m (Type-F)	0% Shale Content (Homogenous Properties)	1.10	Reference
	10% Shale Content (Heterogeneous Properties)	3.41	Reference

Table 3.11.2 – Comparison of Length Scales and Heterogeneity on Relative Performance

Model Type		Objective Function, Difference in Error as a function of Shale Content (%)
4m, 100m, 1m (Type-A)	0% Shale Content (Homogenous Properties)	3.69
	10% Shale Content (Heterogeneous Properties)	
2m, 25m, 1m (Type-F)	0% Shale Content (Homogenous Properties)	2.31
	10% Shale Content (Heterogeneous Properties)	

Upon review of these models, it was observed that placement of reservoir heterogeneities was a dominant feature, in terms of its impact upon performance and the magnitude of the error values. For example, the aforementioned case has the following distribution of facies.

Figure 4.6.1 – Heterogeneous Model, Facies Distribution (*i*, *k*-direction), 10% Shale Content

4m, 100m, 1m Model

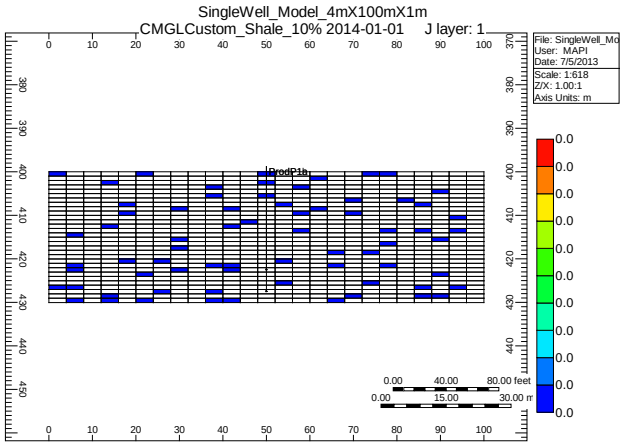

2m, 25m, 1m Model

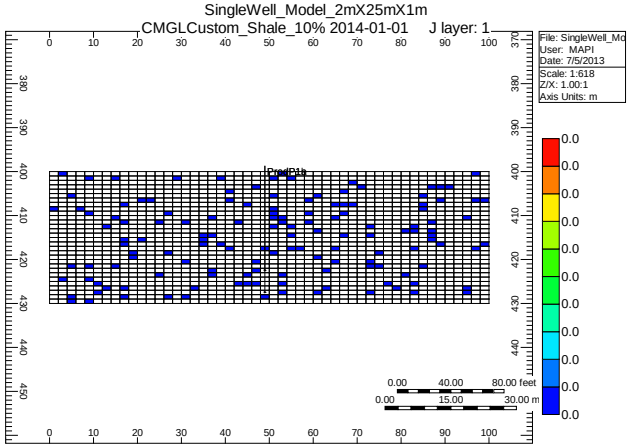

Figure 4.6.2 – Heterogeneous Model, Facies Distribution (*i*, *j*-direction), 10% Shale Content

4m, 100m, 1m Model **2m, 25m, 1m Model**

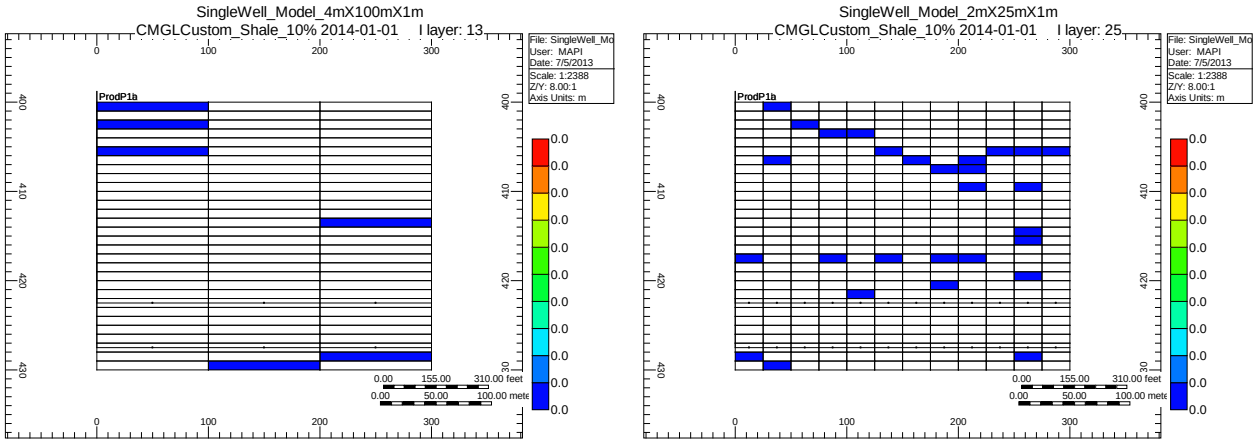

While it has been observed that there is a dependency on length scale when you normalize the volume of non-reservoir, it has also been observed that that dependency can be offset based upon re-alignment of those same proportions. The following set of models highlights that impact upon SAGD performance.

Figure 4.6.3 – Heterogeneous Model, Facies Distribution (*i*, *k*-direction), 10% Shale Content

4m, 100m, 1m Model **2m, 25m, 1m Model**

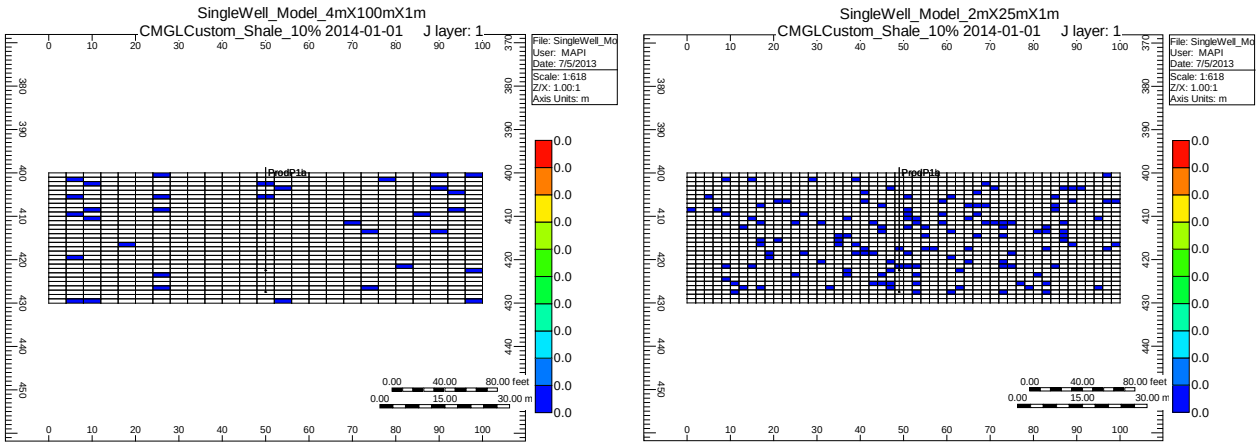

Figure 4.6.4 – Heterogeneous Model, Facies Distribution (*i*, *j*-direction), 10% Shale Content

4m, 100m, 1m Model **2m, 25m, 1m Model**

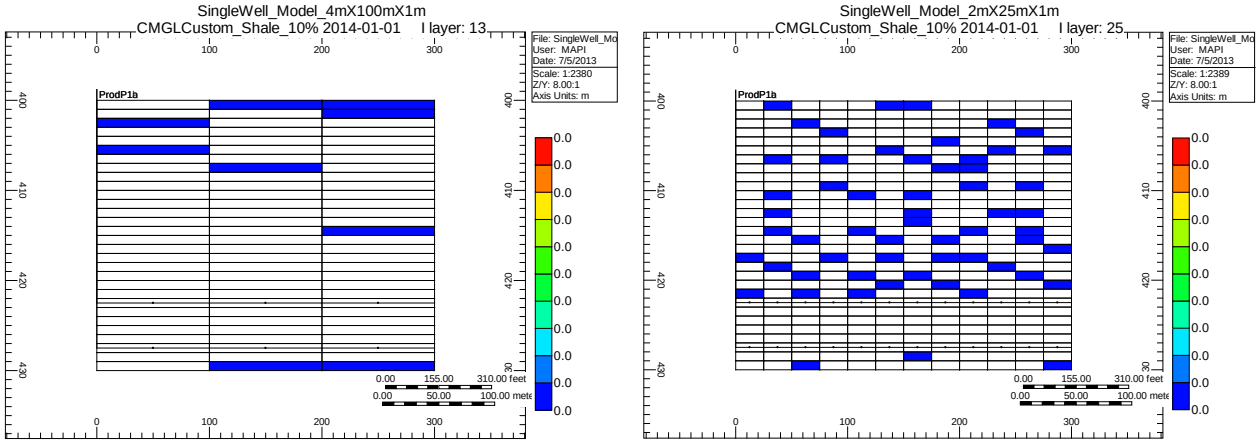

Table 4.6.1 – Revisited Comparison of Length Scales and Heterogeneity on Coarse Model Performance

Model Type		Objective Function, Original Error	
		Coarse Model (%)	Fine Model (%)
4m, 100m, 1m (Type-A)	0% Shale Content (Homogenous Properties)	4.77	Reference
	10% Shale Content (Heterogeneous Properties)	5.41	Reference
2m, 25m, 1m (Type-F)	0% Shale Content (Homogenous Properties)	1.10	Reference
	10% Shale Content (Heterogeneous Properties)	3.71	Reference

Table 4.6.2 – Revisited Comparison of Length Scales and Heterogeneity on Relative Performance

Model Type		Objective Function, Difference in Error as a function of Shale Content (%)
4m, 100m, 1m (Type-A)	0% Shale Content (Homogenous Properties)	0.64
	10% Shale Content (Heterogeneous Properties)	
2m, 25m, 1m (Type-F)	0% Shale Content (Homogenous Properties)	2.61
	10% Shale Content (Heterogeneous Properties)	

Given the same content of reservoir and non-reservoir rock types, the placement of the non-reservoir had a significant impact to the heterogeneous model relative to the fine model or reference case. The coarse model error for Type-A was significantly different, 8.46% and 5.41% respectively. However, the difference in coarse error was significantly less for the Type-F models, 3.41% and 3.71% respectively. The significant reduction in error for Type-A binary model and the increase in error for the Type-F binary model suggest the overriding impact of location of these reservoir heterogeneities as opposed to the length scale assignment itself. The author is not implying that length scale impact is negligible, but through the course of the analysis the hope is an error bar can be assigned to a given shale content for variable length scales, and the magnitude of length scale impact can be quantified. Given a realistic band of uncertainty, the analysis can be simplified for industry models with this variation perpendicular (4m or 2m) and parallel (100m, 50m or 25m) the wellbore.

This implication further motivates the need for a robust tool. The implementation of CMG's SAGD Productivity Index will help quantify the impact of different facies types and proportions while validating the use of these two parameters to recommend upscaling parameters, independent of the length scales discussed within the content of this report.

Figure 4.6.5 - Production Profile of Reconfigured Heterogeneous Distribution (Type-A, 10% Shale Content)

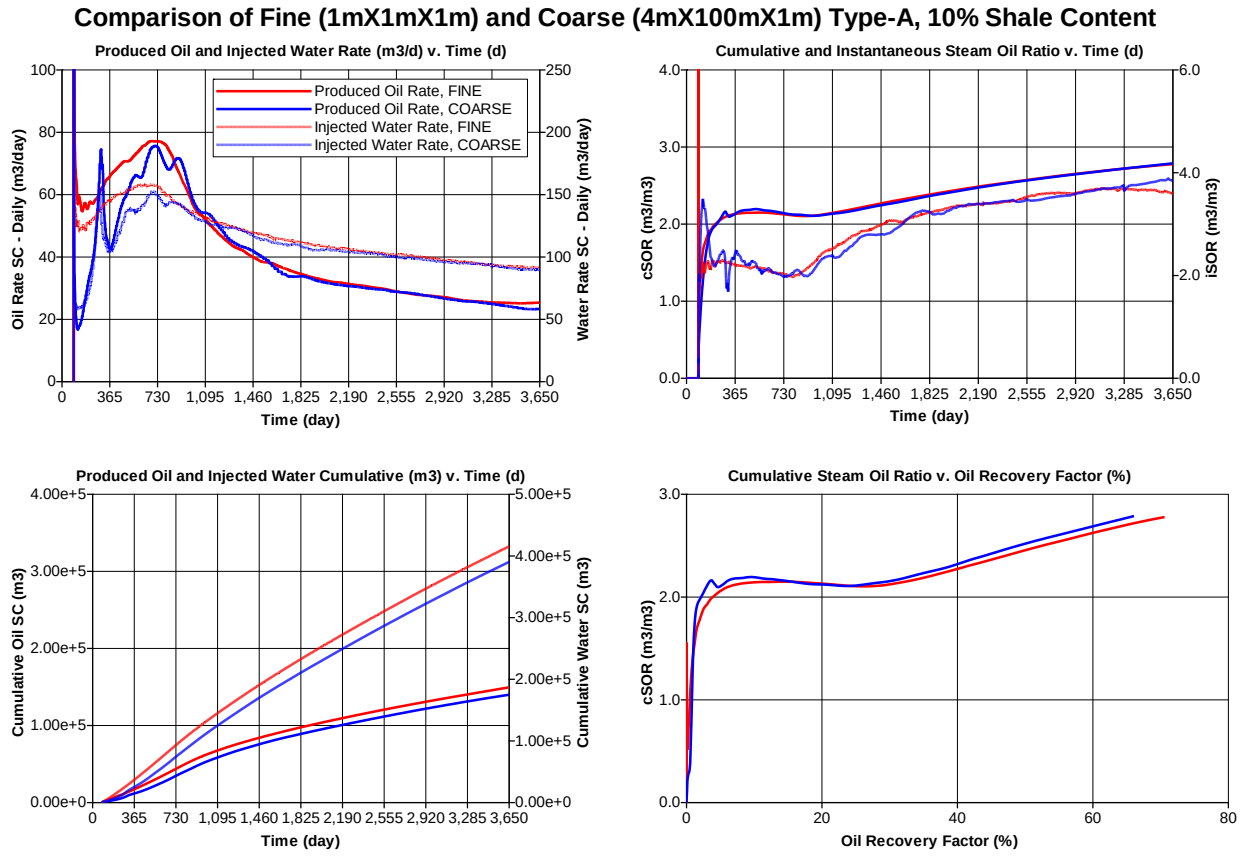

Figure 4.6.6 – Production Profile of Reconfigured Heterogeneous Distribution (Type-F, 10% Shale Content)

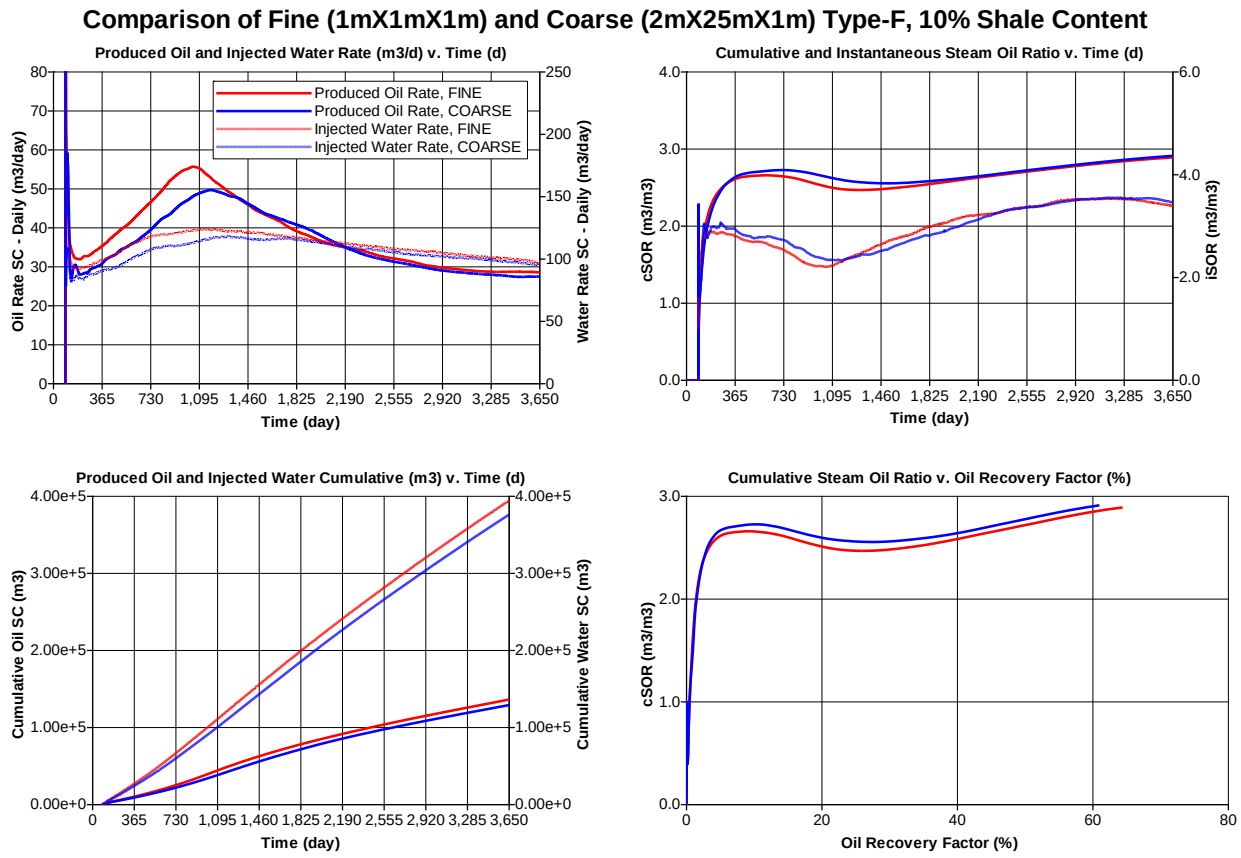

CHAPTER 5 – EVALUATION CRITERIA

5.1 SAGD Productivity Index

The SAGD Productivity Index tool was developed so geostatistical realizations can be quickly preprocessed to provide an indication of SAGD productivity prior to simulation. Based upon the ranking procedure implemented by many geomodellers, such as a net-continuous bitumen or bulk oil weight script, there can be a disconnect between the static ranking and the dynamic result, as location of reservoir heterogeneities with respect to well placement is not captured. Provided three realizations are generated for reservoir simulation studies (p10, p50 and p90), the results might not show a high, medium and low profile. Therefore, CMG has developed this mathematical tool to help streamline the process. The SAGD Productivity Index (SPI) for a realization is determined from the average optimum connectivity of the cells in the realization:

$$SPI = \frac{\sum_{i=Iprod-NI}^{Iprod+NI} \sum_{j=Jheel}^{Jtoe} \sum_{k=Kprod-NK}^{Kprod} C_{max}(i,j,k)}{(2*NI+1)*(Jtoe-Jheel+1)*(NK+1)} \quad (5.1.1)$$

As provided from CMG, *Iprod*, *Jheel*, *Jtoe* and *Kprod* indicate well pair location, with (*i, j, k*) indicating the location of the gridblock. Additionally, *NI*, *NK* indicates the approximate steam chamber size at the conclusion of the well pair's life, relative to the gridblock size[56]. Further details of the tool are attached in **Appendix C** in which CMG has published a brief description of all the components to the process.

5.1.1 SAGD Productivity Set-Up

The CMG SAGD ranking tool is a very straightforward instrument and only requires a few fundamental inputs. Firstly, the Builder^{TM} data files (.DAT) must be conditioned with the appropriate keywords. All the data arrays of interest, such as porosity or permeability, require the read option keyword '*ALL' be employed. For example, the porosity array is defined on the following basis:

**POR *ALL*
*Number of Gridblocks$_i$*Property Value$_i$ Number of Gridblocks$_{i+1}$*Property Value$_{i+1}$*

The 'Model Options' section within the tool requires an indication of growth potential as well as the directional permeability. The steam chamber size estimation was based upon a review of several representative models of different dimensions. It was concluded that chamber growth was approximately 80% of the vertical and 80% of the horizontal dimension during the life of the SAGD pair. That is a function of the fact that steam chamber development is first dominated by vertical chamber rise, then horizontal chamber development upon communication with the overburden. **Table 5.1.1.1** highlights the various inputs required to allow the model to have an SPI computed.

Table 5.1.1.1 – Model Options with CMG's SAGD Productivity Index (SPI), (4m, 100m, 1m) Grid Dimensions

Estimated Steam Chamber Size		
Height (gridblocks)	Width (gridblocks)	
24	20	
Gridblock Size		
i-direction (meters)	*j*-direction (meters)	*k*-direction (meters)
4	100	1
Clean Sand Permeability		
PERM, *i* (mD)	PERM, *j* (mD)	PERM, *k* (mD)
5,000	5,000	4,000

As a preliminary check, the productivity index of the three models mentioned earlier (Model A, Model #1 and Model#2) that have identical distributions (5% shale by volume) but with different spatial orientations, were first compared to ensure a difference in result was noted as a function of heterogeneity location,

Table 5.1.1.2 – Comparison of SAGD Productivity Index (SPI) of Model #1, Model #2 and Model A

Model	**Productivity Index**
Model #1	0.93397
Model #2	0.96063
Model A	0.95021

As indicated by the production profiles, Model #2 performs better in terms of production and thermal efficiency, so the incremental increase in productivity index is honoured in the well pair's performance. Whereas, the performance of Model #1 and Model A are very similar, which is reflected in their similar productivity index values.

Upon grouping all the productivity indexes for the binary models and facies-based models, there is a strong correlation between shale context and potential productivity.

Figure 5.1.1.1 – Relationship between Shale Content by Volume and SAGD Productivity Index for all Binary Models

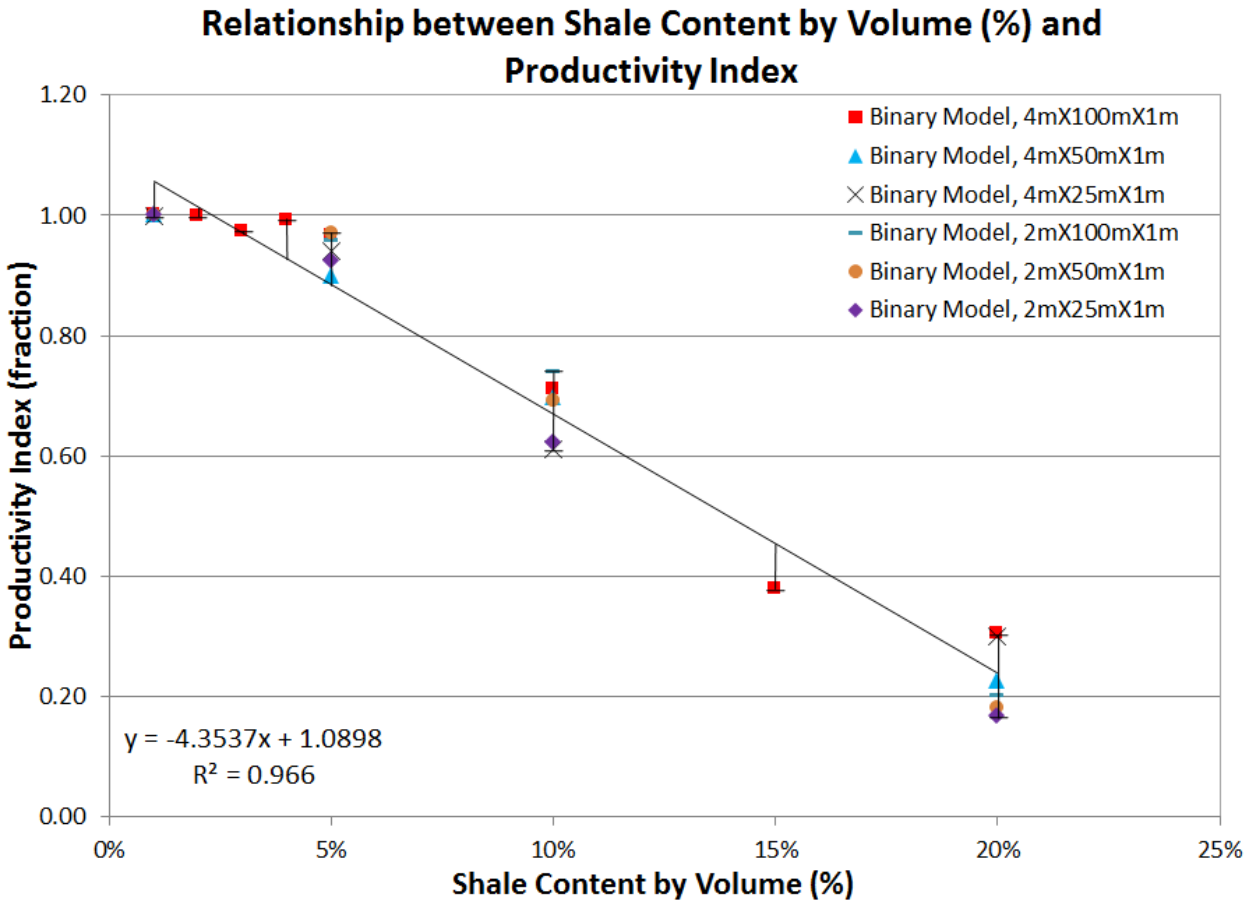

Table 5.1.1.3 – Error Band and Variation in SPI for Given Shale Content

Shale Content by Volume (%)	Error Band for Given Shale Content (High Value, Low Value) (%)	Maximum Variation in SPI (High Value, Low Value) (fraction)
1	(+0.00,-4.42)	(+0.00,-0.05)
2	(+0.00,-0.40)	(+0.00,-0.00)
3	(+1.54,0.00)	(+0.03,-0.00)
4	(+8.31,0.00)	(+0.08,-0.00)
5	(+11.29,+3.20)	(+0.10,+0.03)
10	(+13.35,-6.69)	(+0.09,-0.04)
15	(+0.00,-13.36)	(+0.00,-0.06)
20	(+38.83,-24.11)	(+0.09,-0.05)

The error bands can be thought of as the variation observed in the models as a function of length scale relative to shale content. The impact of the location of reservoir heterogeneities is captured in the degree of connectivity or SPI. However, it was observed that there was not a strong impact between length scales and shale content in skewing the result because manipulation in length scale could also affect connectivity by limiting or increasing lateral continuity of reservoir barriers. Therefore, for the purpose of the analysis the impact of the length scales can be minimized. Of the 28 binary model data-points available 22 were selected, because some models were not appropriate due to numerical convergence problems or non-representative SAGD chamber behaviour. For the remaining 22 data-points, like model types were lumped together and an average term was taken to improve the strength of the correlation. Below are the groups of data, organized into like-distributions.

Table 5.1.1.4 – Binary Models, 1% Distribution

Binary Model Association	Productivity Index	Parameters			
		PERM, *i*	**PERM, *j***	**TH, *i***	**TH, *j***
Type-A	1.0000	1.13	8.13	1.17	2.17
Type-B	1.0000	1.19	5.13	1.17	2.17
Type-C	0.9994	1.19	7.75	1.17	5.67
Type-D	1.0000	1.06	1.38	1.00	10.92
Type-E	1.0000	1.06	6.63	1.00	9.75
Type-F	0.9995	1.25	5.88	1.17	8.58
Average	*0.9999*	*1.15*	*5.81*	*1.11*	*6.54*

Table 5.1.1.5 – Binary Models, 2% Distribution

Binary Model Association	Productivity Index	Parameters			
		PERM, *i*	**PERM, *j***	**TH, *i***	**TH, *j***
Type-A	1.0000	1.19	2.88	1.17	10.33

Table 5.1.1.6 – Binary Models, 3% Distribution

Binary Model Association	Productivity Index	Parameters			
		PERM, *i*	**PERM, *j***	**TH, *i***	**TH, *j***
Type-A	0.9746	1.56	6.63	1.00	3.33

Table 5.1.1.7 – Binary Models, 4% Distribution

Binary Model Association	Productivity Index	Parameters			
		PERM, *i*	**PERM, *j***	**TH, *i***	**TH, *j***
Type-A	0.9949	1.19	7.00	1.17	12.08

Table 5.1.1.8 – Binary Models, 5% Distribution

Binary Model Association	Productivity Index	Parameters			
		PERM, *i*	**PERM, *j***	**TH, *i***	**TH, *j***
Type-A	0.9803	1.56	8.13	1.00	7.42
Type-C	0.9408	1.25	9.25	1.17	13.25
Type-D	0.9600	1.13	8.50	1.00	9.17
Type-E	0.9706	1.13	4.38	1.00	12.08
Type-F	0.9076	1.25	6.25	1.17	9.17
Average	*0.9524*	*1.26*	*7.30*	*1.07*	*10.22*

Table 5.1.1.9 – Binary Models, 10% Distribution

Model	Productivity Index	Parameters			
		PERM, *i*	**PERM, *j***	**TH, *i***	**TH, *j***
Type-A	0.7816	1.69	2.13	1.00	12.67
Type-C	0.6106	1.63	10.00	1.00	12.67
Type-D	0.7405	1.19	9.25	1.00	13.83
Type-F	0.5792	1.19	4.00	1.00	13.83
Average	*0.6789*	*1.42*	*6.34*	*1.00*	*13.25*

Table 5.1.1.10 – Binary Models, 20% Distribution

Model	Productivity Index	Parameters			
		PERM, *i*	**PERM, *j***	**TH, *i***	**TH, *j***
Type-C	0.3002	1.56	9.25	1.17	11.50
Type-D	0.2013	1.31	9.63	1.00	10.33
Type-E	0.1805	1.31	8.13	1.00	15.00
Type-F	0.1814	1.25	6.25	1.00	13.83
Average	*0.2120*	*1.36*	*8.31*	*1.04*	*12.67*

The performance indexes for each distribution were tabulated and organized into figures.

Figure 5.1.1.2 – Cross-Plot of SPI and Parameter Values

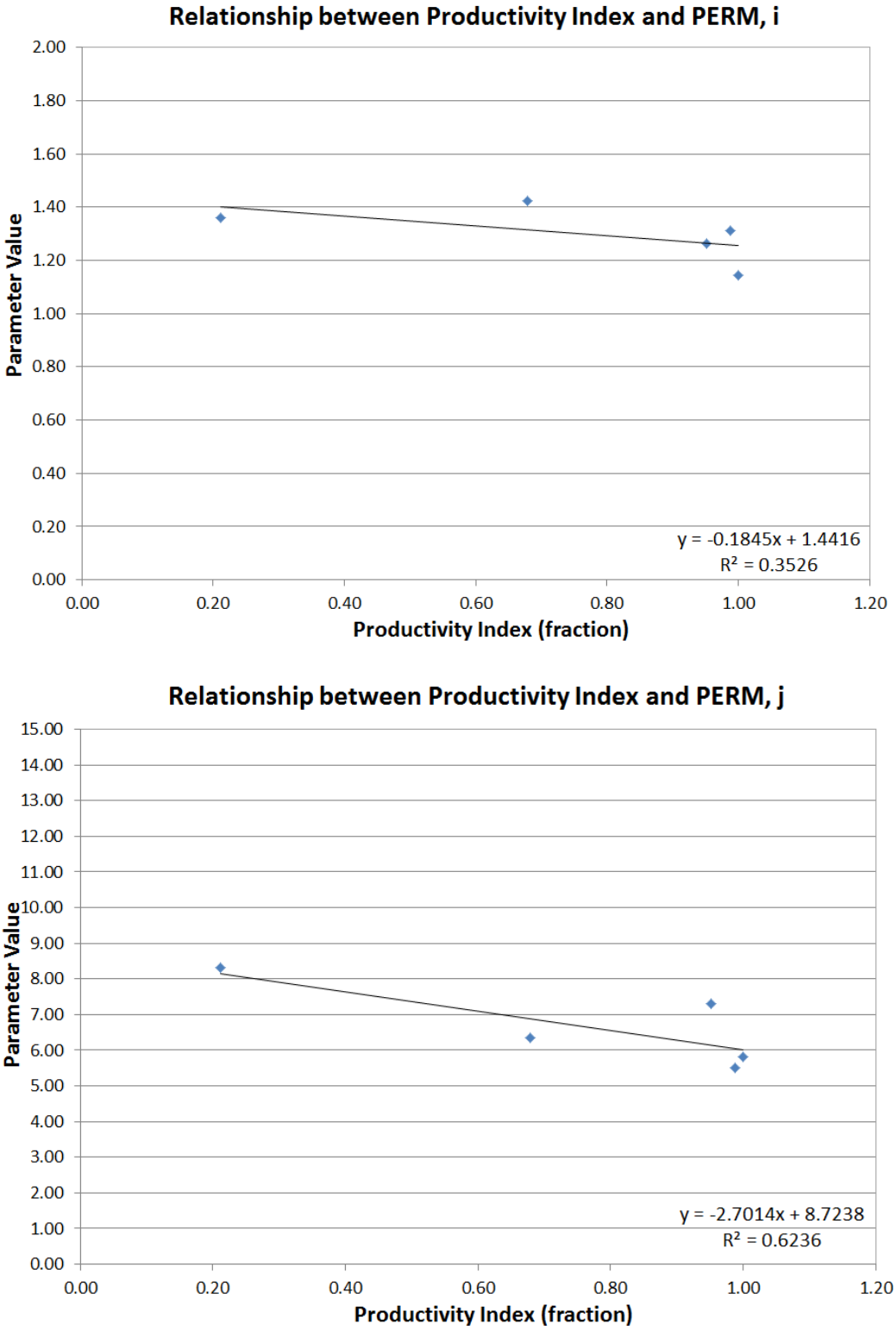

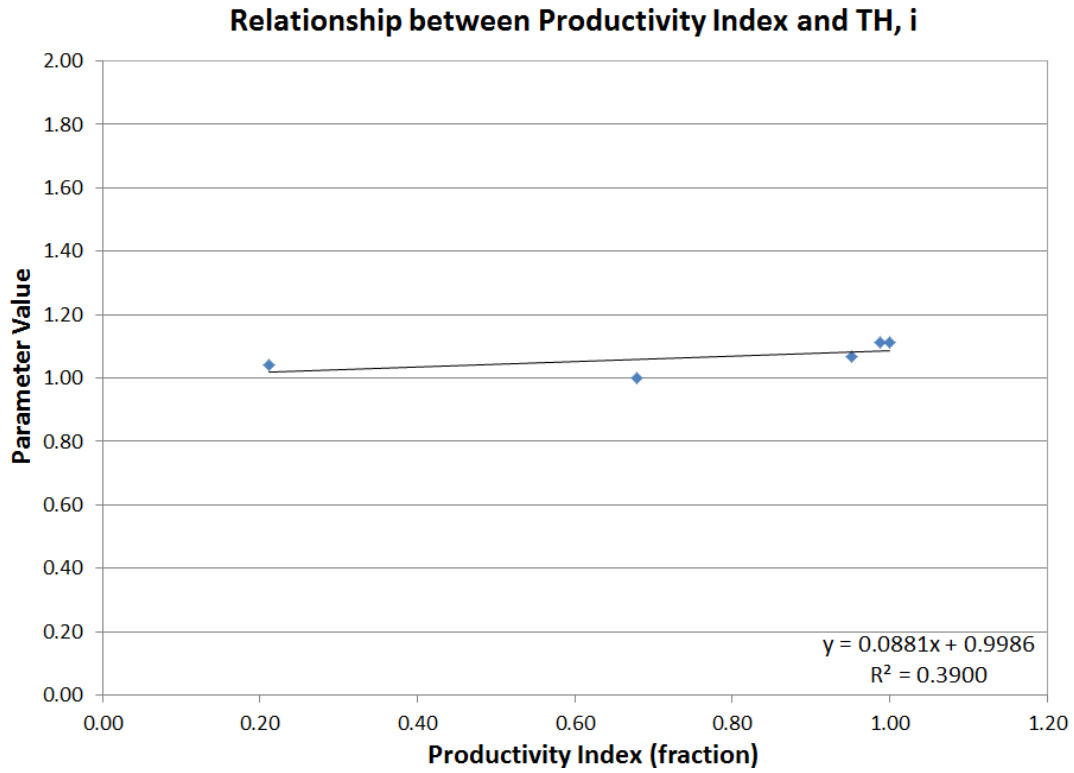
Relationship between Productivity Index and TH, i
Parameter Value
Productivity Index (fraction)
y = 0.0881x + 0.9986
R² = 0.3900
2.00
1.80
1.60
1.40
1.20
1.00
0.80
0.60
0.40
0.20
0.00
0.00
0.20
0.40
0.60
0.80
1.00
1.20

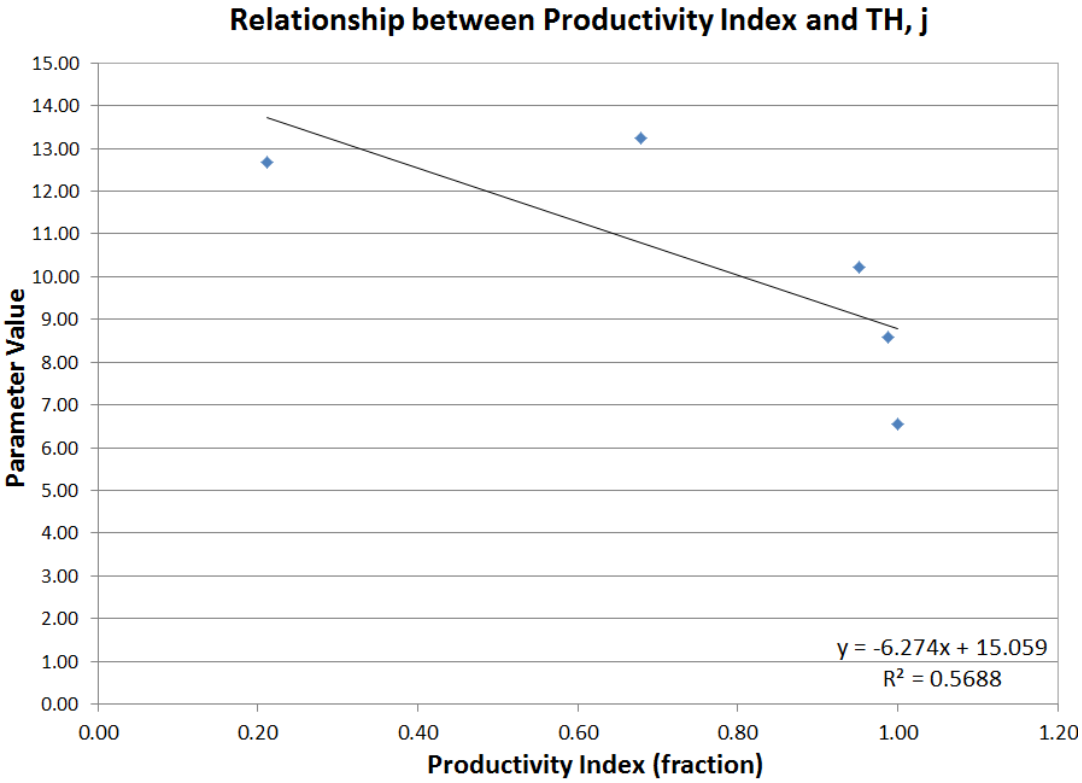
Relationship between Productivity Index and TH, j
Parameter Value
Productivity Index (fraction)
y = -6.274x + 15.059
R² = 0.5688
15.00
14.00
13.00
12.00
11.00
10.00
9.00
8.00
7.00
6.00
5.00
4.00
3.00
2.00
1.00
0.00
0.00
0.20
0.40
0.60
0.80
1.00
1.20

As presented earlier, a parameter that will be used to judge the extent to which the data is correlatable will be the Coefficient of Determination (R-Squared, R^2). The Coefficient of Determination is a statistical measure that evaluates the proximity of the data points from the proposed linear regression. The better the linear regression fits the data the greater the likelihood the R^2 term will converge to 1. A principle limitation in our work is the size of the sample set. Due to the limited data-points, any single data-point will have a greater effect on the trend for the data-set. As a result, it is assumed the Coefficient of Determination could be improved if more models and data was available for review, however, it is anticipated that it would not have a big impact upon the suggested parameters. It should be noted that while the Coefficient of Determination is much lower in the *i*-direction metrics, the absolute deviation is relatively small and therefore would have much lower impact than the *j*-direction metrics which would have the biggest impact.

Table 5.1.1.11 – Equations Representing the Relationship between SPI and Parameter Values

Parameter	Equation
PERM, *i*	Parameter Value = (-0.185*SPI) + 1.442
PERM, *j*	Parameter Value = (-2.701*SPI) + 8.724
TH, *i*	Parameter Value = (0.088*SPI) + 0.999
TH, *j*	Parameter Value = (-6.274*SPI) + 15.059

Based upon the variability observed with the thermal conductivity parameter parallel the wellbore (*j*-direction), it was anticipated that the TH, j parameter would afford the greatest variability and scatter – which is presented in **Figure 5.1.1.2**.

5.2 Application of Equations to Facies-based Models

The intention of the report was to develop a work-flow based upon the binary models, after which the results could be tested against the more representative "geomodel" (geological model) types, which are dependent on different facies proportions. The binary models were easier to evaluate but have less applicability to industrial projects. Binary model types are most relevant to preliminary decision gates and projects in their infancy where coarse forecasts are acceptable and type-well representations are frequently used. Therefore, all four facies-based models proposed earlier will be analyzed with the recently presented equations. **Table 5.2.1** highlights the sensitivity analysis that will be performed. It is assumed this combination of models is an acceptable sample size.

Table 5.2.1 – Facies-based Sensitivity

Sensitivity	Facies-based Model Association	Depositional Environment
1	Type-A' (4m, 100m, 1m)	Uniform
		Coarsening Upwards
		Fining Upwards
		Channel
2	Type-B' (4m, 50m, 1m)	Uniform
		Channel
3	Type-C' (4m, 25m, 1m)	Coarsening Upwards
4	Type-D' (2m, 100m, 1m)	Fining Upwards
5	Type-E' (2m, 50m, 1m)	Coarsening Upwards
6	Type-F' (2m, 25m, 1m)	Fining Upwards

The equations representing the relationship between the SAGD Productivity Index and parameter values will be utilized to project the magnitude of the matching parameters required. It is hypothesized that the proposed parameter values will noticeably improve the match of the coarse models to the fine models. The results will then be compared against the 'Original Error' relationship defined earlier as a quantitative indicator for success. An 'Absolute Percent Improvement' value can be seen as the improvement from applying the matching parameters to the coarse models, however, the absolute relationship does not differentiate if the projection is higher or lower than the fine model reference. Only if the projection worsens the result will it be noted as a negative result. In addition, the actual history matched models (History Matched Values) for the Type-A' sub-set will be highlighted to show the significant improvement if this exercise could be run on an individual model basis and not generalized (Forecasted Values).

Table 5.2.2 – Type A' Facies-based Model Associations (Forecasted Values)

Sensitivity	Depositional Environment	Productivity Index	Forecasted Parameter Values			
			PERM, *i*	PERM, *j*	TH, *i*	TH, *j*
1	Uniform	0.6105	1.33	7.07	1.05	11.23
	Coarsening Upwards	0.2767	1.39	7.98	1.02	13.32
	Fining Upwards	0.7260	1.31	6.76	1.06	10.50
	Channel	0.8192	1.29	6.51	1.07	9.92

Table 5.2.3 – Type A' Facies-based Model Associations (Forecasted Percent Improvement)

Sensitivity	Depositional Environment	Productivity Index	Coarse Model Original Error (%)	Modified Coarse Model Original Error (%)	*Absolute Percent Improvement (%)*
1	Uniform	0.6105	9.90	3.34	*66.3*
	Coarsening Upwards	0.2767	2.21	1.98	*10.4*
	Fining Upwards	0.7260	8.11	2.66	*67.2*
	Channel	0.8192	6.79	3.64	*46.4*

Table 5.2.4 – Type A' Facies-based Model Associations (History Matched Values)

Sensitivity	Depositional Environment	Productivity Index	Forecasted Parameter Values			
			PERM, *i*	PERM, *j*	TH, *i*	TH, *j*
1	Uniform	0.6105	1.44	9.63	1.17	12.67
	Coarsening Upwards	0.2767	1.38	1.00	1.50	4.50
	Fining Upwards	0.7260	1.19	4.38	1.50	1.58
	Channel	0.8192	1.31	9.63	1.33	12.67

Table 5.2.5 – Type A' Facies-based Model Associations (HM Percent Improvement)

Sensitivity	Depositional Environment	Coarse Model Original Error (%)	Actual History Matched Original Error (%)	*Absolute Percent Improvement (%)*
1	Uniform	9.90	0.97	*90.2*
	Coarsening Upwards	2.21	0.52	*76.5*
	Fining Upwards	8.11	0.96	*88.1*
	Channel	6.79	1.12	*83.5*

Table 5.2.6 – Type B' Facies-based Model Associations (Forecasted Values)

Sensitivity	Depositional Environment	Productivity Index	Forecasted Parameter Values			
			PERM, *i*	PERM, *j*	TH, *i*	TH, *j*
2	Uniform	0.5971	1.33	7.11	1.05	11.31
	Channel	0.7876	1.30	6.60	1.07	10.12

Table 5.2.7 – Type B' Facies-based Model Associations (Forecasted Percent Improvement)

Sensitivity	Depositional Environment	Productivity Index	Coarse Model Original Error (%)	Modified Coarse Model Original Error (%)	*Absolute Percent Improvement (%)*
2	Uniform	0.5971	12.81	1.61	*87.4*
	Channel	0.7876	6.12	1.00	*83.7*

Table 5.2.8 – Type C' Facies-based Model Associations (Forecasted Values)

Sensitivity	Depositional Environment	Productivity Index	Forecasted Parameter Values			
			PERM, *i*	PERM, *j*	TH, *i*	TH, *j*
3	Coarsening Upwards	0.3657	1.37	7.74	1.03	12.76

Table 5.2.9 – Type C' Facies-based Model Associations (Forecasted Percent Improvement)

Sensitivity	Depositional Environment	Productivity Index	Coarse Model Original Error (%)	Modified Coarse Model Original Error (%)	*Absolute Percent Improvement (%)*
3	Coarsening Upwards	0.3657	11.33	3.71	*67.3*

Table 5.2.10 – Type D' Facies-based Model Associations (Forecasted Values)

Sensitivity	Depositional Environment	Productivity Index	Forecasted Parameter Values			
			PERM, *i*	PERM, *j*	TH, *i*	TH, *j*
4	Fining Upwards	0.7077	1.31	6.81	1.06	10.62

Table 5.2.11 – Type D' Facies-based Model Associations (Forecasted Percent Improvement)

Sensitivity	Depositional Environment	Productivity Index	Coarse Model Original Error (%)	Modified Coarse Model Original Error (%)	*Absolute Percent Improvement (%)*
4	Fining Upwards	0.7077	2.16	3.01	*-39.4*

Table 5.2.12 – Type E' Facies-based Model Associations (Forecasted Values)

Sensitivity	Depositional Environment	Productivity Index	Forecasted Parameter Values			
			PERM, *i*	PERM, *j*	TH, *i*	TH, *j*
5	Coarsening Upwards	0.3593	1.38	7.75	1.03	12.80

Table 5.2.13 – Type E' Facies-based Model Associations (Forecasted Percent Improvement)

Sensitivity	Depositional Environment	Productivity Index	Coarse Model Original Error (%)	Modified Coarse Model Original Error (%)	*Absolute Percent Improvement (%)*
5	Coarsening Upwards	0.3593	8.47	6.27	*26.0*

Table 5.2.14 – Type F' Facies-based Model Associations (Forecasted Values)

Sensitivity	Depositional Environment	Productivity Index	Forecasted Parameter Values			
			PERM, *i*	PERM, *j*	TH, *i*	TH, *j*
6	Fining Upwards	0.5495	1.34	7.23	1.05	11.61

Table 5.2.15 – Type F' Facies-based Model Associations (Forecasted Percent Improvement)

Sensitivity	Depositional Environment	Productivity Index	Coarse Model Original Error (%)	Modified Coarse Model Original Error (%)	*Absolute Percent Improvement (%)*
6	Fining Upwards	0.5495	6.03	6.69	*-10.9*

As indicated by the 'Percent Improvement' metric, the application of the SPI-Parameter formulation has provided a noticeable improvement to the original coarse model, despite the relationship to length scales. It should be noted that two instances highlighted the need for further refinement as the analytical solution worsened the result, which will be addressed further in **Section 6.1**. Ultimately, the coarse model 'Original Error' varied significantly throughout the models, with no discernible relationship or logic between length scale and depositional type. In this way, the user can have confidence that their model definition and configuration is appropriate for this application.

All production profiles are presented in **Appendix D, Figures D.1 – D.10**. The production profiles afford a visual appreciation as to the improvement in the coarse model with upscaling parameters relative to the fine model output.

5.3 Modelling Assumptions and Limitations

Inherent to many studies, there are assumptions that impact the validity and applicability of the results. The purpose of this section is to highlight those assumptions and make suggestions as to strengthen this body of work and enhance its value for the future while notating obvious limitations.

Some fundamental assumptions include:

(1) Dynamic SAGD Parameters

The dynamic parameters or operating constraints within the models were held constant, for example, bottom-hole injection pressure, maximum and minimum liquid rates, producer pressure (inter-well ΔP), steam quality, maximum steam production, etc. A simple sensitivity analysis was performed at the start of the study to access the impact of varying these simulation parameters. The overall observation is that only the bottom-hole pressure and steam quality could potentially have an impact upon the universality of the results, as it affected the rate of temperature development within the models. An increase in bottom-hole injection pressure and saturated steam temperature accelerated chamber development and rate of recovery within all models. Despite a reduction in thermal efficiency, the SAGD process was effectively enhanced, however, the relative change from the coarse model approximation to the fine model approximation was held constant and the impact of the injection pressure could be normalized in this sense. Ultimately, representative operating parameters were selected based upon published industry documentation[57-59], and it was believed this was the most appropriate value to carry forward. An improvement for future work-flows could be to consider a wider range of well and

operating constraints to verify the impact is nominal and ensure no systematic bias is being built into the analytical approximation. Regardless, throughout the duration of the report an overriding thought was that if a parameter was held constant throughout the period of the analysis, then its impact could be minimized and results were relative.

(2) STARS™ Sink-Source Modelling Approach

As mentioned in prior sections, the type of simulation configuration used during this study was sink-source modelling. Whereby, each gridblock with a well definition acts as a node for either steam injection or emulsion production. The performance of that node is independent of the wellbore nodes adjacent to them, and there is no dependence on wellbore hydraulics. Fundamentally, this assumption is an acceptable approach for modelling SAGD performance within a pay interval, as indicated by the work performed in industry[33]. However, for the benefit of the study, verifying the result with a discretized well would be useful. Only if certain reservoir features were not being honoured as understood operationally, would the result potentially change.

In addition, it was verified within the models that the wellbore configuration was equivalent in the coarse and the fine model. For example, as the gridblock count increased parallel the wellbore, additional injection and production nodes were added to the reduced gridblock volumes, as highlighted in **Figure 5.3.1 – 5.3.2**. The rate of energy input and temperature for the entire length of the well was comparable for the different configurations, with the only variation occurring as a function of reservoir properties and grid size.

Figure 5.3.1 – Schematic of Well Definition Parallel the Wellbore

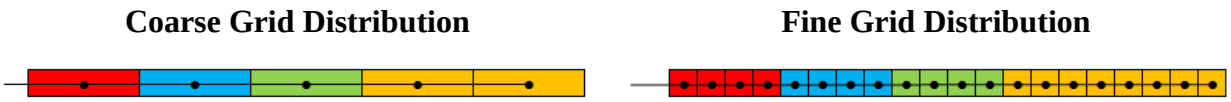

Figure 5.3.2 – Temperature Distribution upon Conversion to SAGD for Type-B' Model

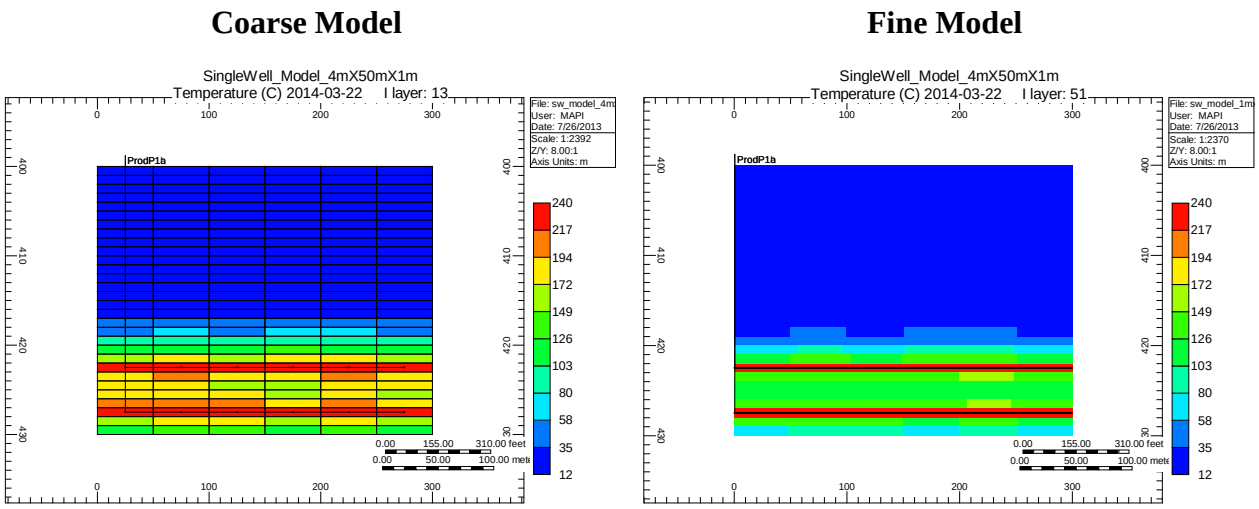

Figure 5.3.3 – Energy Investment during the Circulation Period

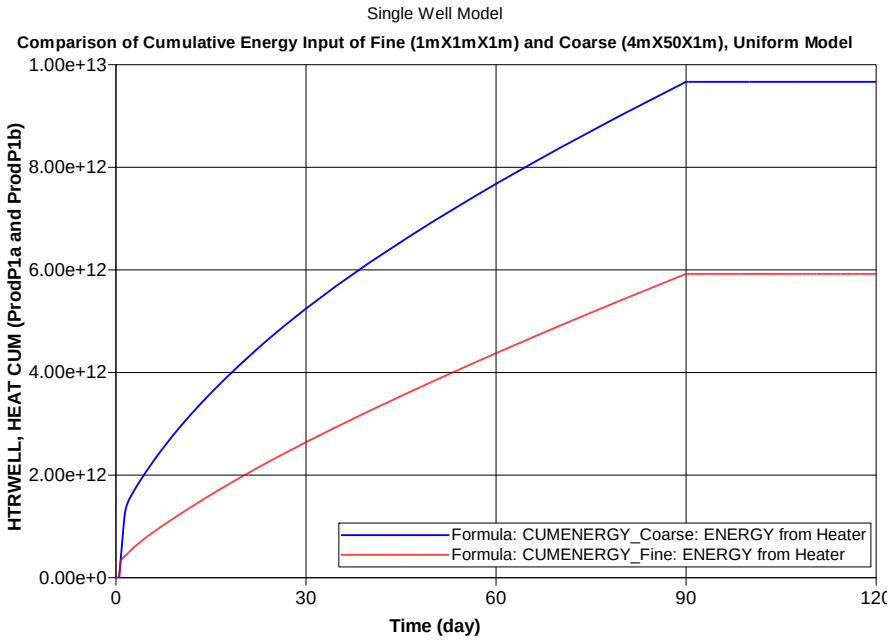

It should be noted that **Figure 5.3.2 – 5.3.3** supports the fundamental statement of this paper, that given normalized production parameters, the temperature signature is inherently different in the model as a function of grid definition. The heater well configuration can achieve the temperature set-point (240^{o}C) in the fine model quicker than the coarse model. The difference in energy required on a block-basis changes the timing and sequencing of the SAGD process.

(3) Fine Gridding as Reference Data

When reviewing core analysis, some geological features are on the magnitude of centimeters and significant variation can occur over small dimensions. Therefore, it is fair to say the grid coarseness of (1m, 1m, 1m) could still be inappropriate for being considered the reference case or case representative of reality. However, due to the nature of the simulations and the effective properties for each gridblock, the fine gridded models are the maximum limit for grid refinement for numerical modelling. It would be impossible given current resources to capture geological features on a finer scale. Therefore, no recommendations are made for further improvement on the reference cases.

(4) Fundamental Reservoir Inputs

The fundamental reservoir inputs for the simulations (PVT, relative permeability curves and thermal properties) were all based upon default parameters or sourced from representative files within the CMG data-base. In addition, the property assignment per facies type was maintained and universally applied. There was no specific rock type assignment. In this sense, the inputs are highly generalized but were necessary for performing this type of analysis. However, for further refinement of this work, more effort can be made into PVT characterization and impact on

manipulating these parameters. For example, the viscosity profile will have a big impact on energy requirement for bitumen mobilization, which will affect the rate of heat development within the model. Therefore, PVT characterization in its own right will impact the production profiles significantly. Additionally, the thermal conductivity multipliers are directly linked to the default or base values, which would likely change as the magnitude of the base values are altered. While the permeability multipliers are a function of absolute permeability, the relative permeability inputs, including end-point definitions, will have an effect on the flow of bitumen production and the ability to void the chamber to allow further chamber growth. In that way, temperature propagation is directly linked to convective flows. It is not expertly known how manipulation of these fundamental inputs would affect the result. As a result, it would be a beneficial exercise to examine a wider range of reservoir inputs, including GOR impact and directional relative permeability.

(5) CMOST™ Optimization Method

The process of history matching was based upon one method within CMOST™, referred to as the Designed Exploration Controlled Evolution (DECE) Optimization method. While extensive justification was sought to employ this technique, other techniques could be considered in the future to verify the validity of the parameters, such as use of the Particle Swarm Optimization (PSO) and Brute Force methods. The justification for Brute Force is to better understand the non-unique solution sets being generated by DECE. By running Brute Force all combination of parameter values are tested so there is no risk of non-unique solutions. However, the application of the Brute Force method would have to be selective as the simulation time associated with that work would not be practicable for all cases.

Whereas, the PSO method would be better served as a practical full-scale alternative than to the Brute Force search method. The PSO method is most similar with the evolutionary computing techniques such as Genetic Algorithms (GA). It is initially populated with random solutions and searches for optima by updating generations. Effectively, potential solutions (particles) 'fly' through problem space by following current optimum particles. There are several advantages to PSO approach which include the fact that the PSO approach will continue searching for optimum values until the maximum number of simulation calls is reached. The PSO method also employs the use of a repository to reduce the number of simulation calls required for a given number of solutions. This repository option enables the user to restart the optimization if necessary to see if a better optimum can be achieved, or revert back to a previously constructed repository of results. This technique is absent with the DECE method. As the performance of the PSO to the DECE is not known, this is a good area of study in the future. The focus would be to run the same cases using the two approaches to determine if the distribution of result is the same. If differences are noted, further investigation can be performed, such as, considering selective use of the Brute Force method which is more expensive to run but would improve the understanding of non-unique solution sets.

(6) SAGD Productivity Index and Ranking Method

The most challenging part of the work-flow was developing an approach to consider the impact of gridding with respect to reservoir quality. It was concluded that the effect of gridding could be minimized if the reservoir quality was emphasized. As a result, the SAGD Productivity Index was employed to rank the connectivity of the cells within the models. The tool focuses on connectivity of cells to be able to be reached by stream chamber growth and allow for bitumen

production into the producer. If the grid dimensions vary significantly, but the reservoir quality is high then the connectivity of the cell, which is the ratio of the average permeability for the actual gridblock to the average permeability for the clean sand (as indicated in **Appendix C**), has nominal dependence on gridblock sizes. Ultimately, the ability to transmit heat and drain fluids is mostly comparable. This inference is indicated in more detail in **Section 3.11**. Fundamentally, the assumption is that the index is properly treating the connectivity of these cells which directly effects the analytical approximation.

(7) History Matching Approach

As mentioned earlier in the modelling and project assumptions section, the results are a function of the CMOST^{TM} history matching process. However, if the user were to still normalize the impact of different history matching optimization methods, then the configuration is still limited in the values that can be proposed. A fundamental assumption was the extent of the parameter inputs. As indicated in **Figure 5.3.1**, the minimum or default multiplier was 1, which would imply no change to the values. However, the maximum multiplier was assumed based upon the gridding dimensions and understanding of the physical process. In only a few instances was the upper limit on any multiplier achieved, so it can be assumed that the magnitude and the increment of each multiplier (for example, 0.1 increment in the PERM, *i* parameter instance) is valid and no further sensitivity work needs to be performed. As a validation for the process, those 'best job' cases that were returning multiplier values near the upper or maximum multiplier limit could be re-assessed using a broader range and/or smaller increments. Ultimately, the goal was to achieve universal multipliers that improved overall performance whereby more refined increments would not be necessary.

Table 5.3.1 – Revisited Parameter Inputs

Parameter Name	Default Multiplier	Value Generator Method	Minimum Multiplier	Maximum Multiplier	Number of Values
PERM, *i*	1	Arithmetic Sequence	1	5	100
PERM, *j*	1	Arithmetic Sequence	1	20	100
TH, *i*	1	Arithmetic Sequence	1	10	100
TH, *j*	1	Arithmetic Sequence	1	30	100

A fundamental limitation includes:

(8) Number and Type of Models

The nature in which the models were constructed is unique to this study. The objective of building two unique model types (binary and facies-based) was two-fold. Firstly, the binary configuration focused on control and awareness of the impact of reservoir and non-reservoir with respect to length scale. As the values were discrete, it would allow the user to focus on the impact of non-reservoir rock in systematically defined increments, and forecast any challenges or limitations early on. However, these types of models are neither representative of reality nor comparable to geological models. Therefore, a second approach employing facie-based models was proposed to broaden the applicability of the values and verify the binary models could capture the influence properly. Inherent in this approach is potentially the biggest limitation of the work, and that is if the binary models do not properly capture the effect of the reservoir and non-reservoir rock types with respect to varying length scales, then the foundation of the analytical work is incorrect. However, in expanding the approach more confidence could be developed as to the precision of these approximations. Another weakness of the data-set it is it is

limited in the number of data-points that could be generated, as a result of the extensive simulation time required for the models. For example, the run-time to generate the 'best-job' simulation parameters for the (4m, 25m, 1m) 10% shale distribution was approximately 95 hours.

Regardless, the number and type of models used should be expanded to develop a more robust data-set in which to tune the current correlations. Additional data would support the ability of the binary models to be able to predict the correct impact of reservoir heterogeneities coupled with variable dimensions.

As an example, **Table 4.0.1** proposes an updated set of binary model configurations, and expands upon **Table 5.3.2.**

Table 5.3.2 – Revisited Depositional Quantities

Model Association	**Coarse Dimensions (*i, j, k*)**	**Fine Dimensions (*i, j, k*)**	**Non-Reservoir Content in Increments of 1% (Percent by Volume)**
Type-A (Base Case)	4m, 100m, 1m	1m, 1m, 1m	[1, 20]
Type-B	4m, 50m, 1m	1m, 1m, 1m	[1, 20]
Type-C	4m, 25m, 1m	1m, 1m, 1m	[1, 20]
Type-D	2m, 100m, 1m	1m, 1m, 1m	[1, 20]
Type-E	2m, 50m, 1m	1m, 1m, 1m	[1, 20]
Type-F	2m, 25m, 1m	1m, 1m, 1m	[1, 20]

Additionally, variations on the facies-based models could be produced and ran to replicate a different set of realizations like one would expect from a geological work-flow.

5.4 Impact on Commercial Projects

The perceived benefit of this work-flow may be limited, but the ability to improve one's forecast has significant implications. Firstly, from a full field production profile, many business planning decisions are based upon a certain vintage of reservoir models. However, the grid coarseness decision is often taken with less thought and without full understanding of its implication. Routinely, the grid coarseness is a function of hardware and software limitations, but tends to stay rigid for the duration of the project. In that way, older model vintages can be compared more easily to earlier vintages provided other parameters are not manipulated significantly.

The decision to maintain grid resolution is more significant when more marginal drainage areas with greater reservoir heterogeneities are considered for production and included in forecasts. The increase in reservoir variability will result in greater disparity between the coarse and fine grid cases and more error. It has been shown that approximately 10% uplift in cumulative production can occur and 5% improvement in thermal efficiency parameters, such as cSOR when this discrepancy is acknowledged. As mentioned in **Section 3.5**, these models represent one-third a conventional well pair. If you extrapolate this one-third of the production to a well with a standard well length (~900m) and 100% well contribution, the 10% mentioned prior becomes significant. More relevant is when the uplift associated with a single well pair is extrapolated amongst several well pads. For example, the cumulative bitumen uplift suggested earlier corresponds to 12,250 m^3 for one-third a pair and 36,750 m^3 for 100% well conformance of a 900m horizontal. This contribution multiplied over a 50 well pair (approximately a 5 well pad configuration) results in a total bitumen contribution of 1.8375 million m^3. This can significantly change project economics and the economic viability of certain areas.

Of equal interest is the impact of simulation run-times. As highlighted in **Figure 5.4.1 – 5.4.2**, whereby several models are compared between their coarse model and their fine model run-time, it becomes obvious that it is less expensive to run coarse models in favour of fine models. But the ability to run a coarse model coupled with upscaling parameters, allows the engineer to improve their forecast while running with the greatest efficiency. This is increasingly more important when multiple well pair models want to be simulated with complex PVT characterization, such as the introduction of solvent with steam, where the interaction between pairs is of paramount importance, but the improved predictive ability allows for tuning of solvent use and recovery. In addition, the improved accuracy of the models will benefit the engineer in terms of generating a history match, as the prediction already couples some elements of a history matching exercise.

Table 5.4.1 – Representative Simulation Run-Times for Binary Models

Binary Model Association	Non-Reservoir Content (%)	Coarse Model (hh:mm:ss)	Fine Model (hh:mm:ss)
Type-A	5	00:00:47	92:05:24
Type-A	10	00:00:46	101:02:36
Type-F	5	00:30:40	125:08:57
Type-F	10	00:31:40	146:47:44

Table 5.4.2 – Representative Simulation Run-Times for Facies-based Models

Facies-based Model Association	Depositional Environment	Productivity Index	Coarse Model (hh:mm:ss)	Fine Model (hh:mm:ss)
Type-A’	Channel	0.8192	00:01:13	51:18:27
Type-F’	Fining Upwards	0.5495	00:19:13	190:18:27

CHAPTER 6 – CONCLUSIONS AND RECOMMENDATIONS

6.1 Conclusions

While reservoir simulation inherently has limitations, it is still a widely used and respected forecasting tool for companies to evaluate different resource plays. As a result, efforts are continually made to improve the processes in which we apply to simulation work-flows.

Throughout the report, observations were made as to the impact of different grid definitions or length scales relative to variation in reservoir quality. The work also took into consideration the location of heterogeneities on the performance of SAGD wells and how it impacts numerical forecasts.

The primary focus of the conclusion section is to revisit the observations made during the report coupled with the limitations already identified, to highlight the extent to which this work-flow is applicable.

- It was observed that there is a strong correlation between shale content by volume and the 'Original Error' parameter. Indicating that 'Original and Delta Error' increases as the reservoir becomes less homogenous.
- The original plot of parameter values with respect to 'Original and Delta Error' for all binary model types was poor, motivating the need for a different tool to generate a correlation.

- The SAGD Productivity Index built by CMG is a valuable tool for generating a relationship between different reservoir qualities, as it relates to connectivity of gridblocks and thus its impact on ‘Original Error’.
- The impact of different length scales in homogenous models is evident when you review the geometry of the steam chamber and impact on production. However, relative to models with reservoir heterogeneities, these differences are minor and are often negligible from a project perspective. The impact of different length scales in homogenous models is most evident in the ramp-up period of SAGD as the steam chamber is growing most rapidly.
- The location and quantity of reservoir heterogeneities relative to well location has a significant impact upon performance. As noted in **Section 3.11** the difference can be approximately 1-5% of the Objective Function ‘Original Error’ difference, which is a function of shale content, despite identical length scales.
- While length scales do have a quantifiable impact upon simulation, for the purpose of this project and to generalize the correlations for the size of the given sample set, they were absorbed into the productivity index parameter. Specifically, based upon error bars in **Section 5.1**, the impact of length scales could be normalized when considering grid variation of 4m to 2m perpendicular to the well and 100m to 25m parallel the well. However, it should be noted that the error bars associated with higher shale content tended to have the largest variation and uncertainty.
- If fine grid resolution cannot be utilized within a SAGD reservoir simulation, thermal conductivity and permeability multipliers can be employed to improve the predictive ability of the coarse model.

- During the course of the analysis, it was also observed the DECE optimization method was capable of generating non-unique solutions for the same model distributions. It was concluded that different combination of the parameters can generate comparable, if not identical results. The user can manipulate some of the results, as long as the improvement to the base models is maximized, further supporting generalized equations for matching purposes.
- Despite different initial length scales for different depositional types, there was the possibility to generate similar SPI values, and therefore similar forecast parameter values. However, as each model had a unique 'Original Error' value, the magnitude of the improvement would vary. It is understood that the two values are fundamentally linked, but the magnitude of impact would need to be analyzed on a case-by-case basis. A larger subset of samples would help verify the magnitude of its impact for certain cases.
- As hypothesized, the scatter associated with the SPI and parameter values was greatest for the *j*-direction (parallel to the well pair) as the variation in length scale was greatest. Additional models would help tune these values further. However, for the SPI and parameter values in the *i*-direction (perpendicular to the well pair), the values had little variation. In the case of the permeability multiplier the values fluctuated between approximately 1.2 and 1.4 while the values thermal conductivity multiplier fluctuated between approximately 1.0 and 1.15. In this way, it was concluded that future forecasted values could be assigned constants (average values of the ranges highlighted above) for the multipliers in the *i*-direction and not sourced from the SPI and parameter value formulation in **Section 5.1.1**.
- Ultimately, the upscaling parameters were effective in matching the three cumulative metrics as well as improving oil rate and the steam-oil ratio both with respect to time and

recovery factor. For example, **Appendix D**, **Figure D.1 – Figure D.10** highlights the improvement to the rate data on a yearly basis, which is intended to smooth the daily oscillations.

- The results from employing the upscaling parameters is promising with the 'Absolute Percent Improvement' representing an improvement as significant as 85% on some models with the average improvement being approximately 50%.

- However, those instances where the upscaling parameters were ineffective or less effective should also be noted. When the coarse model 'Original Error' was small, like in the Type A' Coarsening Upwards facies-based model case, the improvement was small (~10%). Additionally, in the Type D' fining upwards facies-based model case, the parameter values over-estimated the result. It was reasoned that an 'Original Error' less than or equal to 3.0 started to neutralize the effectiveness in the correlations and should not be used in these instances.

- Additionally, the instance of Type F' fining upwards facies-based model, the 'Original Error' was appropriate for application of the parameters, indicating a difference between the coarse and fine model, despite the most refined coarse (*i, j*) grid dimensions of (2m, 25m). However, it can't be explained why this particular combination of depositional model, 'Original Error' value and forecasted parameter values yielded a small negative result. This result is considered erroneous to the data-set. Upon review of the production profile in **Appendix D, Figure D.10**, it is an instance of over-prediction of the productive potential. Therefore, additional model types need to be simulated to confirm this threshold of behaviour and support the universal use of upscaling parameters on all coarse models.

- On average the upscaling parameters systematically over-predicted the performance of the fine model. Though often a significant absolute improvement on the coarse model, the parameters were often optimistic. By scaling down the magnitude of the parameters by a set

percentage, it is reasoned that the matches could be improved by minimizing cases of exaggerated prediction. This would also benefit Type A' and D' cases, as indicated above, as the degree of improvement required is less significant. The extent to which the parameters should be scaled is not expertly known.

- An alternative procedure for checking the accuracy of the coarse gridded model result without running the fine gridded model case is to consider models from producing fields with a significant amount of historical data, which effectively represents what is being captured with the fine gridded model. By comparing the forecast of the coarse model, as exported by the geomodeller, with the coarse model coupled with upscaling parameters, the user can identify improvements relative to the historical data. This process could be applied prior to the history matching sensitivity and save efforts during history matching.

6.2 Recommendations

(1) Test Dynamic Upscaling with One Parameter

All runs were performed by coupling the multipliers for permeability and dynamic upscaling, in both the *i*-direction and *j*-direction. However, to get a better appreciation for the ability of one parameter to improve upon the 'Original Error' the optimization runs could be run with a single parameter, in one direction as well as both directions. For example, permeability multiplier in the *j*-direction could be ran then the permeability multiplier for both the *i*-direction and *j*-direction (TH, *i* and TH, *j*) could be implemented. Additionally, the parameters in strictly the *i*-direction could be run (PERM, *i* and TH, *i*) as well as the *j*-direction (PERM, *j* and TH, *j*). In this way, more effort is made to understand the relative impact of each parameter in each respective

direction. This would also likely influence the magnitude of the values, so a significant amount of new raw data would have to be post-processed. For the confines of this report, it would have been impractical to perform such an analysis.

(2) Directional Parameters

As an alternative to applying parameters with specific magnitudes, directional parameters could be assigned per facies type. This would require a more robust understanding of relative permeability and thermal conductivity characterization, and it would be insufficient to apply generic values or definitions. However, if each rock type was assigned a certain configuration for each direction, and that data was tuned based upon different distribution and quantity of reservoir rock types on a block basis, then multipliers would not be required in favour of this single solution. The concern is that it could potentially generalize the solution and lose relevance but would be easier to implement and could also offer more applicability.

(3) Examination of Convection in the Steam Chamber

A major element of this study was the growth of the steam chamber at the bitumen-steam interface, in which conduction was considered dominant. Heat transfer into the block volume and the time required to achieve mobilization was analyzed extensively. However, some thought can be given to the application of convection or convective multipliers in these models. It was assumed that the temperature within the simulated chambers is constant, so no temperature gradient exists within the steam zone itself (as highlighted by the Marx-Langenheim Model in **Appendix E**), and therefore be stated that convective heating is negligible within the chamber. However, convective heating can occur at the bitumen-steam interface and is an important heat

transfer mechanism within the SAGD process. Sharma and Gates (2011)[60] explained this behaviour through initial water mobility. It was stated that while the results demonstrated convective heating is a significant contributor to heat transfer at the boundary of the steam chamber, it does not necessarily increase oil production if limited by the relative oil permeability. In addition, Mazda and Gates (2013)[61] analyzed the role of convective heat flux parallel and normal to the steam chamber-bitumen interface. They concluded that the results supported the idea that outflow convection plays a minor role in heat transfer within the SAGD process and the heat flux is approximately less than 10% of the conductive heat flux normal to the chamber edge.

The role of convective heat transfer within SAGD could be considered for future studies and the possibility of adapting the mode(s) of heat transfer within the study.

(4) Sensitivity on Specific Placement of Reservoir Heterogeneities

While outside the scope of the original study, a sensitivity analysis could have been performed to better understand the impact of reservoir heterogeneities relative to placement within the reservoir interval. It had been identified throughout the course of the study that as low quality reservoir grouped around the wellbore, performance decreased significantly, but it was never explicitly quantified. A relationship could be developed with respect to the change in the coarse model 'Original Error' value to understand the link between the percentage of poor quality reservoir and location to the change observed in the 'Original Error'. It would enhance the understanding of what drives changes in the 'Original Error' parameter.

(5) Application of a Dynamic Upscaling Tool

As indicated in **Sections 2.1** and **2.2**, the implementation of a dynamic gridding feature, ideally a commercially tuned and widely tested and calibrated feature, would be a valuable check to this work-flow. Knowledge and an extensive review about gradient thresholds would have to be performed in order to properly apply the dynamic gridding algorithm of choice, however, it can help determine the frequency and quantity of amalgamated and de-amalgamated cells and the predictive ability of the coarse models coupled with upscaling parameters.

Ultimately, the user knows there is limitation in this work, but that it is still able to provide significant insight into the impact of reservoir heterogeneities with respect to varying grid dimensions. Ideally, with new information and models this study could be further tuned.

6.3 Pareto Principle, 80-20 Rule

Throughout the thesis research, the author was motivated by the Pareto Principle, or 80-20 Rule. An interpretation of the Pareto Principle suggests “80% of all constructive results originate from the most focused 20% effort.” The focus was on the project details that afforded the greatest benefit to future users. By placing emphasis on the information most relevant to future users, the conclusions would more practical. The principle fear was developing a work-flow that had a limited scope in terms of applicability and usability. But by focusing on a certain configuration of models, it would allow the user to filter and screen large sets of data in a timely manner. Furthermore, the author has tried to allow others to build and analyze a comparable approach to verify or improve upon the base objective. As suggested in **Section 6.1,** the application of this

work-flow could be applied prior to the process of history matching, which is often extensive and considers a significant amount of variables. Ideally, it can help minimize the amount of history matching related work and improve the front-end of that task. As highlighted in the **Section 5.3** and **6.2**, there are many areas where this work could further develop and evolve, but those details were less relevant to the big picture. Ultimately, the author was seeking to understand from the process and apply the results than derive a perfect solution.

REFERENCES

(1) Energy Resources Conservation Board ST98-2013. 2013. Alberta's Energy Reserves 2012 and Supply/Demand Outlook 2013–2022, Section 3 – Crude Bitumen (accessed September 2, 2013).

(2) Energy Resources Conservation Board ST98-2013. 2013. Alberta's Energy Reserves 2012 and Supply/Demand Outlook 2013–2022, Section 3 – Crude Bitumen, 3-2 (accessed September 2, 2013).

(3) Card, C.C., Chakrabarty, N., Gates, I.D. 2006. Automated Global Optimization of Commercial SAGD Operations. Paper SPE 2006-157-EA presented at the Canadian International Petroleum Conference, 13 – 15 June 2006, Calgary, Alberta.

(4) Johnston, D.H. 2013. Practical Applications of Time-lapse Seismic Data. Society of Exploration and Geophysicists (SEG) 2013 Distinguished Instructor Short Course. Practical Applications of Time-lapse Seismic Date: 160-163.

(5) Begg, S.H., Carter, R.R., and Dranfield, P. 1989. Assigning Effective Values to Simulator Gridblock Parameters for Heterogeneous Reservoirs. SPE Res Eng **4** (4): 455-463. SPE 16754-PA.

(6) White, C.D. and Horne, R.N. 1987. Computing Absolute Transmissibility in the Presence of Fine-Scale Heterogeneity, Paper SPE 16011 presented at the SPE Symposium on Reservoir Simulation, 1 – 4 February 1987, San Antonio, Texas.

(7) Durlofsky, L.J. 1992. Representation of Gridblock Permeability in Coarse Scale Models of Randomly Heterogeneous Porous Media. Water Resources Research, **28** (7): 1791-1800.

(8) King, M.J. 1993. Application and Analysis of Tensor Permeability to Cross-Bedded Reservoirs. Paper SPE 26118-MS presented at the SPE Western Regional Meeting, 26-28 May 1993, Anchorage, Alaska.

(9) Pickup, G.E. et al. 1992. A Method for Calculating Permeability Tensors Using Perturbed Boundary Conditions. Presented at the Third European Conference on the Mathematics of Oil Recovery, 17 – 19 June 1992, Delft, Netherlands.

(10) King, P.R. 1989. The Use of Renormalization for Calculating Effective Permeability. *Transport in Porous Media*. **4** (1): 37-58.

(11) King, P.R., Muggeride, A.H. and Price, W.G. 1993. Renormalization Calculations of Immiscible Flow. *Transport in Porous Media*. **12** (3): 237-240.

(12) Christie, M.A. 1996. Upscaling for Reservoir Simulation. J. Cdn. Pet. Tech **48** (11): 1004-1010. SPE 37324-MS.

(13) Soedarmo, E. 1994. Length-Dependent Pseudo Function: An Improved Up-scaling Method in Black Oil Simulation. Paper SPE 28754-MS presented at the SPE Asia Pacific Oil and Gas Conference, 7-10 November 1994, Melbourne, Australia.

(14) Jacks, H.H., Smith, O.J.E., Mattax, C.C. 1973. The Modeling of a Three-Dimensional Reservoir with a Two-Dimensional Reservoir Simulator – The Use of a Dynamic Pseudo Functions. SPE Journal **13** (3): 175-185. SPE 4071-PA.

(15) Kyte, J.R., Berry, D.W. 1975. New Pseudo Functions to Control Numerical Dispersion. SPE Journal **15** (4): 269-276. SPE 5105-PA.

(16) Lasseter, T.J., Waggoner, J.R., Lake, L. W. 1986. Reservoir Heterogeneities and their Influence on Ultimate Recovery. *Reservoir Characterization*. Academic Press, Orlando.

(17) Kossack, C.A., Aasen, J.O., Opdal, S.T. 1989. Scaling-Up Laboratory Permeability and Rock Heterogeneities with Pseudo Functions for Field Simulations. Paper SPE 18436-PA presented at the SPE Symposium on Reservoir Simulation, 6 – 8 February 1989, Houston, Texas.

(18) Stone, H.L. 1991. Rigorous Black Oil Pseudo Functions. Paper SPE 21207-MS presented at the SPE Symposium on Reservoir Simulation, 17 – 20 February 1991, Anaheim, California.

(19) Alabert, F.G., Corre, B. 1991. Heterogeneity in a Complex Turbiditic Reservoir: Impact on Field Development. Paper SPE 22902-MS, presented at the SPE Annual Technical Conference & Exhibition, 6 – 9 October, 1991, Dallas, Texas.

(20) Guérillot, D., Verdiére, S. Different Pressure Grids for Reservoir Simulation in Heterogeneous Reservoirs. Paper SPE 29148-MS presented at the SPE Symposium on Reservoir Simulation, 12 – 15 Feb 1995, San Antonio, Texas.

(21) Verdiére, S., Guérillot, D., Thomas, J.M. 1996. Dual Mesh Method for Multiphase Flows in Heterogeneous Reservoirs. Presented at the Fifth European Conference on the Mathematics of Oil Recovery, 3 – 6 September 1996, Leoben, Austria.

(22) Taggart, I.J., Soedarmo, E. 1995. Limitations in the Use of Pseudo Functions for Upscaling Reservoir Simulation Models. Paper SPE 29126-MS presented at the SPE Reservoir Simulation Symposium, 12 – 15 February 1996, San Antonio, Texas.

(23) Guedes, S.S., Schiozer, D.J. 1999. An Implicit Treatment of Upscaling in Numerical Reservoir Simulation. Paper SPE 51937-MS presented at the SPE Reservoir Simulation Symposium, 14-17 February 1999, Houston, Texas.

(24) Ponting, D.K. 1989. Corner Point Geometry in Reservoir Simulation. Presented at the First European Conference on the Mathematics of Oil Recovery, 1 – 4 July 1989, Oxford, England.

(25) Agut, I. 1998. Flexible Streamline Grids for Reservoir Simulation. Paper SPE 49072-MSpresented at the SPE Annual Technical Conference and Exhibition, 27 –30 September, New Orleans, Louisiana.

(26) Garcia, M., Ecole, N., Andre, G., Aziz, K. 1990. An Automatic Grid Generation and Adjustment Method for Modelling Reservoir Heterogeneities. SPE Res Eng **7** (7): 278-284. SPE 21471-PA.

(27) Lacroix, S., Renard, G., Lemonnier, P., Taieb, C. 2003. Enhanced Numerical Simulations of IOR Processes Through Dynamic Sub-Gridding. Paper SPE 2003-087 presented at the Canadian International Petroleum Conference, 10 – 12 June 2003, Calgary, Alberta.

(28) Christensen, J.R., Darche, G., Dechelette, B., Ma, H., Sammon, P.H. 2004, Applications of Dynamic Gridding to Thermal Simulations. Paper SPE 86969-MS presented at the SPE International Thermal Operations and Heavy Oil Symposium and Western Regional Meeting, 16 – 18 March 2004, Bakersfield, California.

(29) Builder™ Pre-Processing Applications, Version 2012 User Guide. 2012. Calgary, Alberta: Computer Modeling Group Ltd.

(30) STARS™ Advanced Process and Thermal Reservoir Simulator, Version 2012 User Guide. 2012. Calgary, Alberta: Computer Modeling Group Ltd.

(31) CMOST™ Computer Assisted History Matching, Optimization and Uncertainty Assessment Tool, Version 2012 User Guide. 2012. Calgary, Alberta: Computer Modeling Group Ltd.

(32) Results Graph and Results Report, Version 2012 User Guide. 2012. Calgary, Alberta: Computer Modeling Group Ltd.

(33) Gillis, K.A., Palmgren, C., Thimm, H.F. 2000. Simulation of Gas Production in SAGD. Paper SPE 65500-MS presented at the SPE/CIM International Conference on Horizontal Well Technology, 6-8 November 2000, Calgary, Alberta.

(34) Deng, X., Huang. H., Zhao, L. et al. 2010. Simulating the ES-SAGD Process with Solvent Mixture in Athabasca Reservoirs. J. Cdn. Pet. Tech **49** (1): 38-46. SPE 132488-PA.

(35) Law, D.H.S. and Nasr, T.N. 2003. Field-Scale Numerical Simulation of SAGD Process with Top-Water Zone. J. Cdn. Pet. Tech **42** (8): 32-38. JCPT Paper No. 03-08-01.

(36) Alberta Energy Regulator (AER). 2013. In-situ Progress Reports, 2013. http://www.ercb.ca/data-and-publications/activity-and-data/insitu-progress (accessed September 2, 2013)

(37) Fustic, M., Hubbard, S.M., Spencer, R. et al. 2012. Recognition of down-valley translation in tidally influenced meandering fluvial deposits, Athabasca Oil Sands (Cretaceous), Alberta, Canada. Elsevier Marine and Petroleum Geology, **29** (2012): 219-232.

(38) @RISK^{TM} Risk Analysis and Simulation Add-In for Microsoft Excel, Version 5.5. 2010. Ithaca, NY: Palisade Corp.

(39) Prothero, D.R., Schwab, F. 1996. *Sedimentary Geology: An Introduction to Sedimentary Rocks and Stratigraphy*. United States: W.H. Freeman and Company: 159-168.

(40) Prothero, D.R., Schwab, F. 1996. *Sedimentary Geology: An Introduction to Sedimentary Rocks and Stratigraphy*. United States: W.H. Freeman and Company: 134-140.

(41) Gates, I.D., Wang, J. 2011. Evolution of In Situ Oil Sands Recovery Technology in the Field: What Happened and What's New? Paper SPE 150686-MS presented at SPE Heavy Oil Conference and Exhibition, 12-14 December 2011, Kuwait City, Kuwait.

(42) @RISK^{TM} Risk Analysis and Simulation, Version 5.5. 2010. Ithaca, NY: Palisade Corp. Risk Discrete Formulation: 488-490.

(43) @RISK^{TM} Risk Analysis and Simulation, Version 5.5. 2010. Ithaca, NY: Palisade Corp. Risk Normal Formulation: 544-546.

(44) Aziz, K., Settari, A. 1979. *Petroleum Reservoir Simulation*. 11-14, 2002. Calgary, Alberta: Blitzprint Ltd.

(45) Holman, J.P. 1963. *Heat Transfer Ninth Edition*. 1-24, Ninth Edition 2002. New York, NY: McGraw-Hill

(46) Butler, R.M. 1997. *Thermal Recovery of Oil and Bitumen*. 285-300, Fifth Printing 2008. Calgary, Alberta: GravDrain Inc.

(47) Akin, S. 2005. Mathematical Modeling of Steam-Assisted Gravity Drainage. SPE Res Eval & Eng **8** (5): 372-376. SPE 86963-PA.

(48) Butler, R.M. 1985. A New Approach to the Modeling of Steam-Assisted Gravity Drainage. J. Cdn. Pet. Tech**. 24 (3):** 42-51. JCPT Paper No. 85-03-01.

(49) Ferguson, F.R.S., Butler, R.M. 1988. Steam-Assisted Gravity Drainage Model Incorporating Energy Recovery from a cooling Steam Chamber. J. Cdn. Pet. Tech. **27** (5): 75-83.

(50) Gotawala, D.R., Gates, I.D. 2008. Steam Fingering at the Edge of a Steam Chamber in a Heavy Oil Reservoir. Cdn. J. Chem. Eng. **86** (10): 1011-1022.

(51) Reis, J.C. 1992. A Steam-Assisted Gravity Drainage Model for Tar Sands: Linear Geometry. J. Cdn. Pet. Tech. **31** (10): 14-20. JCPT Paper No. 92-10-01.

(52) Reis, J.C. 1993. A Steam-Assisted Gravity Drainage Model for Tar Sands: Radial Geometry. J. Cdn. Pet. Tech. **32** (8): 43-48. JCPT Paper No. 93-05-05.

(53) Sharma, J., Gates, I.D. 2010. Multiphase Fluid Flow at the Edge of a Steam Chamber. Cdn. J. Chem. Eng. **88** (3): 312-321.

(54) STARS™ Advanced Process and Thermal Reservoir Simulator, Version 2012 User Guide. 2012. Calgary, Alberta: Computer Modeling Group Ltd. Other Reservoir Properties – Rock Types: 273.

(55) CMOST™ Computer Assisted History Matching, Optimization and Uncertainty Assessment Tool, Version 2012 User Guide. 2012. Calgary, Alberta: Computer Modeling Group Ltd. Designed Exploration Controlled Evolution (DECE) Optimization: 227-228.

(56) Computer Modeling Group Ltd. Ranking Geostatistical Realizations for SAGD Process. 2013.

(57) Ito, Y., Hirata, T., Ichikawa. M. 2004. The Effect of Operating Pressure on the Growth of the Steam Chamber Detected at the Hangingstone SAGD Project. J. Cdn. Pet. Tech. **43** (1): 47-53. JCPT Paper No. 04-01-05.

(58) Collins, P. M. 2007. The False Lucre of Low-Pressure SAGD. J. Cdn. Pet. Tech. **46** (1): 20-27. JCPT Paper No 07-01-02.

(59) Shin, H., Polikar, M. 2007. Review of Reservoir Parameters to Optimize SAGD and Fast-SAGD Operating Conditions. J. Cdn. Pet. Tech. **46** (1): 35-41. JCPT Paper No 07-01-04.

(60) Sharma, J., Gates, I.D. 2011. Convection at the Edge of a Steam-Assisted-Gravity-Drainage Steam Chamber. SPE Journal **16** (3): 503:512. SPE 142432-PA.

(61) Mazda, I., Gates, I.D. 2013. Understanding the Convection Heat-Transfer Mechanism in the Steam-Assisted Gravity Drainage Process. SPE Journal **18** (6): 1202-1215. SPE 167258-PA.

(62) Settari, A. 2009. Topics in Reservoir Simulation, 2012. Formulation of Flow Equations, Section 1.2 – Flow Equations for Multiphase, Multicomponent Flow.

(63) Carlslaw, H.S., Jaeger, J.C. 1959. *Conduction of Heat in Solids*. Second Edition 1986. Oxford, U.K.: Oxford University Press.

(64) Marx, J.W., Langenheim, R.H. 1959. Reservoir Heating by Hot Fluid Injection Petroleum Transactions. In Transactions of the Society of Petroleum Engineers, Vol. 216: 312-315.

APPENDICES

Appendix A Governing Equations for Reservoir Simulation

In reservoir simulation, the basis for numerical modelling involves segmenting the reservoir into gridblocks of predetermined dimensions. During a dynamic reservoir simulation, the flow equations are applied between neighbouring gridblocks while honouring and solving the material balance equation (equation of continuity). The reservoir flow equations are a function of the conservation of mass, which states that for any volume element that the rate of mass accumulation is equal to the mass into the system minus the mass out of the system.

The equation of continuity describes the rate of change of density of a fixed point due to the changes in the mass velocity vector, $\rho \boldsymbol{v}$[62]. In vector notation, the equation of continuity is given by:

$$-\nabla \cdot (\rho \boldsymbol{v}) = \frac{\delta}{\delta t}(\rho \phi) \mp q \tag{A.1}$$

Where ∇ represents the gradient operator with units of reciprocal length, $\rho \boldsymbol{v}$ is the mass velocity vector with units of mass/area-time, t represents time, $\rho \phi$ is the density-porosity term with units mass/volume.

These processes can also include a sink (production) and source (injection) component in the given gridblock, as denoted by q with units of volume/time.

With respect to hydrocarbon reservoirs, the equation of continuity must be defined to consider multiphase, multimechanism and/or multicomponent flow. To solve the equation of continuity in space and time, an appropriate procedure must be applied to update the pressure and saturations versus time. For example, consider single phase fluid flow, such as oil, in the x-direction with no sink or source term:

$$\frac{\delta}{\delta x}\left(\lambda \frac{\delta P}{\delta x}\right) = \frac{\delta}{\delta t}\left(\frac{\phi}{B}\right) \tag{A.2}$$

The flow equation can be solved implicitly or explicitly. The explicit formulation and implicit formulation of the flow equation are described in detail in **Appendices A.1 and A.2.**

Due to the conditional instability associated with the explicit method (IMPES, implicit pressure and explicit saturation) most simulators can switch from IMPES to fully implicit method. The explicit method tends to be unstable at larger time steps and the gridblock with the smallest value determines the limiting time-step, as indicated in **Equation A.3**. Whereas, the implicit method is unconditionally stable regardless of the time step-size employed, but is often associated with longer numerical run-times.

$$\Delta t \leq \frac{1}{2}\left(\frac{\mu \phi C}{k}\right)\Delta x^2 = \text{Stability Criteria} \tag{A.3}$$

Additionally, the aforementioned conditions are assumed isothermal. However, SAGD involves the injection of high-pressure steam at saturation temperature, so heat transfer theory must also be coupled within the reservoir simulator. The heat transfer theory presented will included the conductive and convective terms as proposed by Carslaw and Jaeger (1959)[63]. For example,

consider the temperature gradient in the horizontal direction (perpendicular to the steam-bitumen interface):

$$K_{TH}\left(\frac{\delta^2 T}{\delta x^2}\right) - V_c \rho_c c_{Pc}\left(\frac{\delta T}{\delta x}\right) = \rho_r c_P \left(\frac{\delta T}{\delta t}\right) \tag{A.4}$$

Where K_{TH} represents the thermal conductivity with units of mass-length/time^3-temp, V_c represents the condensate convective velocity normal to the chamber edge with units distance/time, ρ_r represents the reservoir (oil sand) density with units of mass/volume, c_P represents the heat capacity with units of mass/time^2-length-temp.

A.1 Explicit Discretization of One-Dimensional Flow Equation (x-direction)

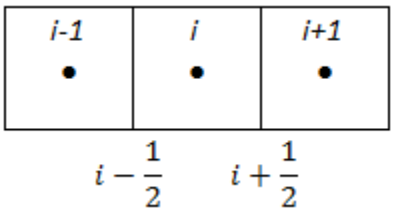

$$\frac{\delta}{\delta x}\left(\lambda\frac{\delta P}{\delta x}\right)=\frac{\delta}{\delta t}\left(\frac{\phi}{B}\right) \tag{A.2}$$

$$\frac{1}{\Delta x}\left[\lambda\frac{\delta P}{\delta x}\Big|_{i+\frac{1}{2}}-\lambda\frac{\delta P}{\delta x}\Big|_{i-\frac{1}{2}}\right]^{n}=\frac{1}{\Delta t}\left[\left(\frac{\phi}{B}\right)_{i}^{n+1}-\left(\frac{\phi}{B}\right)_{i}^{n}\right] \tag{A.1.1}$$

$$\frac{1}{\Delta x}\left[\lambda_{i+\frac{1}{2}}\frac{(P_{i+1}-P_i)^n}{\Delta x}-\lambda_{i-\frac{1}{2}}\frac{(P_i-P_{i-1})^n}{\Delta x}\right]=\frac{1}{\Delta t}\left[\left(\frac{\phi}{B}\right)_{i}^{n+1}-\left(\frac{\phi}{B}\right)_{i}^{n}\right] \tag{A.1.2}$$

$$T=\frac{kA}{\mu B\Delta x}=\frac{\lambda A}{\Delta x} \tag{4.2.1.5}$$

$$T_{i+\frac{1}{2}}(P_{i+1}-P_i)^n-T_{i-\frac{1}{2}}(P_i-P_{i-1})^n=\frac{V}{\Delta t}\left[\left(\frac{\phi}{B}\right)_{i}^{n+1}-\left(\frac{\phi}{B}\right)_{i}^{n}\right] \tag{A.1.3}$$

$$\left[T_{i+\frac{1}{2}}(P_{i+1}-P_i)^n-T_{i-\frac{1}{2}}(P_i-P_{i-1})^n\right]_{x-direction}=\left[\frac{Vc}{\Delta t}[P_i^{n+1}-P_i^n]\right]_{x-direction} \tag{A.1.4}$$

Where x represents the direction of interest with units of length, λ represents the mobility ratio with units of volume/mass-time, P represents the pressure with units of mass/length-time^2, t represents time, ϕ represents the porosity term in fractional terms, B represents the formation volume factor with units of volume/volume, c represents the compressibility within the block with units of reciprocal pressure, V represents the volume of the element, and T represents the temperature in the interface of the element.

A.2 Implicit Discretization of One-Dimensional Flow Equation (x-direction)

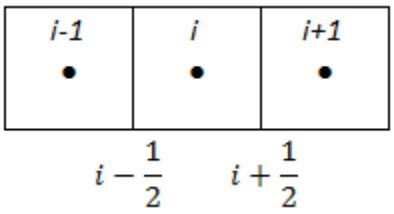

$$\frac{\delta}{\delta x}\left(\lambda\frac{\delta P}{\delta x}\right)=\frac{\delta}{\delta t}\left(\frac{\phi}{B}\right) \tag{A.2}$$

$$\frac{1}{\Delta x}\left[\lambda\frac{\delta P}{\delta x}\Big|_{i+\frac{1}{2}}-\lambda\frac{\delta P}{\delta x}\Big|_{i-\frac{1}{2}}\right]^{n+1}=\frac{1}{\Delta t}\left[\left(\frac{\phi}{B}\right)_i^{n+1}-\left(\frac{\phi}{B}\right)_i^{n}\right] \tag{A.2.1}$$

$$\frac{1}{\Delta x}\left[\lambda_{i+\frac{1}{2}}\frac{(P_{i+1}-P_i)^{n+1}}{\Delta x}-\lambda_{i-\frac{1}{2}}\frac{(P_i-P_{i-1})^{n+1}}{\Delta x}\right]=\frac{1}{\Delta t}\left[\left(\frac{\phi}{B}\right)_i^{n+1}-\left(\frac{\phi}{B}\right)_i^{n}\right] \tag{A.2.2}$$

$$\frac{1}{\Delta x^2}\left[\lambda_{i+\frac{1}{2}}(P_{i+1}-P_i)^{n+1}-\lambda_{i-\frac{1}{2}}(P_i-P_{i-1})^{n+1}\right]=\frac{1}{\Delta t}\left[\left(\frac{\phi}{B}\right)_i^{n+1}-\left(\frac{\phi}{B}\right)_i^{n}\right] \tag{A.2.3}$$

$$T=\frac{kA}{\mu B\Delta x}=\frac{\lambda A}{\Delta x} \tag{4.2.1.5}$$

$$T_{i+\frac{1}{2}}(P_{i+1}-P_i)^{n+1}-T_{i-\frac{1}{2}}(P_i-P_{i-1})^{n+1}=\left[\frac{Vc}{\Delta t}[P_i^{n+1}-P_i^{n}]\right] \tag{A.2.4}$$

$$\left[T_{i+\frac{1}{2}}(P_{i+1})^{n+1}-\left(T_{i+\frac{1}{2}}+T_{i-\frac{1}{2}}-\frac{Vc}{\Delta t}\right)P_i^{n+1}+T_{i-\frac{1}{2}}(P_{i-1})^{n+1}\right]_{x-direction}=\left[\frac{-Vc}{\Delta t}P_i^{n}\right]_{x-direction} \tag{A.2.5}$$

The notation for the implicit discretization is the same as the explicit discretization.

Appendix B CMOST™ Input Files

Builder™ data files (.DAT) were converted to the CMOST™ master file (.CMM) with the necessary syntax. Permeability and thermal conductivity parameters were modified within the data file and summarized in Table B.1 and B.2.

Table B.1 – Keywords for Manipulation of Permeability Parameters in CMOST™

Parameters	Units	.CMM File Notation
Permeability, *i*-direction	mD	*PERMI CON <cmost>this[5,000]=PERMI</cmost>
Permeability, *j*-direction	mD	*PERMJ CON <cmost>this[5,000]=PERMJ</cmost>

Table B.2 – Keywords for Manipulation of Thermal Conductivity Parameters in CMOST™

Parameters	Units	.CMM File Notation
Temperature	^{o}C	12
Rock, *i*-direction	J/m-day-^{o}C	<cmost>this[1]=TH_IMULT*2.74e+5</cmost>
Rock, *j*-direction	J/m-day-^{o}C	<cmost>this[1]=TH_JMULT*2.74e+5</cmost>
Water, *i*-direction	J/m-day-^{o}C	<cmost>this[1]=TH_IMULT*5.35e+4</cmost>
Water, *j*-direction	J/m-day-^{o}C	<cmost>this[1]=TH_JMULT*5.35e+4</cmost>
Oil, *i*-direction	J/m-day-^{o}C	<cmost>this[1]=TH_IMULT*1.15e+4</cmost>
Oil, *j*-direction	J/m-day-^{o}C	<cmost>this[1]=TH_JMULT*1.15e+4</cmost>
Gas, *i*-direction	J/m-day-^{o}C	<cmost>this[1]=TH_IMULT*2,892</cmost>
Gas, *j*-direction	J/m-day-^{o}C	<cmost>this[1]=TH_JMULT*2,892</cmost>
Solid, *i*-direction	J/m-day-^{o}C	<cmost>this[1]=TH_IMULT*2.74e+5</cmost>
Solid, *j*-direction	J/m-day-^{o}C	<cmost>this[1]=TH_JMULT*2.74e+5</cmost>

Appendix C Ranking Geostatistical Realizations for SAGD Process[56]

Ranking Geostatistical Realizations For SAGD Process

Connectivity

The connectivity of a cell (i,j,k) indicates how easily the cell can be reached by the steam chamber and the contained bitumen can be drained to the producer. In this study, the following steps are used to estimate the connectivity of a cell in a realization:

- For the true realization, calculate the harmonic average permeability $Kave_{real}(i,j,k)$ of all the cells in the path for a fluid to flow from the injector to the cell and then back to the producer.

$$\frac{1}{Kave_{real}(i,j,k)} = \frac{1}{Ncell}\sum_{cell=1}^{Ncell}\frac{1}{K_{cell}}$$

  Here, $Ncell$ is the number of cells in the path. K_{cell} is the permeability of a cell which is equal to either the horizontal permeability or the vertical permeability of the cell depending on the flow direction within the cell.
- Assuming all the cells are clean sand, recalculate the harmonic average permeability $Kave_{clean}(i,j,k)$ for the same path.
- The connectivity $C(i,j,k)$ of the cell is equal to the ratio of the average permeability for the true realization to the average permeability for the clean sand case.

$$C(i,j,k) = \frac{Kave_{real}(i,j,k)}{Kave_{clean}(i,j,k)}$$

The calculated connectivity will have the following features:

- Its value ranges from 0 to 1. If all the cells in the path are clean sand, the connectivity is equal to 1. If one of the cells in the path blocks the flow completely (zero permeability), the connectivity is equal to 0.
- Because a cell can be reached by the injector and producer through different paths, a cell can have different connectivity values.

Optimum Path and Optimum Connectivity

Among different paths that connect a cell to the injector and producer, the optimum path is the path that has the largest connectivity for the cell. The largest connectivity is the optimum connectivity $C_{\max}(i,j,k)$ for the cell. In the search of the optimum path, certain rules must be followed to ensure that the optimum path is physically possible in the SAGD process.

SAGD Performance Index

The SAGD Performance Index SPI for a realization is the average optimum connectivity of the cells in the realization.

$$SPI = \frac{\sum_{i=Iprod-NI}^{Iprod+NI}\sum_{j=Jheel}^{Jtoe}\sum_{k=Kprod-NK}^{Kprod} C_{\max}(i,j,k)}{(2*NI+1)*(Jtoe-Jheel+1)*(NK+1)}$$

Here, $Iprod, Jheel, Jtoe, Kprod$ indicates the location of the SAGD well pair; i, j, k indicates the location of a cell (the k index increases downward); NI, NK indicates the approximate steam chamber size at the end of the SAGD project life. If the model has multiple SAGD well pairs, the above formula should be applied to all well pairs.

Appendix D Production Profile Summary

Figure D.1.A – Production Profile, Type-A' Uniform (Actual History Match)

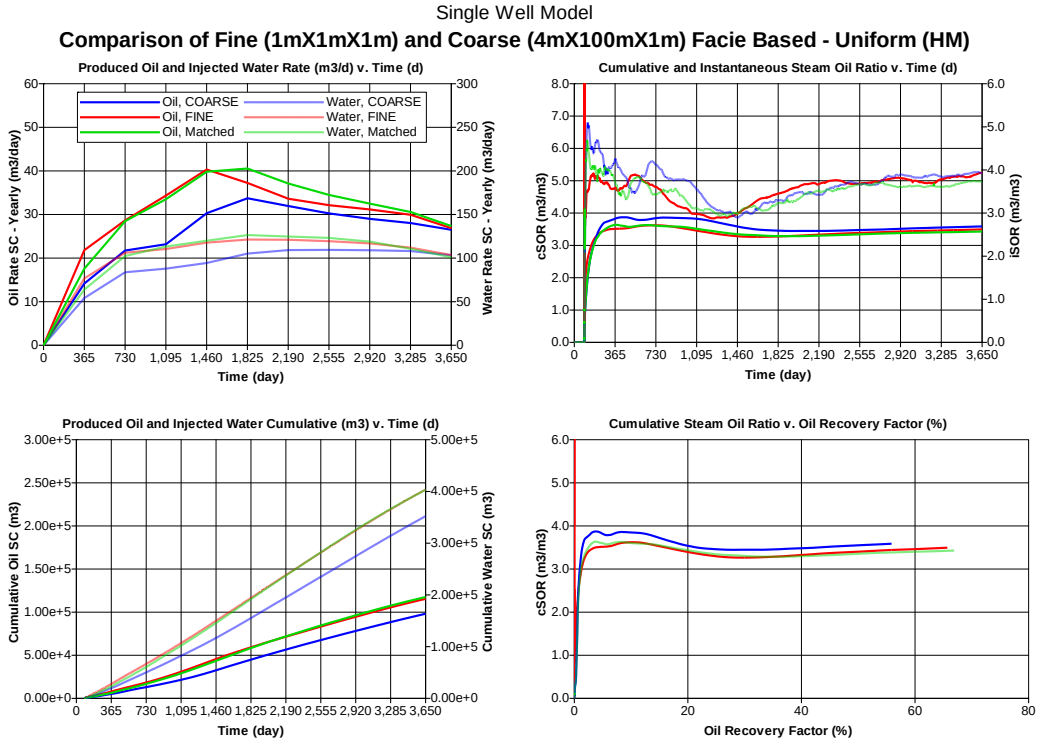

Figure D.1.B – Production Profile, Type-A' Uniform (Forecasted Match)

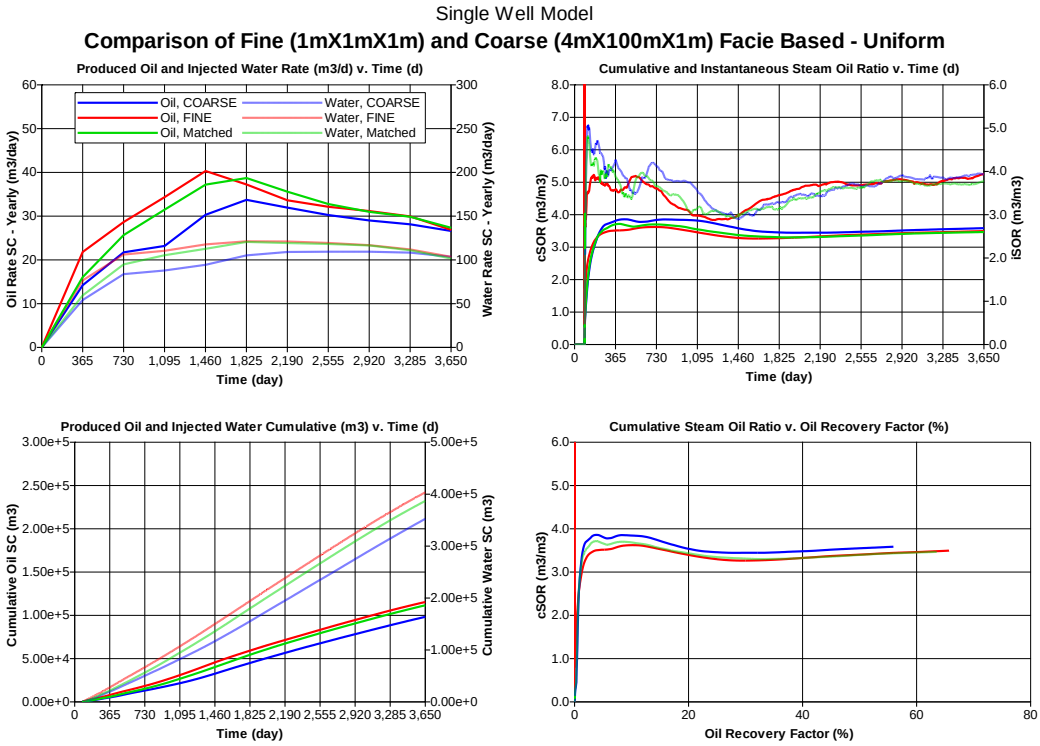

Figure D.2.A – Production Profile, Type-A' Coarsening Upwards (Actual History Match)

Single Well Model

Comparison of Fine (1mX1mX1m) and Coarse (4mX100mX1m) Facie Based - Coarsening Upwards (HM)

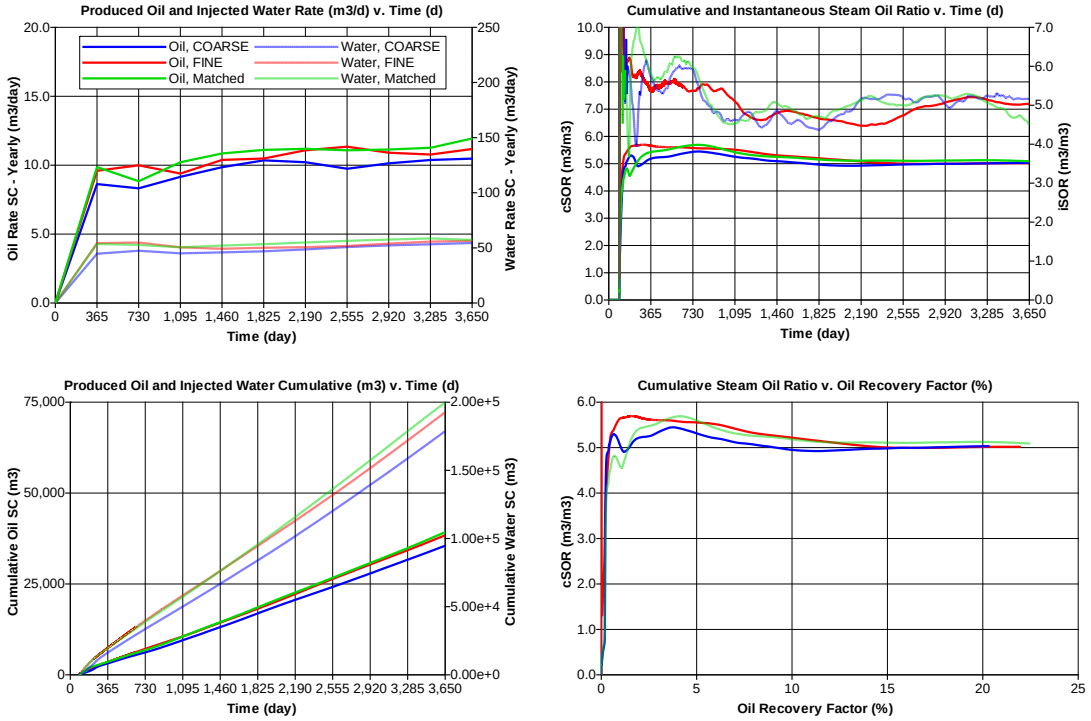

Figure D.2.B – Production Profile, Type-A' Coarsening Upwards (Forecasted Match)

Single Well Model

Comparison of Fine (1mX1mX1m) and Coarse (4mX100mX1m) Facie Based - Coarsening Upwards

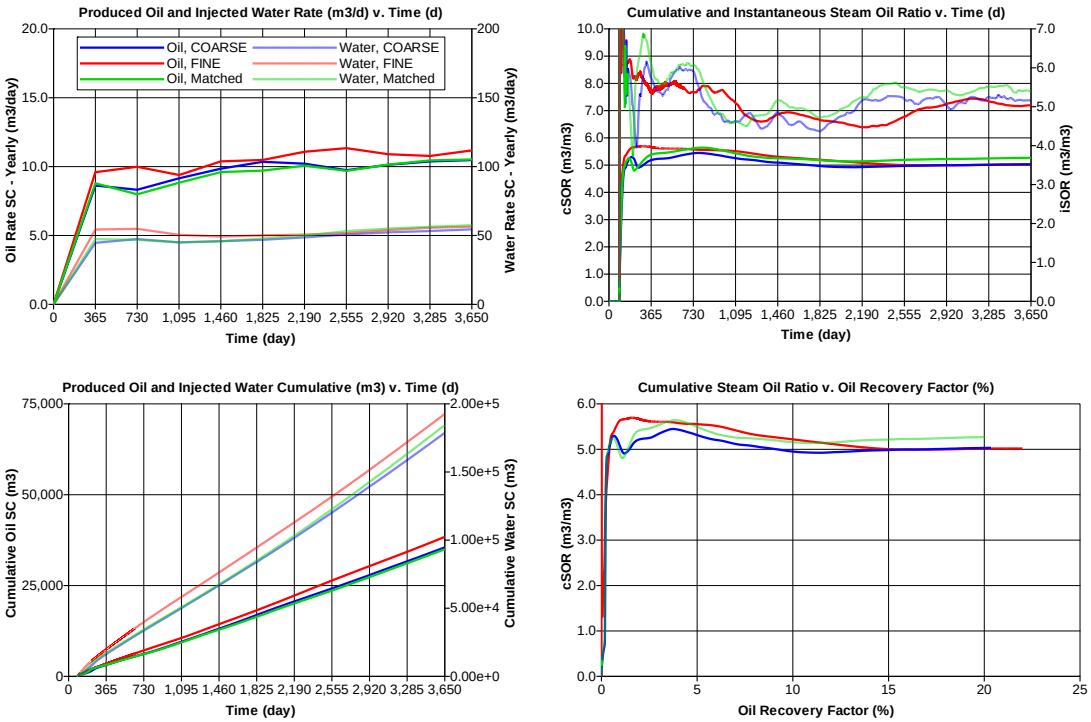

Figure D.3.A – Production Profile, Type-A' Fining Upwards (Actual History Match)

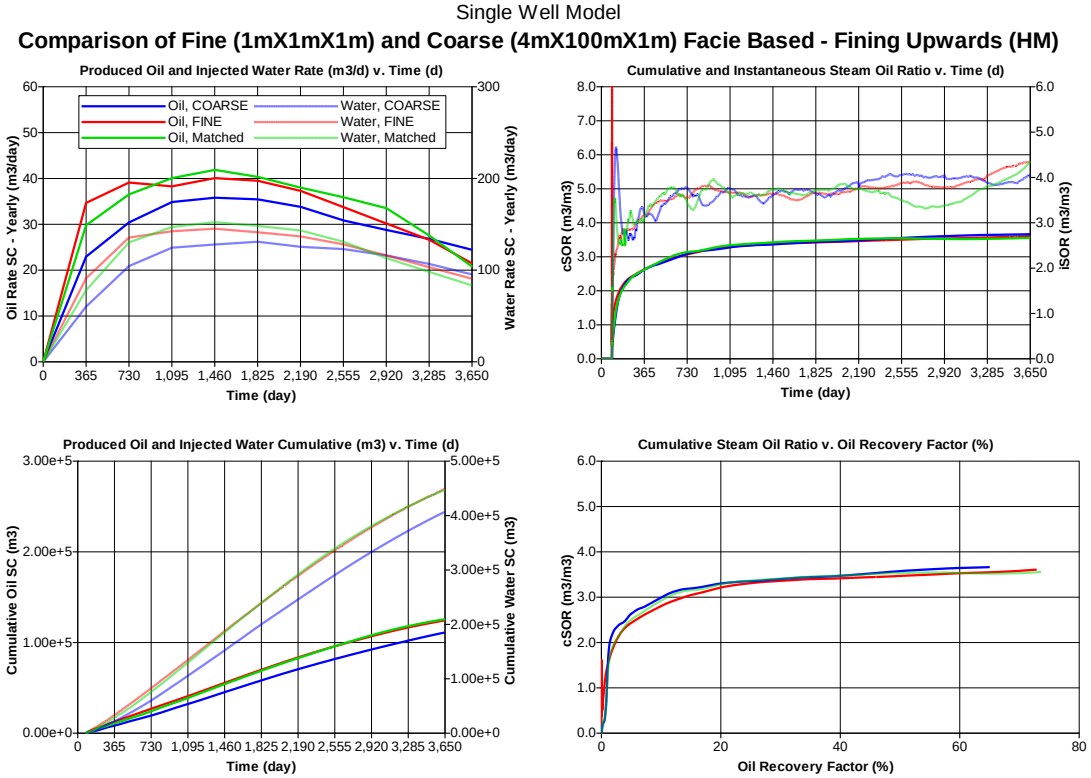

Figure D.3.B – Production Profile, Type-A' Fining Upwards (Forecasted Match)

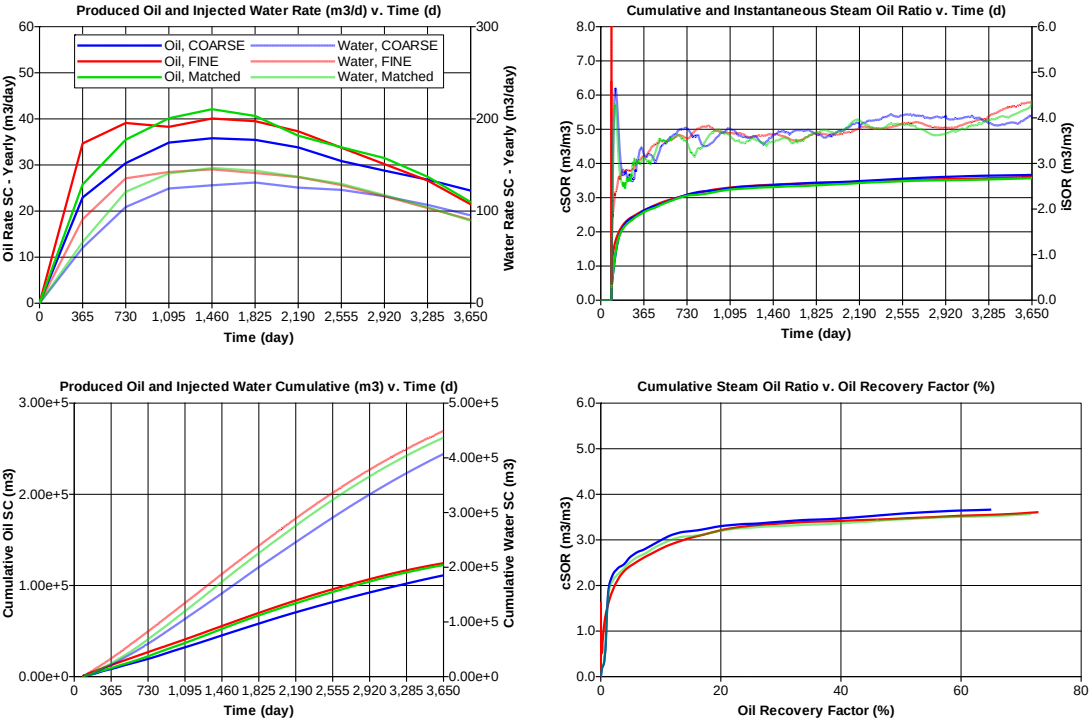

Figure D.4.A – Production Profile, Type-A' Channel (Actual History Match)

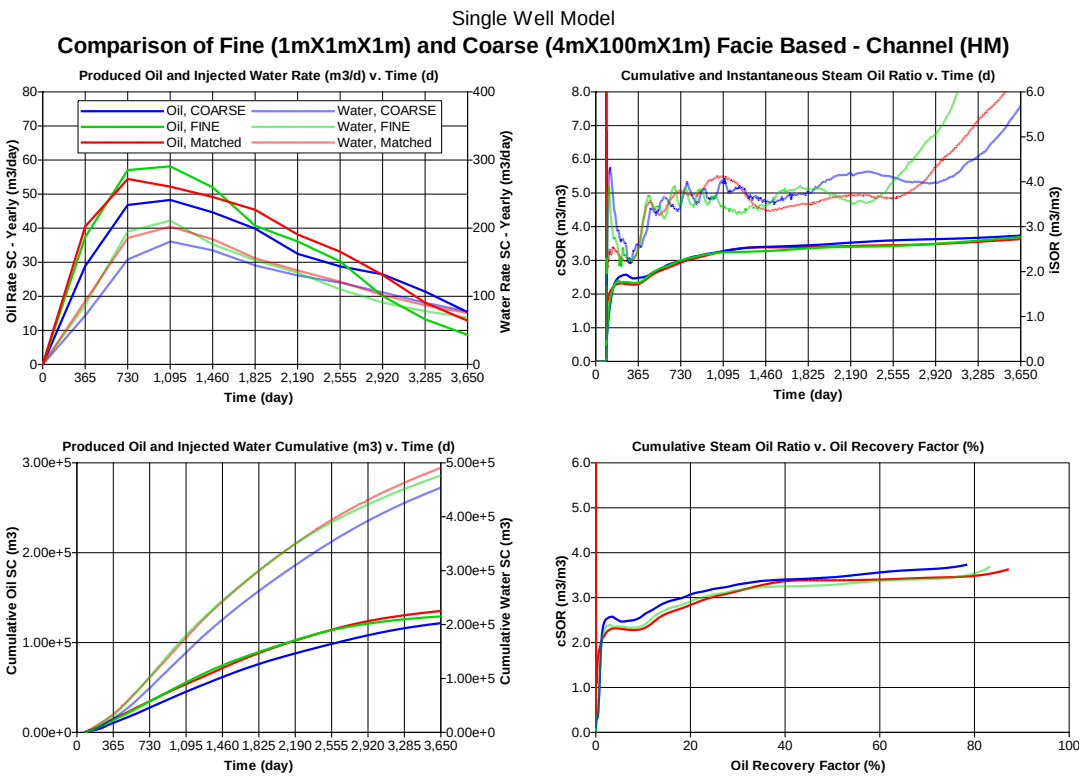

Figure D.4.B – Production Profile, Type-A' Channel (Forecasted Match)

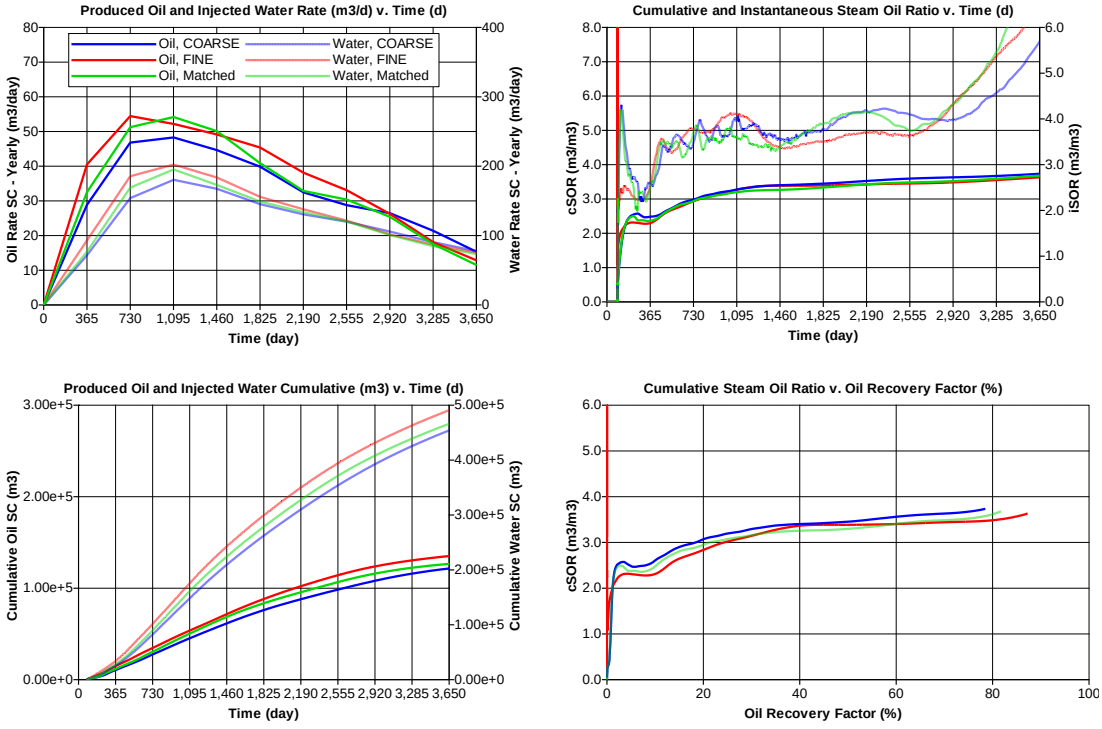

Figure D.5 – Production Profile, Type-B' Uniform (Forecasted Match)

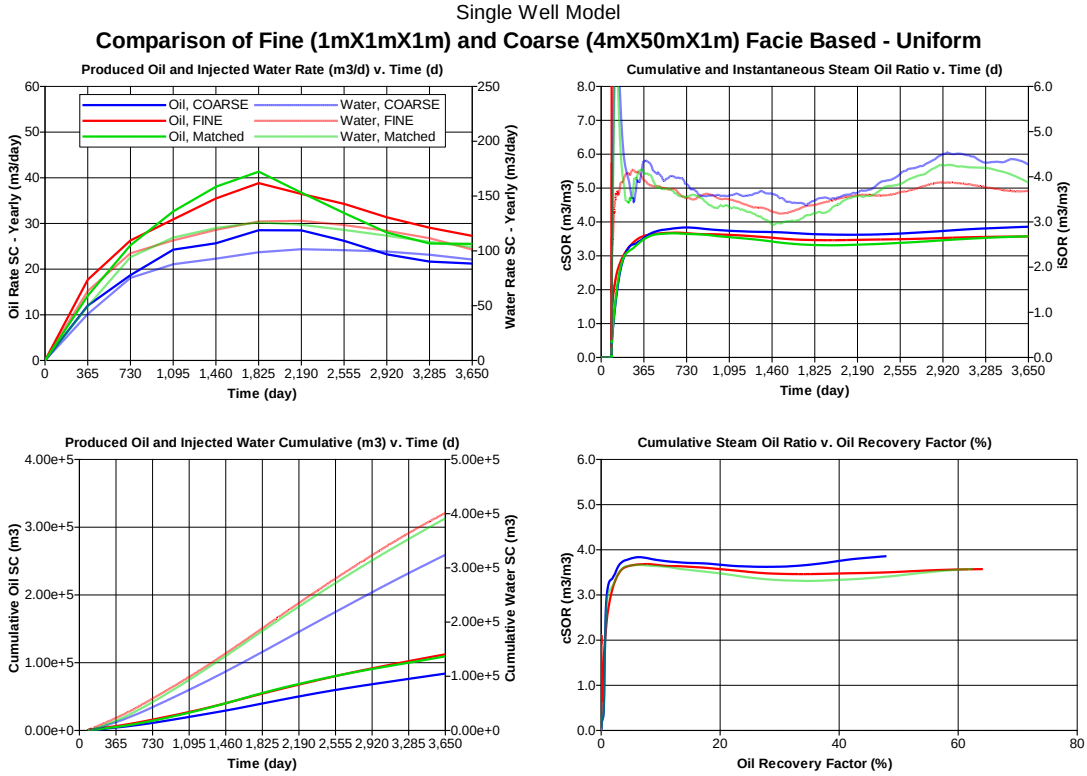

Figure D.6 – Production Profile, Type-B' Channel (Forecasted Match)

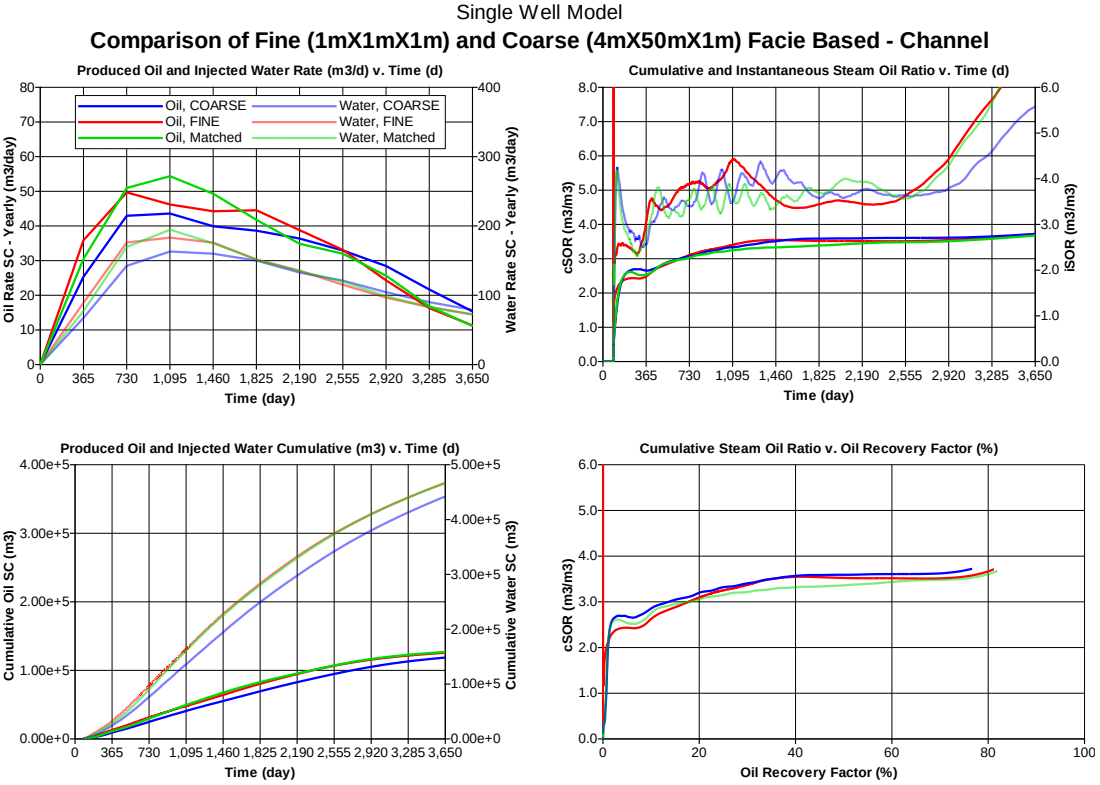

Figure D.7 – Production Profile, Type-C' Coarsening Upwards (Forecasted Match)

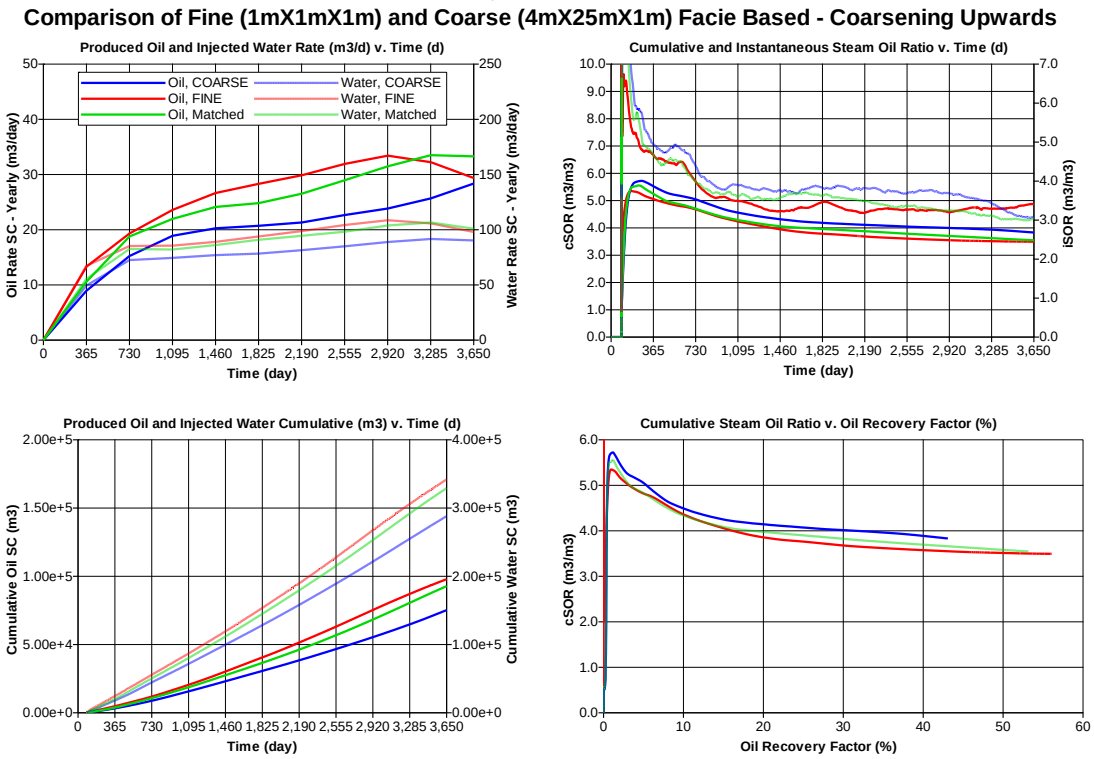

Figure D.8 – Production Profile, Type-D' Fining Upwards (Forecasted Match)

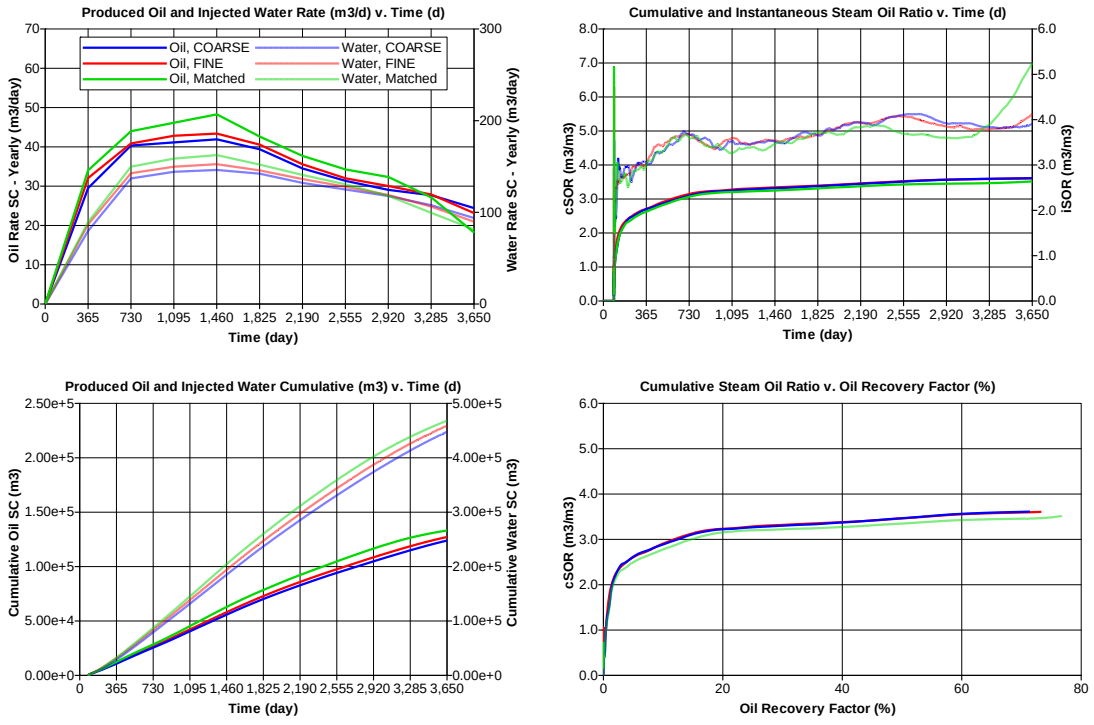

Figure D.9 – Production Profile, Type-E' Coarsening Upwards (Forecasted Match)

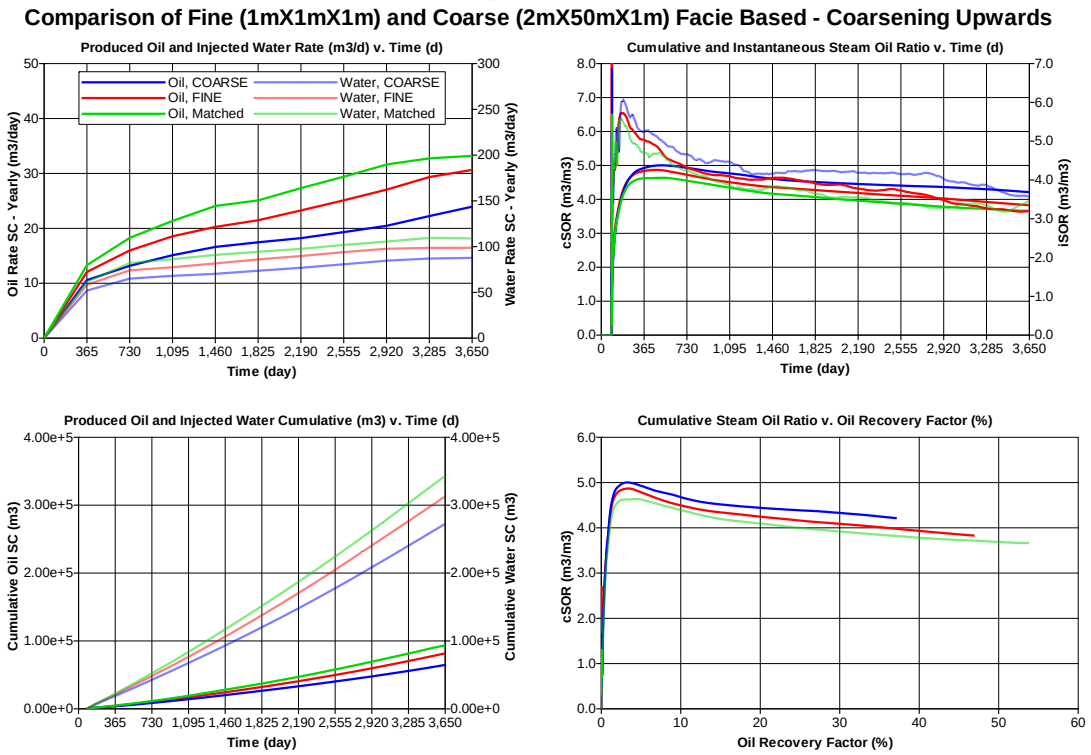

Figure D.10 – Production Profile, Type-F' Fining Upwards (Forecasted Match)

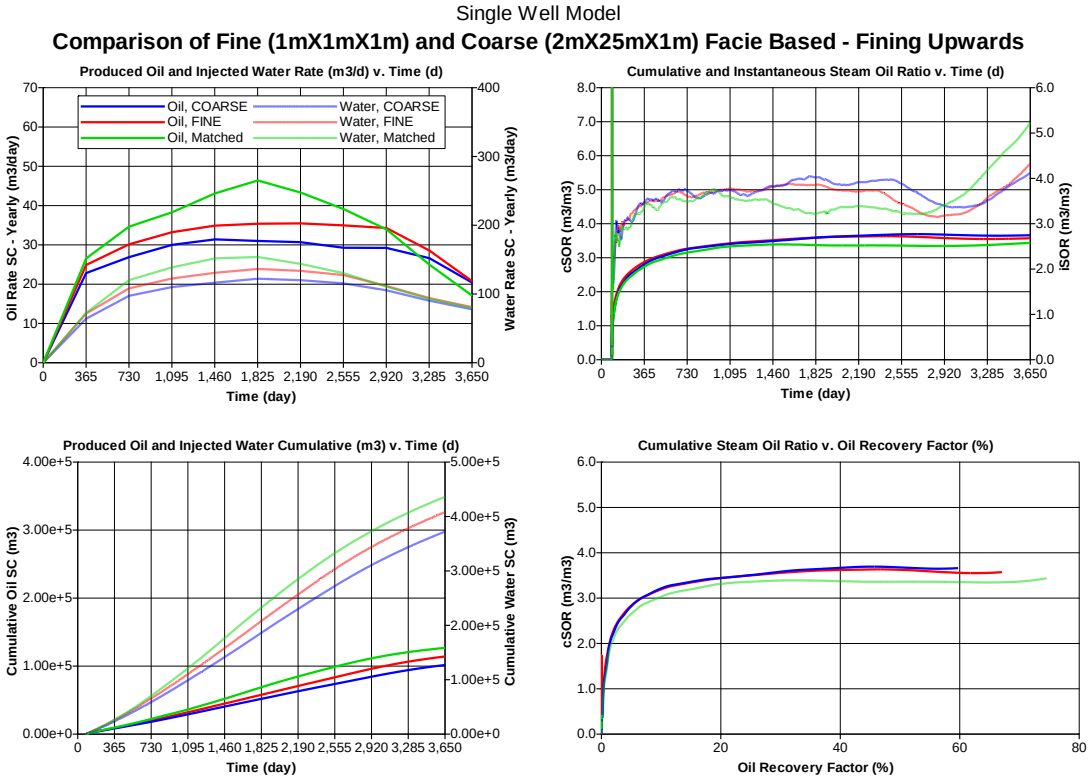

Appendix E Formation Heating by Steam Injection: Marx-Langenheim Model

The principle advantage to use of steam for bitumen recovery is the latent heat steam possess in addition to sensible heat. Conversely, hot water simply carries sensible heat. Steam can transfer all of its latent heat without a change in temperature.

Prior to steam injection into a bitumen rich formation, the initial reservoir temperature is T_R. Once steam is injected, bitumen is displaced and a quantity of oil is produced, creating a void within the reservoir. The steam will then condense while heating the surrounding reservoir rock and fluids. The condensate, while still at saturation temperature T_S, moves ahead of the new wave of steam and preheats the rock at a point beyond the steam front.

It was postulated that the heated zone is at constant steam temperature and a step-change in temperature occurs at the interface between the steam chamber and bitumen interval. The postulation is based upon several assumptions, including:

- Constant injection rate,
- Absence of gravity segregation and pressure drop in the steam zone, and
- Homogenous reservoir interval with uniform thickness,

This profile is highlighted in **Figure E.1**, and is the foundation of the Marx-Langenheim model. Marx-Langenheim (1959)[64] provided a model to explain heating within reservoirs. The growing steam zone is limited in terms of its heat loss rate to the overburden and underburden as well as the heating rate of the rock and fluids to steam temperature, T_S (equivalent to condensed steam).

In that, SAGD performance is expected to vary as a function of non-reservoir rock that serves as a heat sink and causes continual energy loss that doesn't benefit production. The principles developed by Marx-Langenheim helped in the formulation of this work-flow and the idea of chamber development and transfer of heat for steam zone growth.

Figure E.1 - Marx-Langenheim Model, Heating within Reservoirs[64]